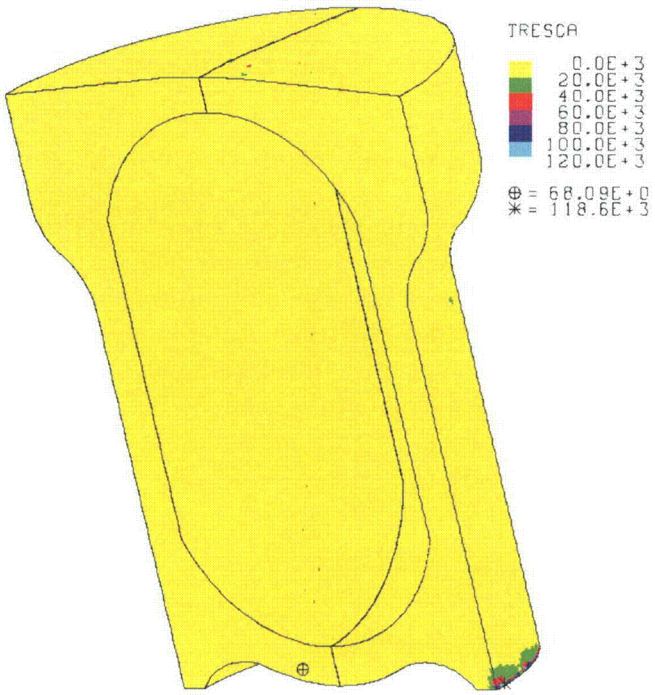

Figure 2-108. NCT SC-2 Side Impact with Support Structure Rotated 45° - Tresca Stress in TB-1

2.12.5.3.1 NCT End and Side Drop Analysis Summary

The two previous sections highlight the fact that the position of the contents within their sample containers and support cradle is essentially unchanged after 4-ft NCT drops. The titanium Inner Cradle remains essentially undeformed and the contents' positions no farther from the T-Ampoule than pre-drop, as well as no plasticity in the TB-1 and the T-Ampoule, all means that HAC and aircraft impact analyses are justified in assuming an undamaged PAT-1 package and contents before those events.

2.12.5.4 Aircraft Accident Impact Analyses

Detailed PAT-1 package models identical to those shown in the previous NCT section, except for neglecting the rolled ring lid ends, were analyzed to determine the response of the T-Ampoule and TB-1 when subjected to the loading of 10 CFR 71.74 (accident conditions for air transport of plutonium). Each combination of package orientation (lid end, side, and CG-over-corner) and contents was analyzed at an initial velocity of 422 ft/sec and each package impacts onto an analytically unyielding target.

The TB-1 was shown in the SAR[1] aircraft impact tests to remain elastic and maintain containment. With similar mass contents, similar TB-1 response would be expected, excepting the possibility of minor localized denting due to more dense contents (solid Pu vs. oxide powder). Effective or von Mises stresses (which capture three-dimensional stress states well and is more conservative than Tresca stress to show avoidance of yielding) were calculated and an acceptance criterion of "below through-thickness yielding" used to demonstrate similar TB-1

behavior as in the original regulatory testing. This also means zero plasticity in the seal area of the TB-1, ensuring similar containment requirements performance of the containment vessel.

A total of twenty-seven high speed impact analyses were conducted for the five potential contents in various orientations; the analyses are listed below in Table 2-18. In the hollow-cylinder (ER cylinder) component models, as well as the sample container models, no credit is taken for the positioning of the cylinders with the tantalum packing foil. Each form contents are assumed to be unconstrained and are placed in the worst orientation and most severe location for each impact. The delta-plutonium in the sample containers is relatively soft and has a greater degree of plasticity, so although its location will affect T-Ampoule loading, its local orientation would not. However, the beryllium composite cylinders are much harder and stronger, so their orientation is always rotated such that they present a sharp corner (CGOC, actually) towards the normal surface of the T-Ampoule, parallel with the impact direction.

Table 2-18. Aircraft Accident Impact Analyses, Components, and Orientations

Run No.	Component	Submodel Orientation
1	831 g Plutonium Metal Hollow Cylinder, alpha Pu	Bottom position, top impact
2	831 g Plutonium Metal Hollow Cylinder, alpha Pu	Bottom position (angled), top impact
3	831 g Plutonium Metal Hollow Cylinder, alpha Pu	Bottom position (angled), CGOC impact
4	831 g Plutonium Metal Hollow Cylinder, alpha Pu	Far side position, side impact
5	831 g Plutonium Metal Hollow Cylinder, alpha Pu	Far side position (angled), side impact
6	731 g Plutonium Metal Hollow Cylinder, alpha Pu	Bottom position, top impact
7	731 g Plutonium Metal Hollow Cylinder, alpha Pu	Bottom position (angled), top impact
8	731 g Plutonium Metal Hollow Cylinder, alpha Pu	Bottom position (angled), CGOC impact
9	731 g Plutonium Metal Hollow Cylinder, alpha Pu	Far side position, side impact
10	731 g Plutonium Metal Hollow Cylinder, alpha Pu	Far side position (angled), side impact
11	SC-1 – Pu	Bottom position, support structure 0°, top impact
12	SC-1 – Pu	Far side position, support structure 0°,side impact
13	SC-1 – Pu	Far side position, support structure 45°, side impact
14	SC-1 – Pu	Bottom position, support structure 0°, CGOC impact
15	SC-1 – Pu	Bottom position, support structure 45°, CGOC impact

Table 2-18. Aircraft Accident Impact Analyses, Components, and Orientations (Continued)

Run No.	Component	Submodel Orientation
16	SC-2 – Pu	Bottom position, support structure 0°, top impact
17	SC-2 – Pu	Far side position, support structure 0°,side impact
18	SC-2 – Pu	Far side position, support structure 45°, side impact
19	SC-2 – Pu	Bottom position, support structure 0°, CGOC impact
20	SC-2 – Pu	Bottom position, support structure 45°, CGOC impact
21	SC-1 – Be	Bottom position, angled Be, support structure 0°, top impact
22	SC-1 – Be	Far side position, angled Be, support structure 0°, side impact
23	SC-1 – Be	Far side position, angled Be, support structure 45°, side impact
24	SC-1 – Be	Bottom position, angled Be, support structure 0°, CGOC impact
25	SC-1 – Be	Bottom position, angled Be, support structure 45°, CGOC impact
26	SC-2 – Pu	Far side position, support structure 45°, side impact, friction 0.4
27	SC-2 – Pu	Far side position, support structure 45°, side impact, friction 0.2

2.12.5.4.1 ER Cylinder Analyses

Ten separate plutonium metal hollow cylinder, high-speed impact analyses were conducted. There are several inherent conservatisms in this model:

1. The tantalum foil used to package the plutonium metal hollow cylinders inside the T-Ampoule is not modeled. The small quantity of energy it would absorb, and load spreading it would provide, is conservatively ignored. In addition, any initial positioning that would be provided by the foil is also ignored. Each analysis is run with the plutonium metal hollow cylinder in a location farthest from the impact surface.

2. The Pu material is modeled using a power-law hardening constitutive model without fracture. Hecker and Stevens[3] present two curves for alpha-plutonium; one curve depicts a very brittle material, and the other represents a finer-grain material with more ductility. To maximize the energy and impulse load applied to the T-Ampoule wall, the plutonium metal was modeled as a continuously hardening material that does not fracture, which is extremely conservative in terms of the reaction loading of the T-Ampoule. This conservatism (stronger alpha material, continuously hardening) allows for the possibility that the cylinder could also consist of delta Pu, if transport of that material were desired instead.

3. The dimensions of the plutonium metal hollow cylinders are conservatively assumed to be the "strongest" possible. Within the bounds of LANL-defined tolerances of machining these cylinders, they are the most resistant to buckling (shortest, thickest wall,

maximum OD and minimum ID, see Figures 2-70and 2-71), which allows for the greatest loading of the T-Ampoule.

2.12.5.4.2 Run 1 - 831-g Plutonium Metal Hollow Cylinder with Bottom Initial Location and a Top Impact

The top end impact model for the plutonium metal hollow cylinder, oriented axially (with the impact direction, as opposed to angled) is shown in Figure 2-109. Note that the cylinder is located at the bottom of the T-Ampoule so that its net impact velocity with the top of the T-Ampoule is maximized. The post-impact deformation is shown in Figure 2-110 and its kinetic energy history in Figure 2-111. Note the similar degree of overpack crush up as compared to the certification test end impact analysis in Figure 2-12, despite the slightly reduced impact velocity of 422 ft/sec versus the tested 445 ft/sec. The plutonium metal hollow cylinder exhibits significant buckling, despite its conservatively "strongest shape" definition.

Equivalent Plastic Strain (EQPS) in the TB-1 vessel is shown in Figures 2-112 and 2-113 to be less than 2.3%, and only in some localized outer contact regions with the redwood overpack. This localized ring of plasticity in the top outer surface of the TB-1 lid is due to a minor contact over closure between the TB-1 and the redwood; it is only a minor modeling artifact. This minor modeling artifact is not a concern because even though it produces elevated localized stresses and even miniscule plasticity, it does not increase through-thickness stresses or in any way negatively affect the integrity of the containment vessel. The von Mises stresses (see Figures 2-114 and 2-115) peak at 147.5 ksi, just above the elevated-temperature minimum yield strength for the TB-1 of 141 ksi, but more importantly, through-thickness TB-1 stress values are in the less-than-50 ksi range, below yield. The time at which the peak value of the von Mises stress occurs coincides with the peak value of the contact force (summed over the lid area). A plot of this force as a function of time is shown in Figure 2-116. A maximum contact load of 66,000 lbs is applied to the inner surface of the TB-1 lid during the impact, which is below the 108,000 lb preload in the bolts. No T-Ampoule elements exceeded the tested B-W strain locus, and the peak Tearing Parameter value (see Table 2-11, High Velocity (Aircraft) Impact Analyses Peak Tearing Parameter Values, run #1) of 0.0528 was below the critical Tearing Parameter value of 1.012 for Ti-6Al-4V.

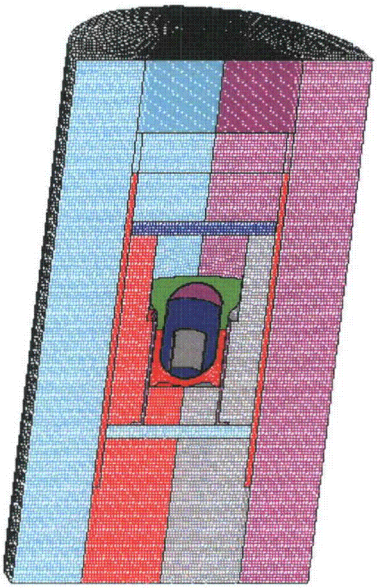

Figure 2-109. Finite Element Mesh for the 831-g, Plutonium Metal Hollow Cylinder, Bottom Position, End Impact

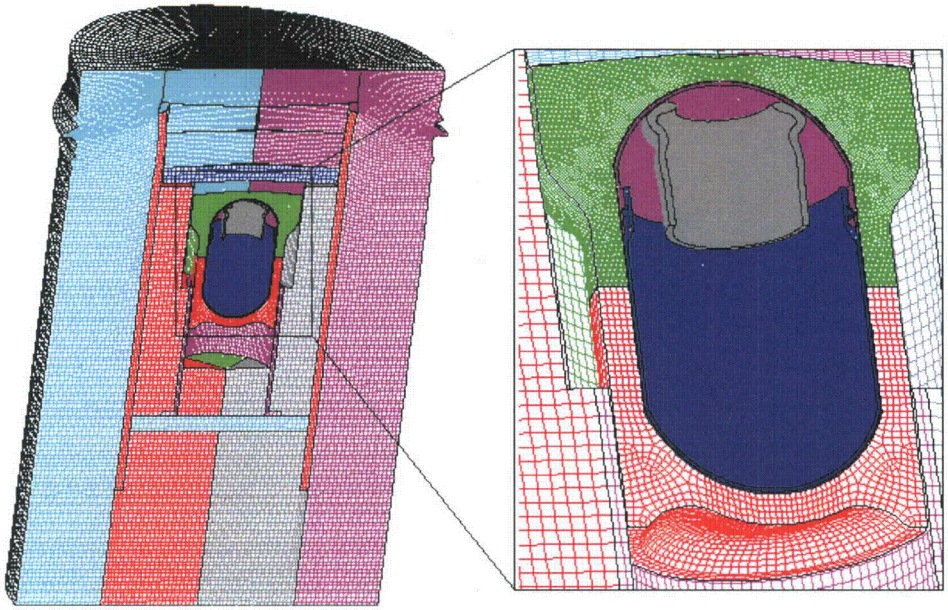

Figure 2-110. Finite Element Mesh for the 831-g, Plutonium Metal Hollow Cylinder, Bottom Position, End Impact – Final Displacement

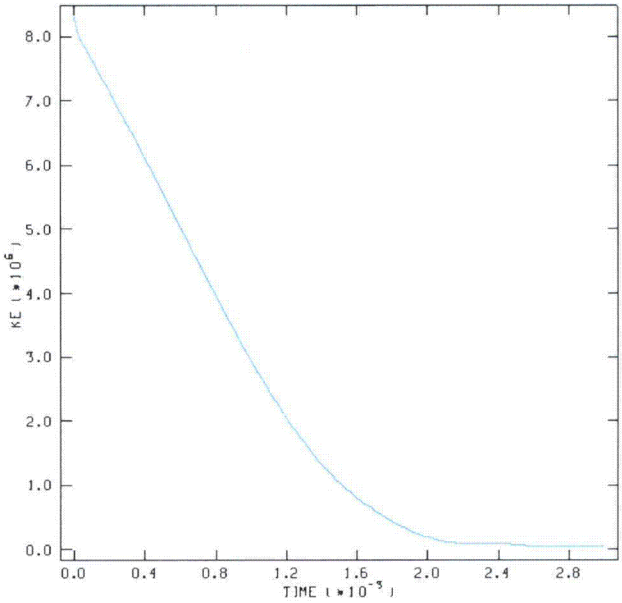

Figure 2-111. Kinetic Energy Time History for the 831-g, ER Cylinder, Bottom Position, End Impact

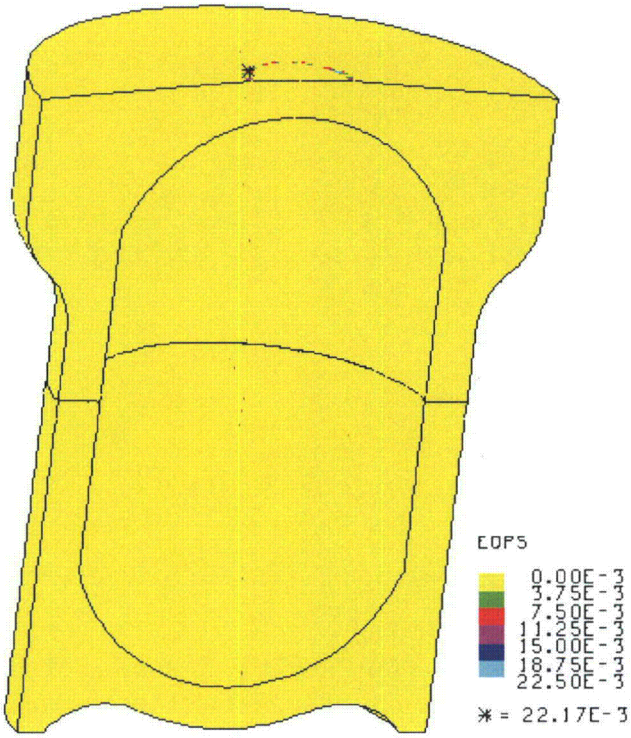

Figure 2-112. EQPS in the TB-1 for the 831-g, ER Cylinder, Bottom Position, End Impact

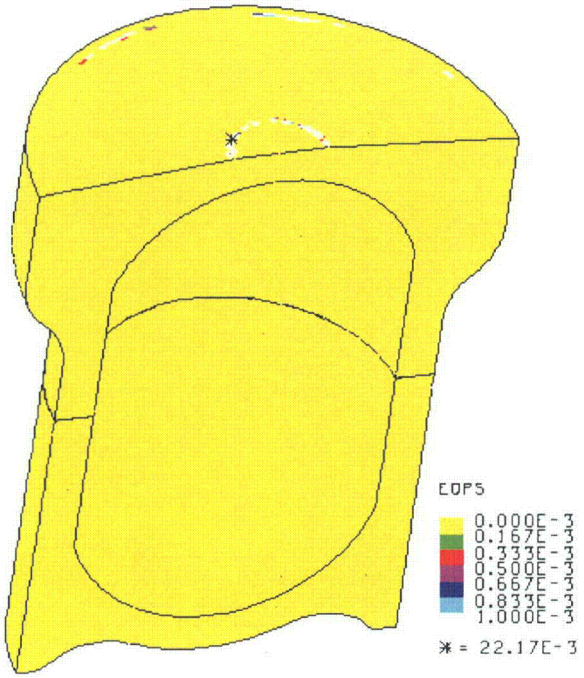

Figure 2-113. EQPS in TB-1 (Range Zoomed in to Show All Elements with non-zero EQPS) for the 831-g, Hollow Cylinder, Bottom Position, End Impact

Figure 2-114. von Mises Stress in the TB-1 for the 831-g Plutonium Metal Hollow Cylinder, Bottom Position, End Impact (Rotated Forward for Ease of Viewing)

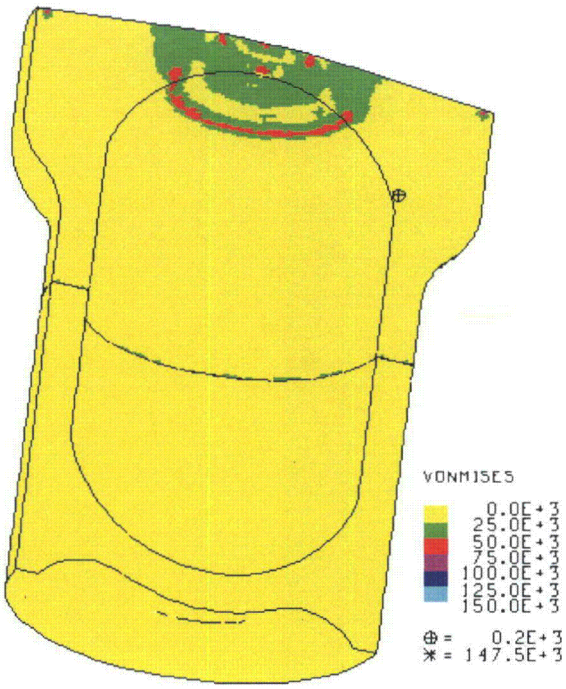

Figure 2-115. von Mises Stress in the TB-1 for the 831-g, Plutonium Metal Hollow Cylinder, Bottom Position, End Impact (Rotated Backward for Ease of Viewing)

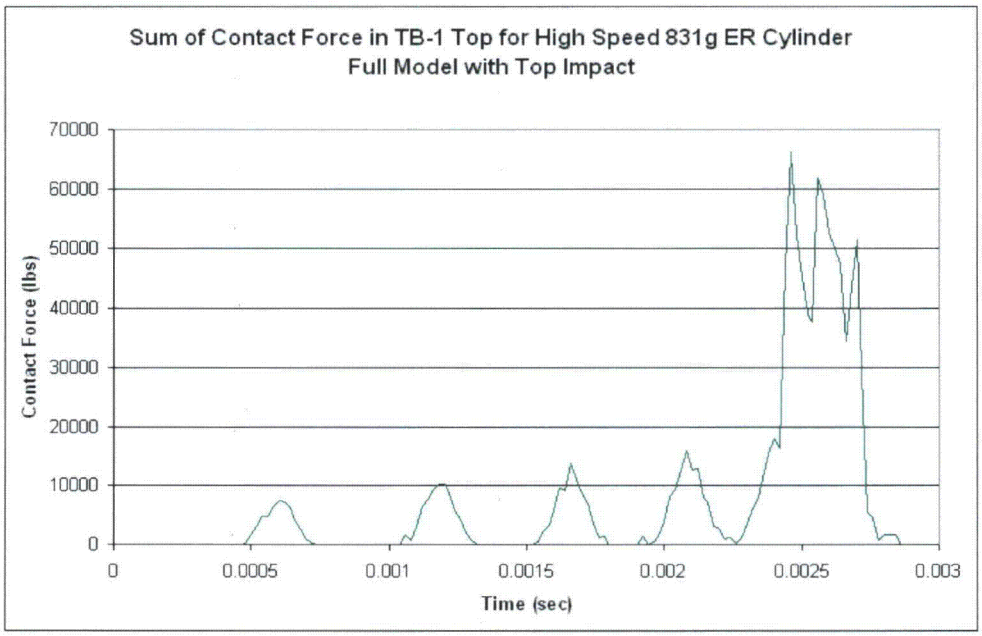

Figure 2-116. Summed Contact Force on the TB-1 Top for a 831-g, Plutonium Metal Hollow Cylinder, Top Impact

2.12.5.4.3 Run 2 - 831-g Angled Cylinder with Bottom Initial Location and a Top Impact

The top end impact model for the plutonium metal hollow cylinder with angled orientation is shown in Figure 2-117. The cylinder is located at the bottom of the T-Ampoule so that its net impact velocity with the top of the T-Ampoule is maximized. The post-impact deformation is shown in Figure 2-118 and its kinetic energy history in Figure 2-119. The plutonium metal hollow cylinder deforms but maintains much of its original shape because of its conservatively assumed "infinitely ductile," with hardening material constitutive model definition (despite its alpha Pu being a relatively brittle material in reality). If the plutonium metal hollow cylinder were modeled as a brittle material with very low ductility, it would effectively shatter and present a much less concentrated load on the T-Ampoule and TB-1.

Average stress-triaxiality versus EQPS is shown in Figures 2-120 and 2-121 for the 19 elements extending beyond the tested Bao-Wierzbicki strain locus. All of these elements are at high stress triaxiality and low EQPS. The Tearing Parameter values for these same 19 elements are shown in Figure 2-122, and all are below the critical Tearing Parameter value of 1.012 for Ti-6Al-4V. These elements are highlighted in red Figure 2-123, but note that these elements are still below even the initiation of a ductile tear.

Peak EQPS in the TB-1 vessel is shown in Figures 2-124 and 2-125 to be about 2.4%, and only in some localized outer contact regions with the redwood overpack (contact modeling artifact). The von Mises stresses (see Figures 2-126 and 2-127) peak at 148.2 ksi, just above the elevated-temperature minimum yield strength for the TB-1 of 141 ksi, but more importantly, through-thickness TB-1 stress values are less than 50 ksi, below yield. The time at which the peak value of the von Mises stress occurs coincides with the peak value of the contact force (summed over the lid area). A plot of this force as a function of time is shown in Figure 2-128. A maximum contact load of 54,509 lbs is applied to the inner surface of the TB-1 lid during the impact.

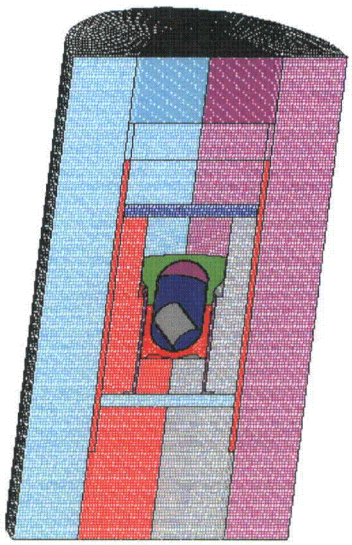

Figure 2-117. Finite Element Mesh for the 831-g, Angled, ER Cylinder, Bottom Position, End Impact

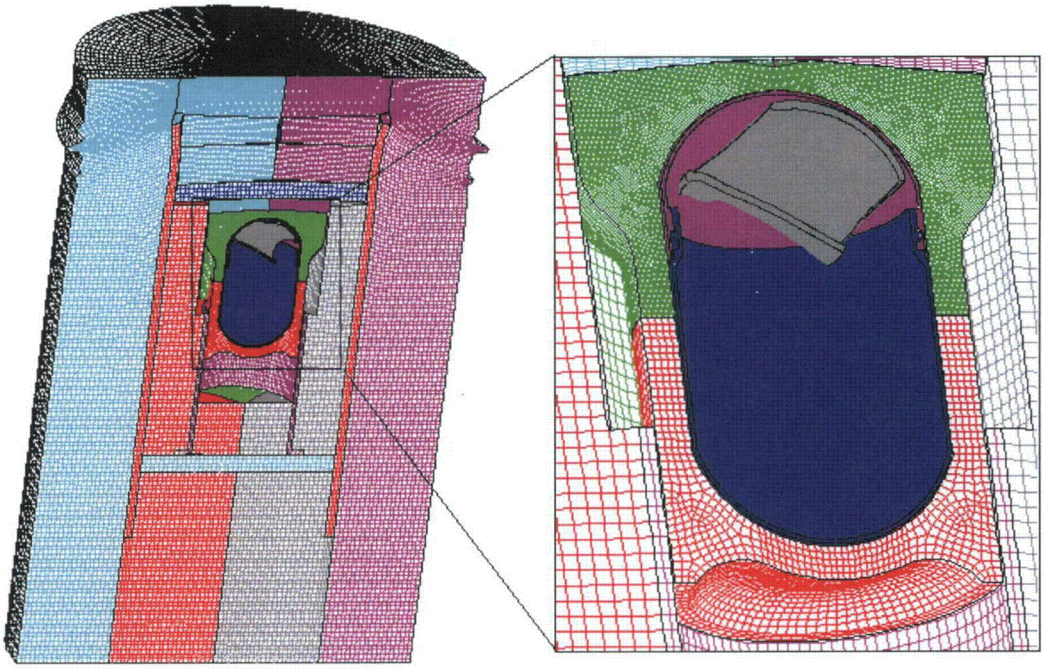

Figure 2-118. Finite Element Mesh for the 831-g, Angled, ER, Cylinder, Bottom Position, End Impact – Final Displacement

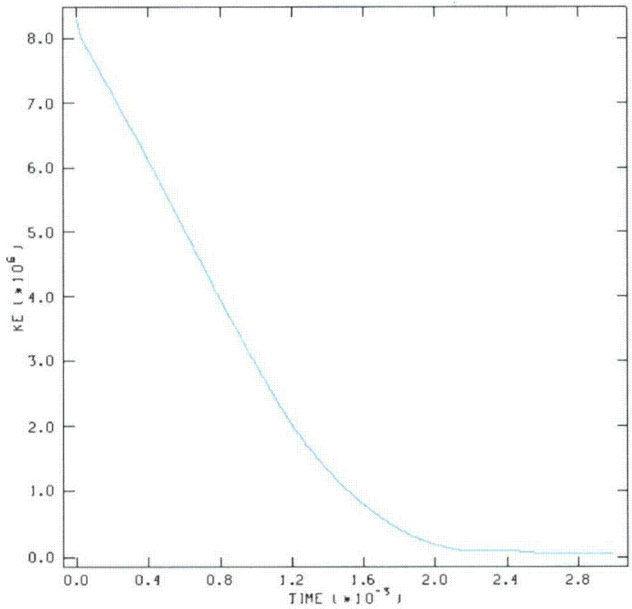

Figure 2-119. Kinetic Energy Time History for the 831-g, Angled, Plutonium Metal Hollow Cylinder, Bottom Position, End Impact

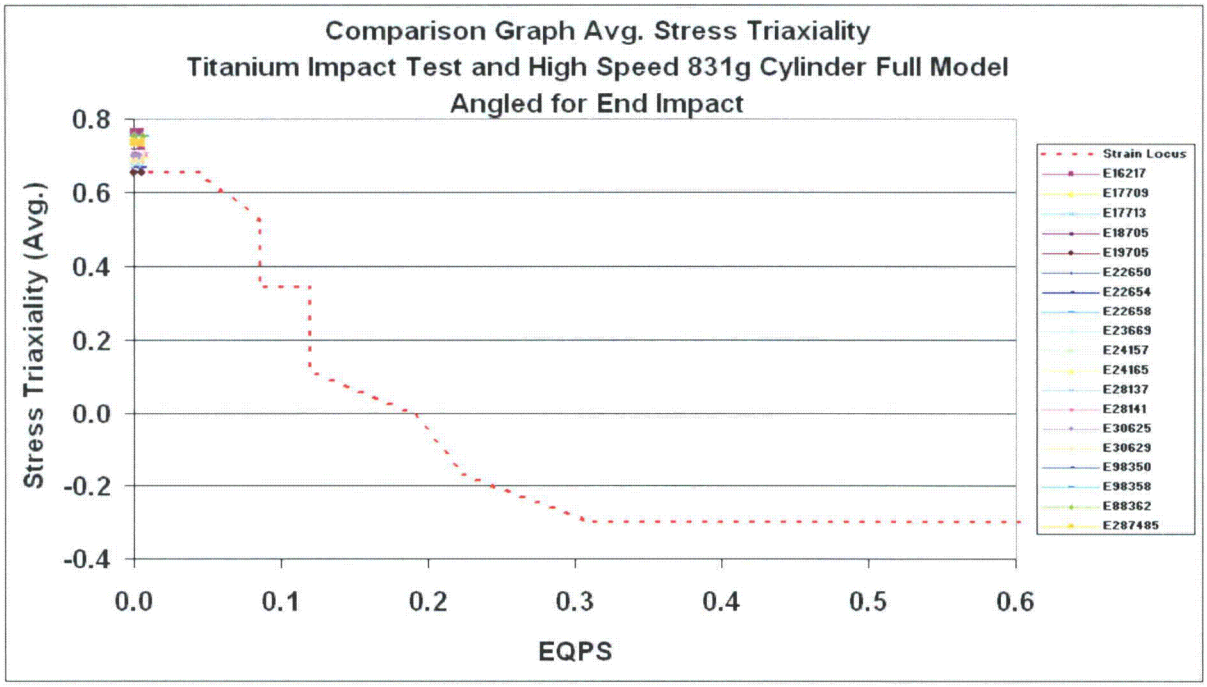

Figure 2-120. Graph of Average Stress Triaxiality versus EQPS of Elements Exceeding the Experimental Strain Locus for the 831-g, Angled, Plutonium Metal Hollow Cylinder, Bottom Position, End Impact

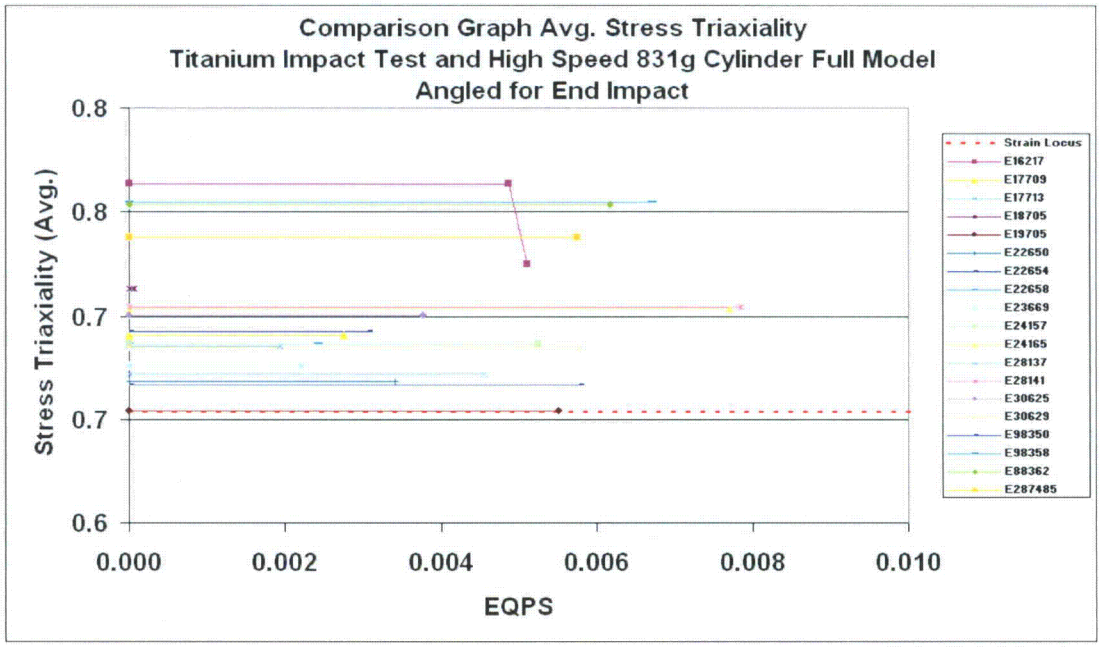

Figure 2-121. Graph of Average Stress Triaxiality versus EQPS of Elements Exceeding the Experimental Strain Locus (Zoomed In) for the 831-g, Angled, Plutonium Metal Hollow Cylinder, Bottom Position, End Impact

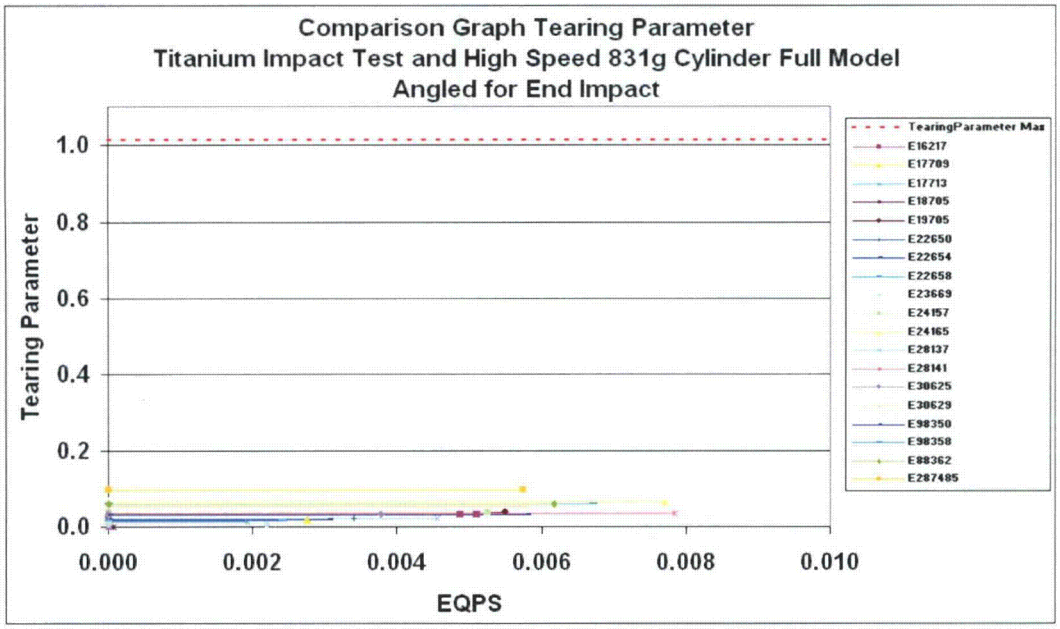

Figure 2-122. Graph of Tearing Parameter versus EQPS for Elements Exceeding the Experimental Strain Locus for the 831-g, Angled, Plutonium Metal Hollow Cylinder, Bottom Position, End Impact

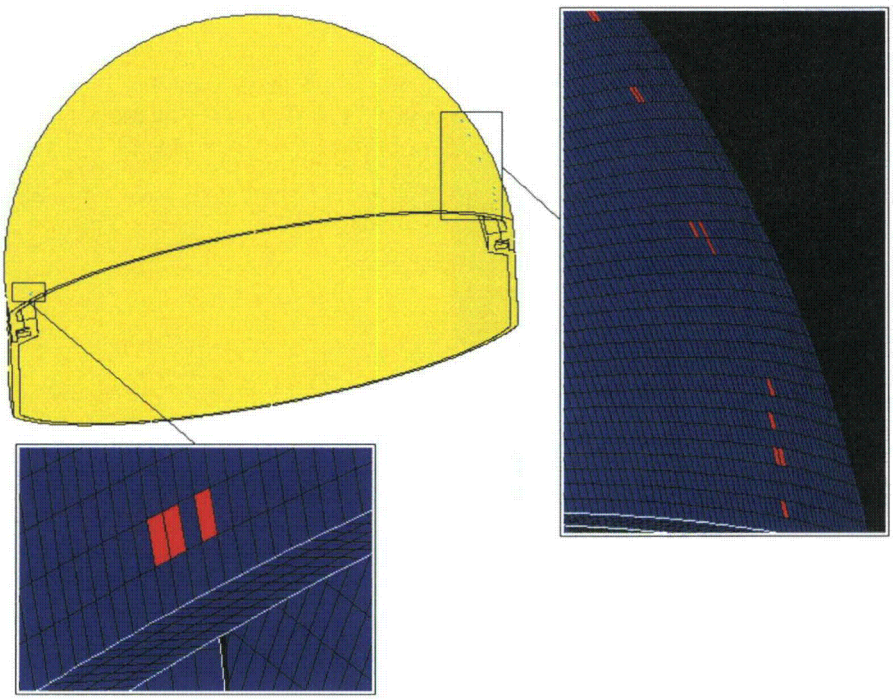

Figure 2-123. Plot of Elements Exceeding the Experimental Strain Locus for the 831-g, Angled, Plutonium Metal Hollow Cylinder, Bottom Position, End Impact

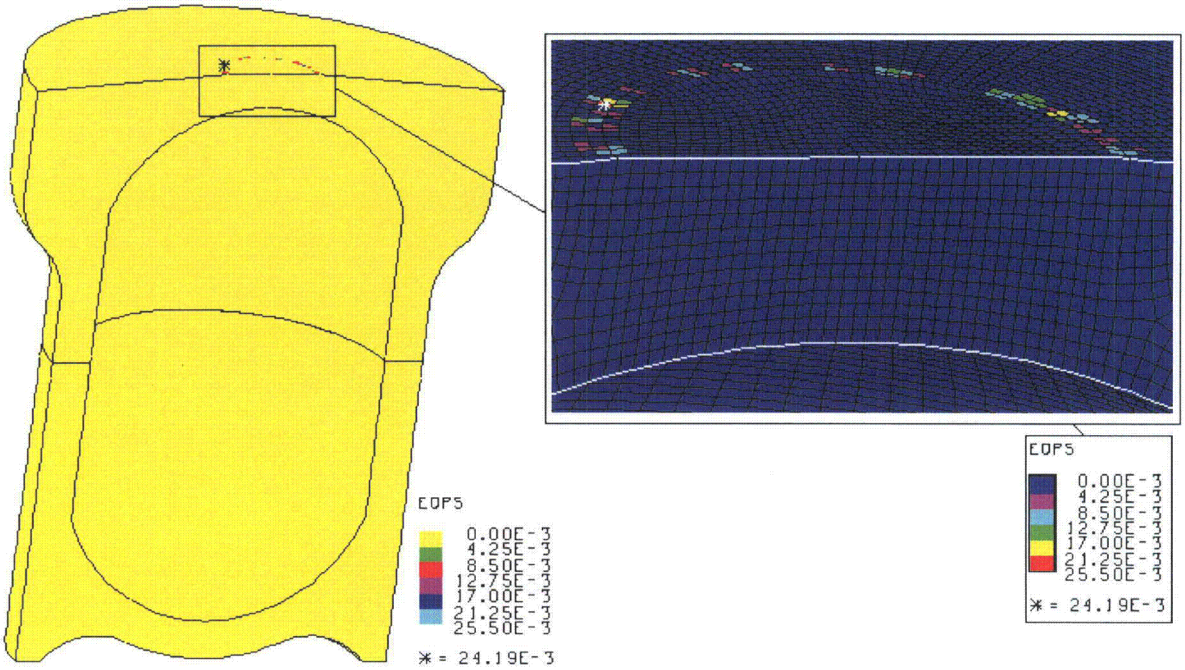

Figure 2-124. Plot of EQPS in the TB-1 for the 831-g Angled, ER, Cylinder, Bottom Position, End Impact

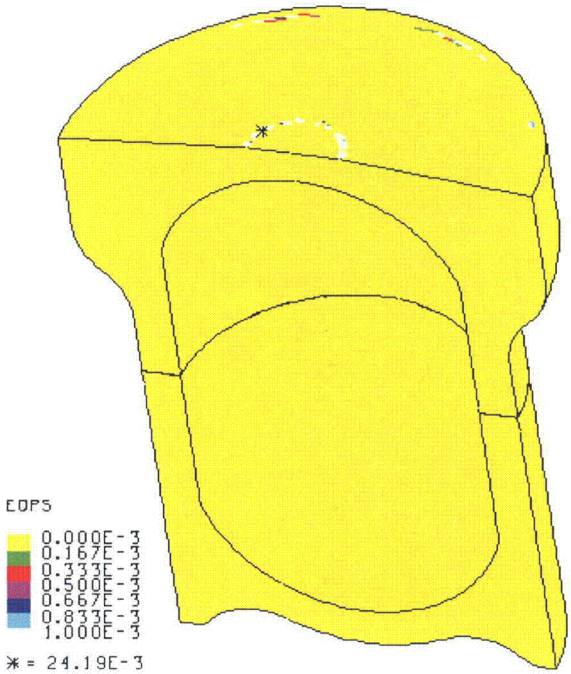

Figure 2-125. Plot of EQPS in the TB-1 (Range Zoomed in to Show all Elements with Non-Zero EQPS) for the 831-g, Angled, Plutonium Metal Hollow Cylinder, Bottom Position, End Impact

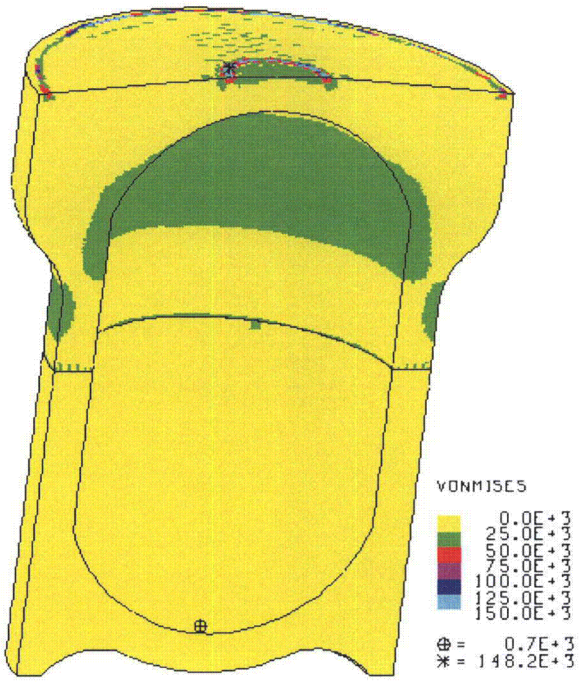

Figure 2-126. Plot of von Mises Stress in the TB-1 for the 831-g, Angled, Plutonium Metal Hollow Cylinder, Bottom Position, End Impact

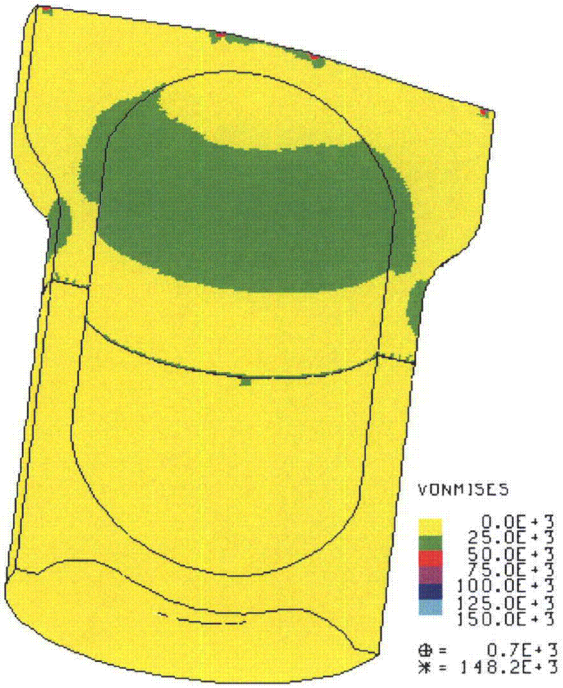

Figure 2-127. Plot of von Mises Stress in the TB-1 for the 831-g, Angled, Plutonium Metal Hollow Cylinder, Bottom Position, End Impact

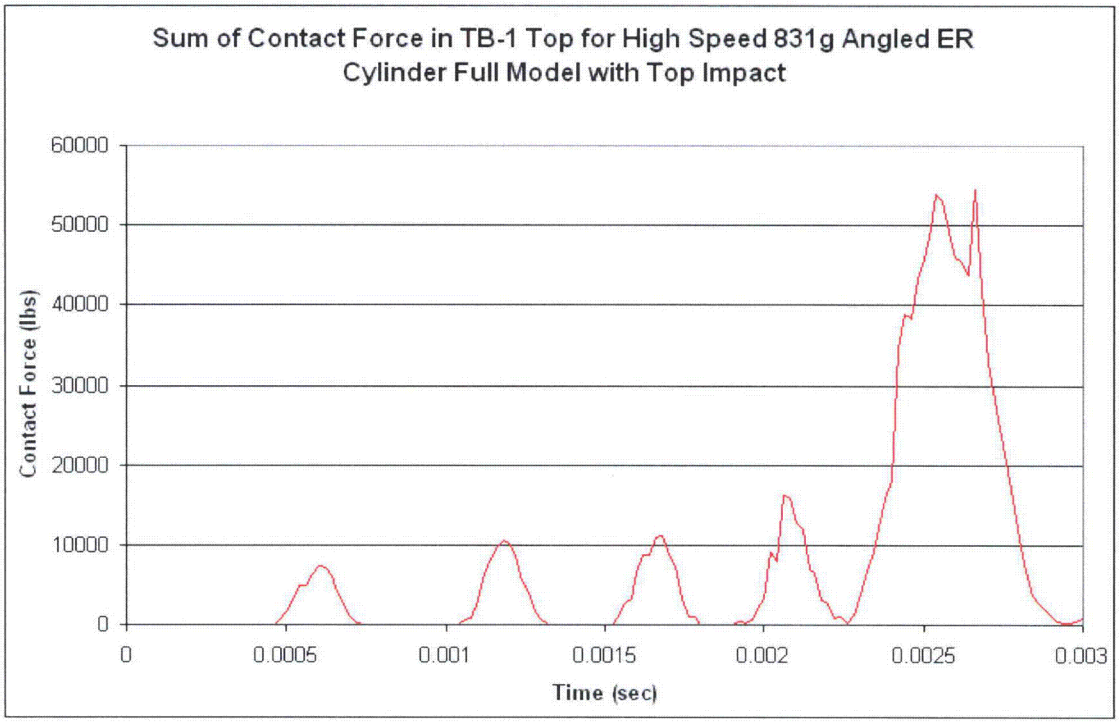

Figure 2-128. Plot of Contact Force in the TB-1 for the 831-g, Angled Plutonium Metal Hollow Cylinder, Bottom Position, End Impact

2.12.5.4.4 Run 3 – 831-g Angled Plutonium Metal Hollow Cylinder with Bottom Initial Location and a CGOC Impact

The lid end CG-over-corner impact model for the plutonium metal hollow cylinder is shown in Figure 2-129. The cylinder is located at the bottom of the T-Ampoule so that its net impact velocity with the top of the T-Ampoule is maximized. The post-impact deformation is shown in Figure 2-130 and its kinetic energy history in Figure 2-131. The plutonium metal hollow cylinder deforms slightly more than the previous case because of the slightly more side-impact-like orientation but maintains much of its original shape because of its conservatively "infinitely ductile" material constitutive model definition. If the plutonium metal hollow cylinder were modeled as a brittle material with very low ductility, it would effectively shatter and present a much less concentrated load on the T-Ampoule and TB-1.

Average stress-triaxiality versus EQPS is shown in Figures 2-132 and 2-133 for the 126 elements extending beyond the tested Bao-Wierzbicki strain locus. All of these elements are at relatively high stress triaxiality and low EQPS. The Tearing Parameter values for these same 126 elements are shown in Figure 2-134 and all are still safely below the critical Tearing Parameter value of 1.012 for Ti-6Al-4V. These elements are highlighted in red in Figures 2-135 through 2-137, but these elements are still below the critical value. Note that this impact analysis case produced the highest value of Tearing Parameter, 0.6177, which still yields a minimum factor of safety of 1.012 divided by 0.6177 equals 1.64 against even the initiation of a ductile tear. With all the analysis conservatisms in the model, the factor of safety is greater, and the T-Ampoule eutectic barrier integrity is maintained.

Peak EQPS in the TB-1 containment vessel is shown in Figures 2-138 and 2-139 to be about 18.5%, although this peak is only in a highly, localized, outer corner region where there is a slight contact over closure issue with the redwood overpack. This is a minor modeling artifact that produces localized plasticity that otherwise would not exist. It occurs when the redwood compresses well into its "lock-up" phase and becomes analytically stiffer than it would realistically be, due to limitations in the orthotropic crush constitutive model of the redwood. Nonetheless, through-thickness plasticity is non-existent and the TB-1 integrity is maintained. The von Mises stresses (see Figure 2-140) peak is 196 ksi (due to the localized redwood contact), above the elevated-temperature minimum yield strength for the TB-1 of 141 ksi, but more importantly, through-thickness TB-1 stress values are less than 35 ksi, below yield.

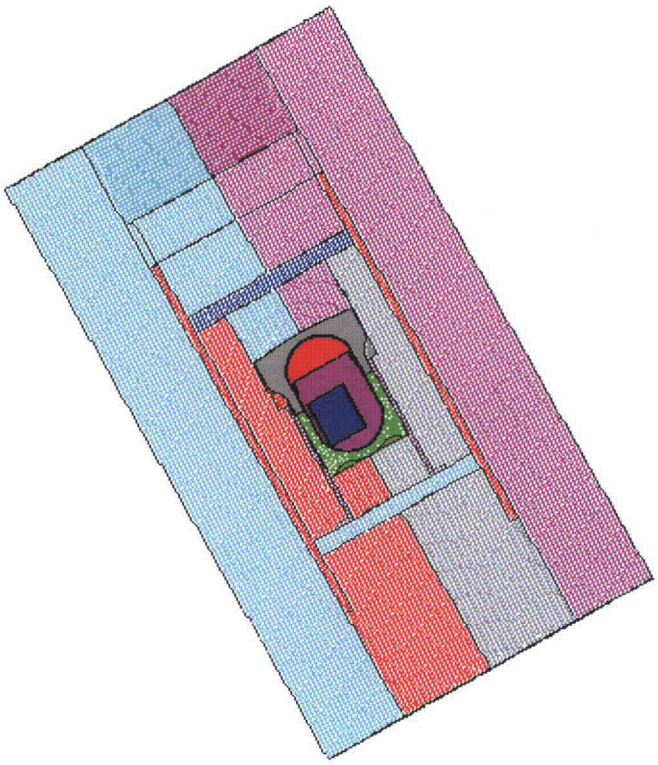

Figure 2-129. Finite Element Mesh for the 831-g, Angled, ER Cylinder, Bottom Position, CGOC Impact

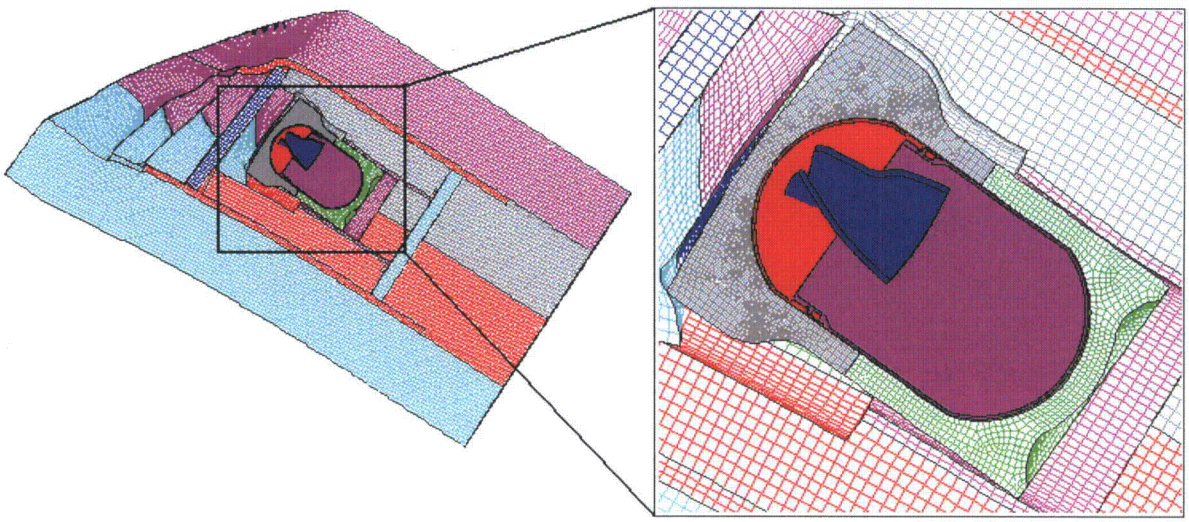

Figure 2-130. Finite Element Mesh for the 831-g, Angled, ER Cylinder, Bottom Position, CGOC Impact – Final Displacement

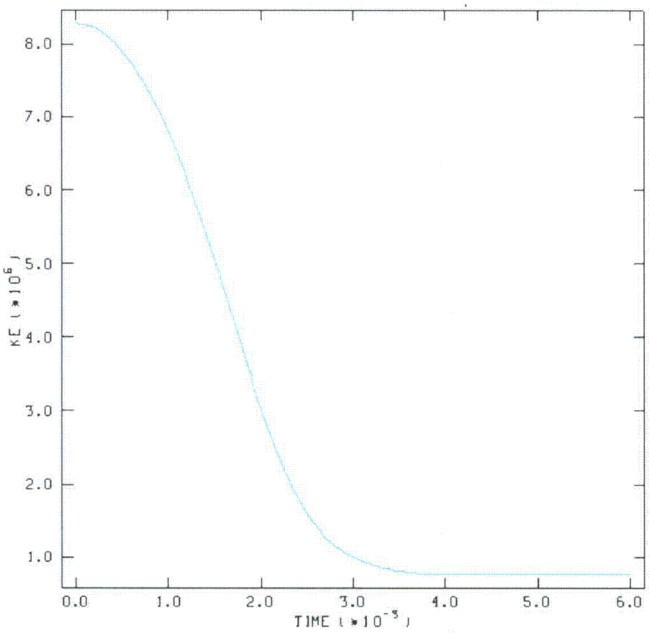

Figure 2-131. Kinetic Energy Time History for the 831-g, Angled, Plutonium Metal Hollow Cylinder, Bottom Position, CGOC Impact

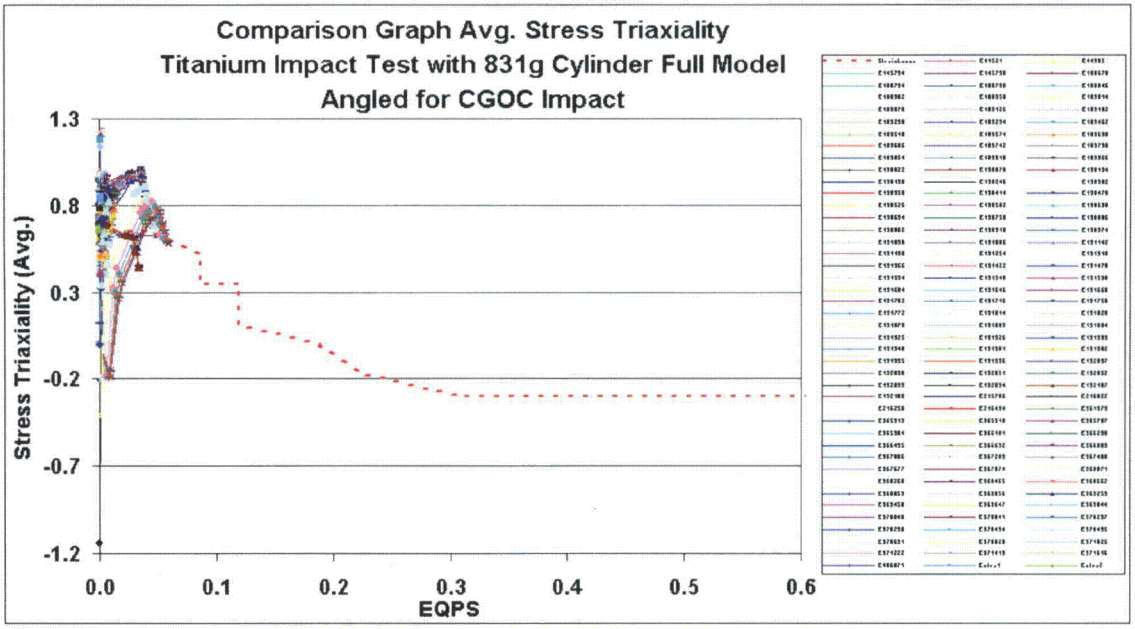

Figure 2-132. Graph of Average Stress Triaxiality versus EQPS of Elements Exceeding the Experimental Strain Locus for the 831-g, Angled, Plutonium Metal Hollow Cylinder, Bottom Position, CGOC Impact

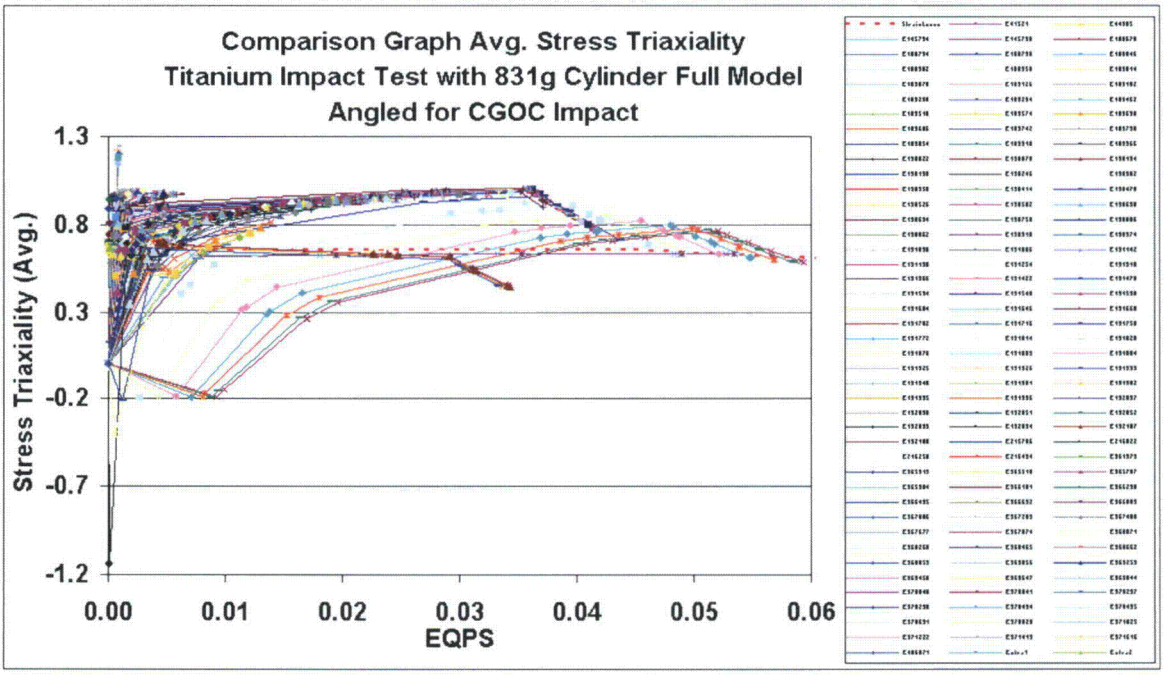

Figure 2-133. Graph of Average Stress Triaxiality versus EQPS of Elements Exceeding the Experimental Strain Locus (Zoomed in) for the 831-g, Angled, Plutonium Metal Hollow Cylinder, Bottom Position, CGOC Impact

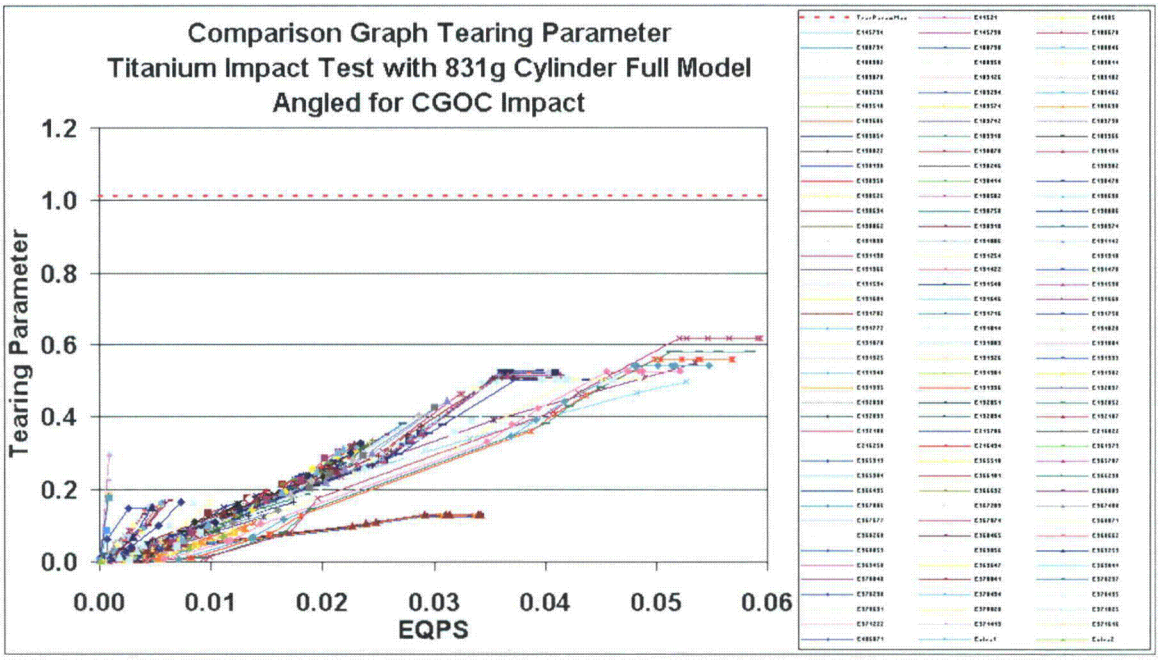

Figure 2-134. Graph of Tearing Parameter versus EQPS of Elements Exceeding the Experimental Strain Locus for the 831-g Angled, Plutonium Metal Hollow Cylinder, Bottom Position, CGOC Impact

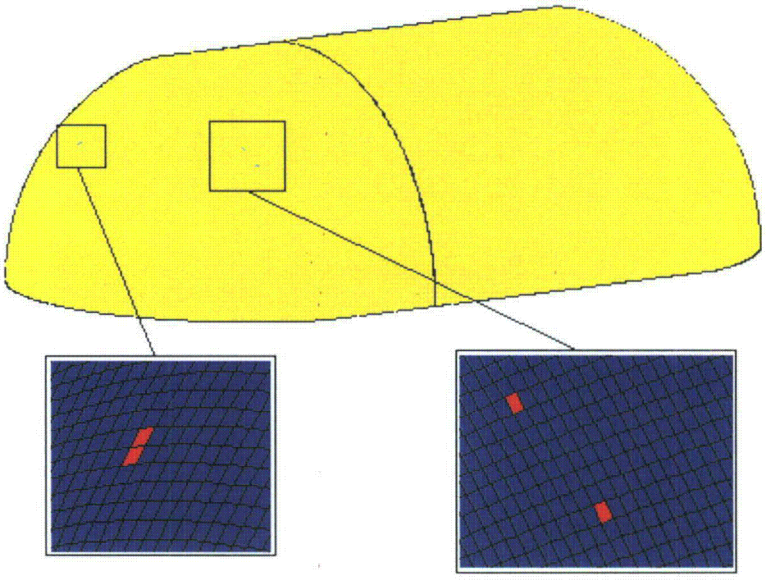

Figure 2-135. Plot of Elements Exceeding the Experimental Strain Locus for the 831-g, Angled, Plutonium Metal Hollow Cylinder, Bottom Position, CGOC Impact

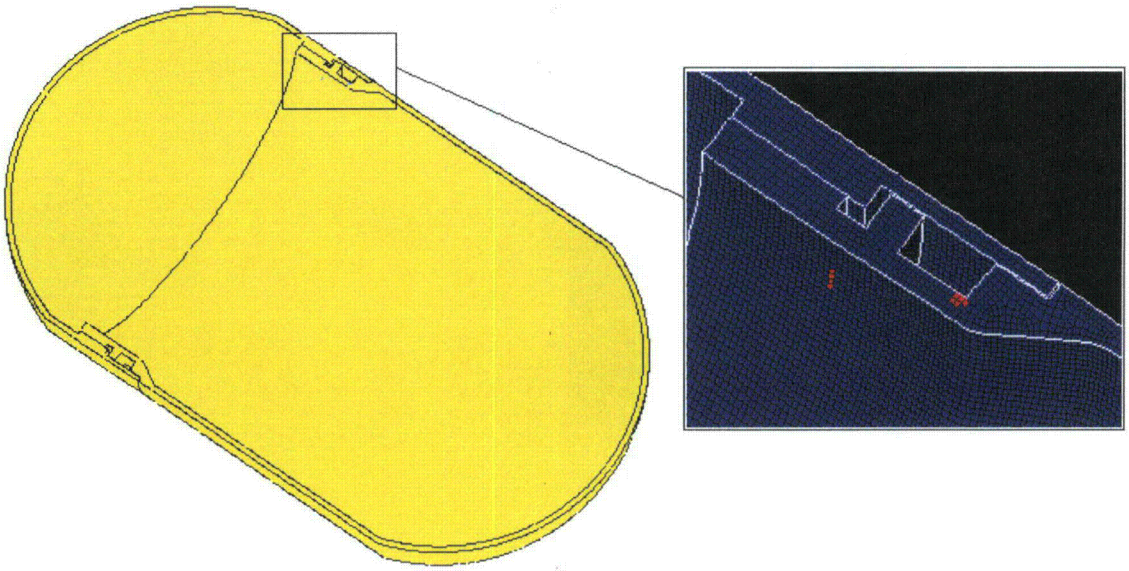

Figure 2-136. Plot of Elements Exceeding the Experimental Strain Locus for the 831-g, Angled, Plutonium Metal Hollow Cylinder, Bottom Position, CGOC Impact

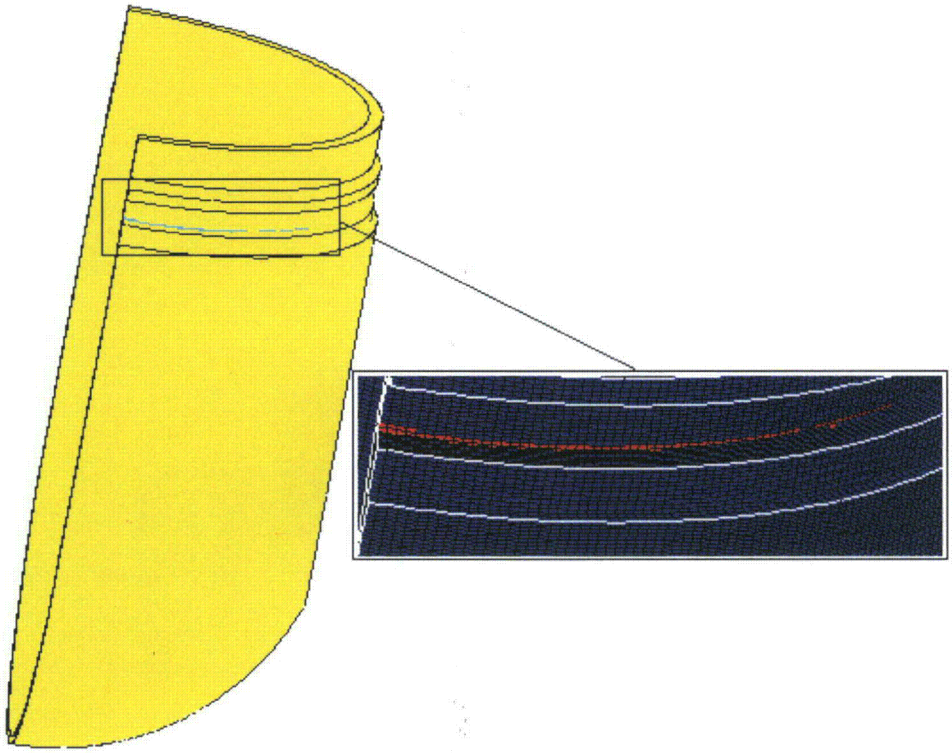

Figure 2-137. Plot of Elements Exceeding the Experimental Strain Locus for the 831-g, Angled, Plutonium Metal Hollow Cylinder, Bottom Position, CGOC Impact

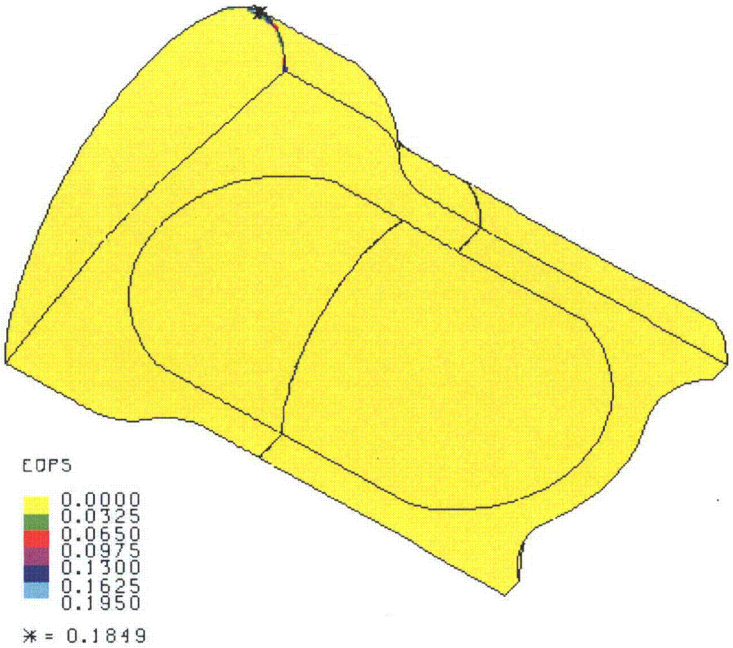

Figure 2-138. Plot of EQPS in the TB-1 for the 831-g, Angled, Plutonium Metal Hollow Cylinder, Bottom Position, CGOC Impact

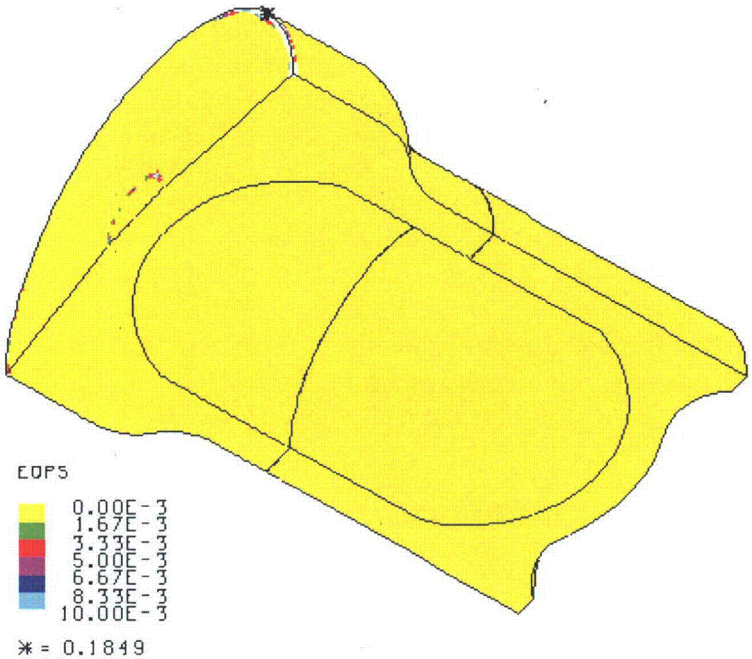

Figure 2-139. Plot of EQPS in the TB-1 for the 831-g, Angled, Plutonium Metal Hollow Cylinder, Bottom Position, CGOC Impact

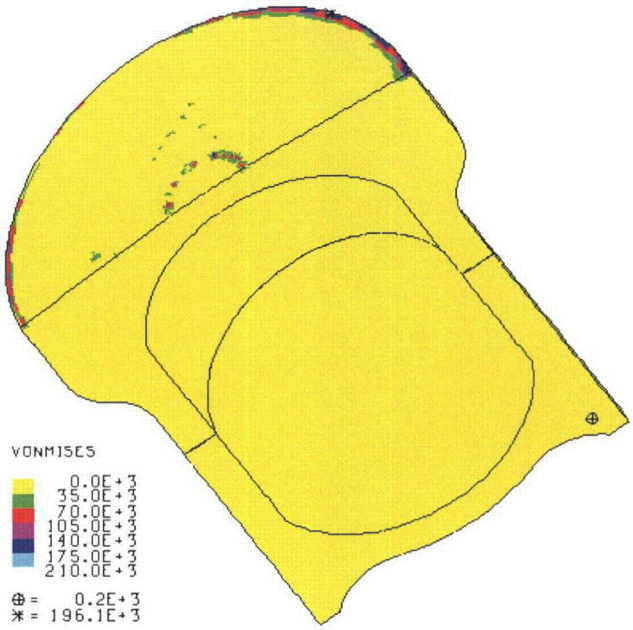

Figure 2-140. Plot of von Mises Stress in the TB-1 for the 831-g, Angled, Plutonium Metal Hollow Cylinder, Bottom Position, CGOC Impact

2.12.5.4.5 Run 4 – 831-g Plutonium Metal Hollow Cylinder Side Impact

The side impact model for the hollow plutonium metal hollow cylinder is shown in Figure 2-141. The cylinder is located at the far side of the T-Ampoule so that its net impact velocity with the side of the T-Ampoule is maximized. The post-impact deformation is shown in Figure 2-142 and its kinetic energy history in Figure 2-143. The plutonium metal hollow cylinder deforms much more than the previous case because of its weaker side-impact orientation.

Average stress-triaxiality versus EQPS is shown in Figures 2-144 and 2-145 for the 67 elements extending beyond the tested Bao-Wierzbicki strain locus. All of these elements are at relatively high stress triaxiality and low EQPS. The Tearing Parameter values for these same 67 elements are shown in Figure 2-146 and all are still below the critical Tearing Parameter value of 1.012 for Ti-6Al-4V. These elements are highlighted in red in Figures 2-147 and 2-148, but these elements are still below the critical value and do not indicate failure; T-Ampoule integrity is maintained.

Peak EQPS in the TB-1 containment vessel is shown in Figures 2-149 and 2-150 to be about 27.4%, although this peak is only in a highly localized outer corner region where there is a slight contact overclosure issue with the redwood overpack. A slight (<1% EQPS) dent is visible in Figure 2-150 from the internal impact of the plutonium metal hollow cylinder with the TB-1 wall (via the T-Ampoule). Through-thickness plasticity is non-existent and the TB-1 integrity is maintained. The von Mises stresses (see Figures 2-151 and 2-152) peak at 222 ksi (due to the localized redwood contact), which is above the elevated-temperature minimum yield strength for the TB-1 of 141 ksi, but more importantly, through-thickness TB-1 stress values are less than 37.5 ksi, below yield.

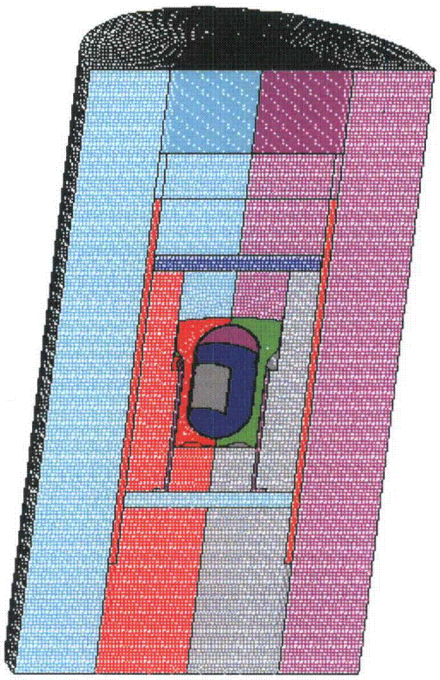

Figure 2-141. Finite Element Mesh for the 831-g, ER, Cylinder, Far Side Position, Side Impact

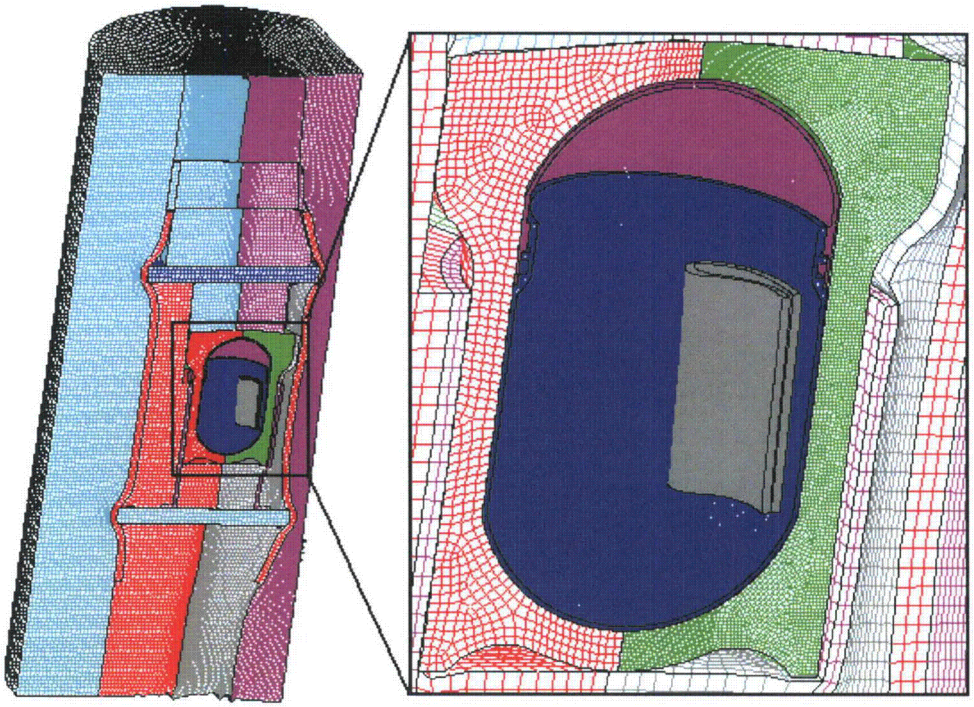

Figure 2-142. Finite Element Mesh for the 831-g, Plutonium Metal Hollow Cylinder, Far Side Position, Side Impact – Final Displacement

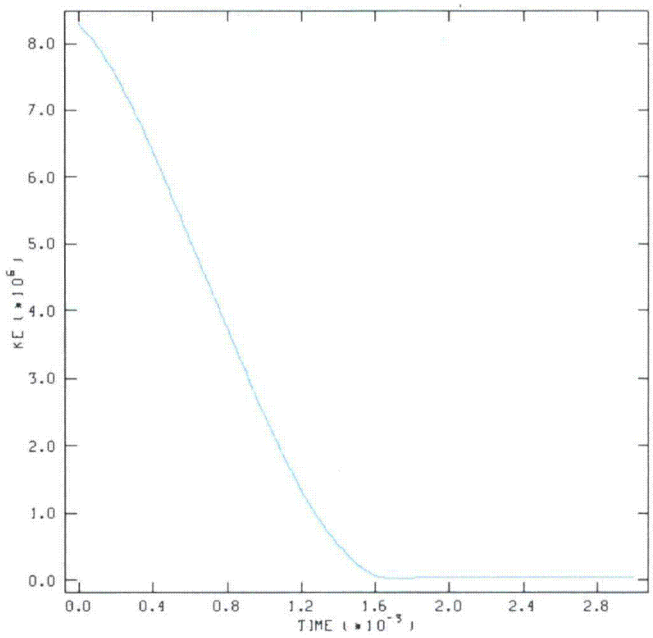

Figure 2-143. Kinetic Energy Time History for the 831-g, ER, Cylinder, Far Side Position, Side Impact

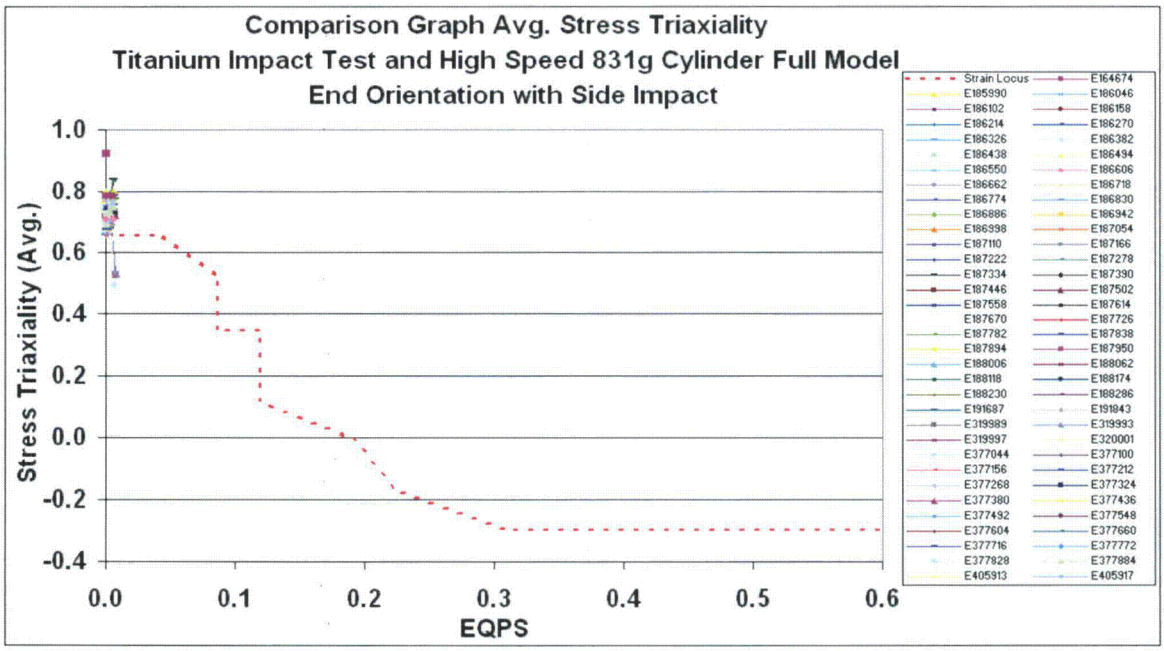

Figure 2-144. Graph of Stress Triaxiality versus EQPS of Elements Exceeding the Experimental Strain Locus for the 831-g, Plutonium Metal Hollow Cylinder, Far Side Position, Side Impact

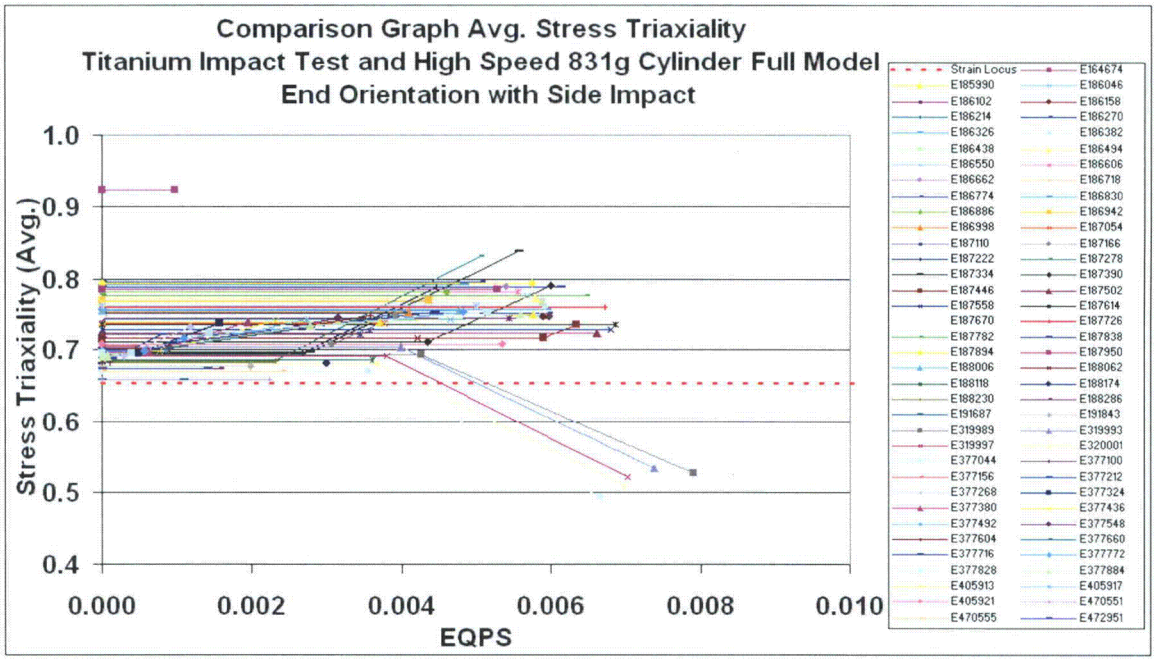

Figure 2-145. Graph of Stress Triaxiality versus EQPS of Elements Exceeding the Experimental Strain Locus (Zoomed In) for the 831-g, Plutonium Metal Hollow Cylinder, Far Side Position, Side Impact

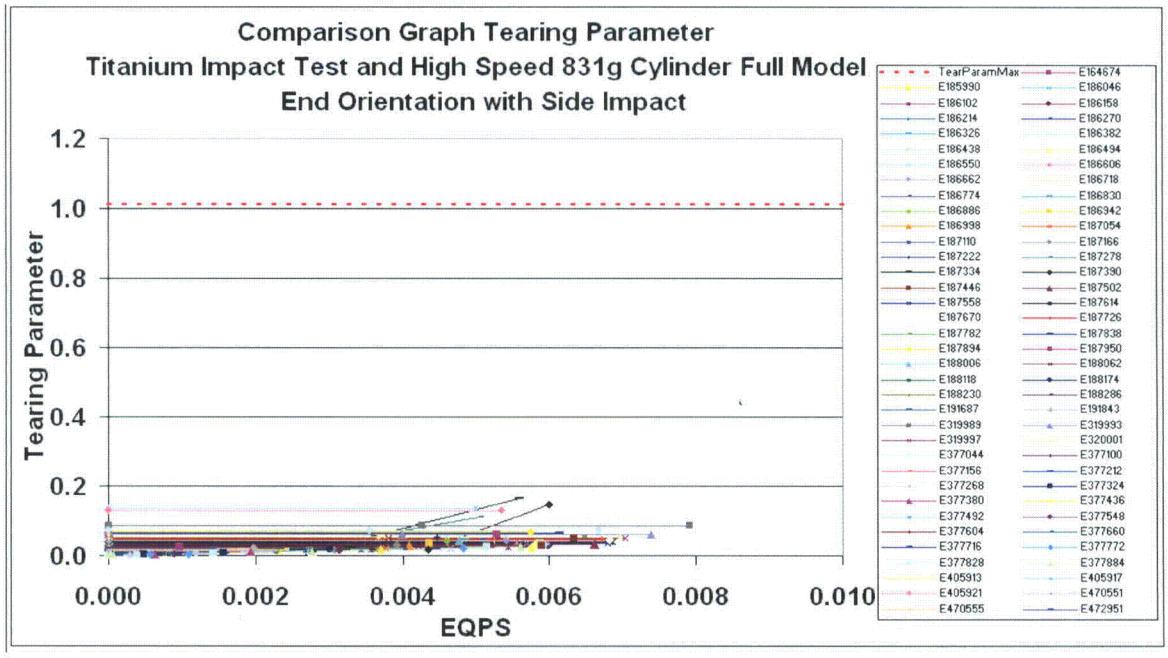

Figure 2-146. Graph of Tearing Parameter versus EQPS of Elements Exceeding the Experimental Strain Locus for the 831-g, Plutonium Metal Hollow Cylinder, Far Side Position, Side Impact

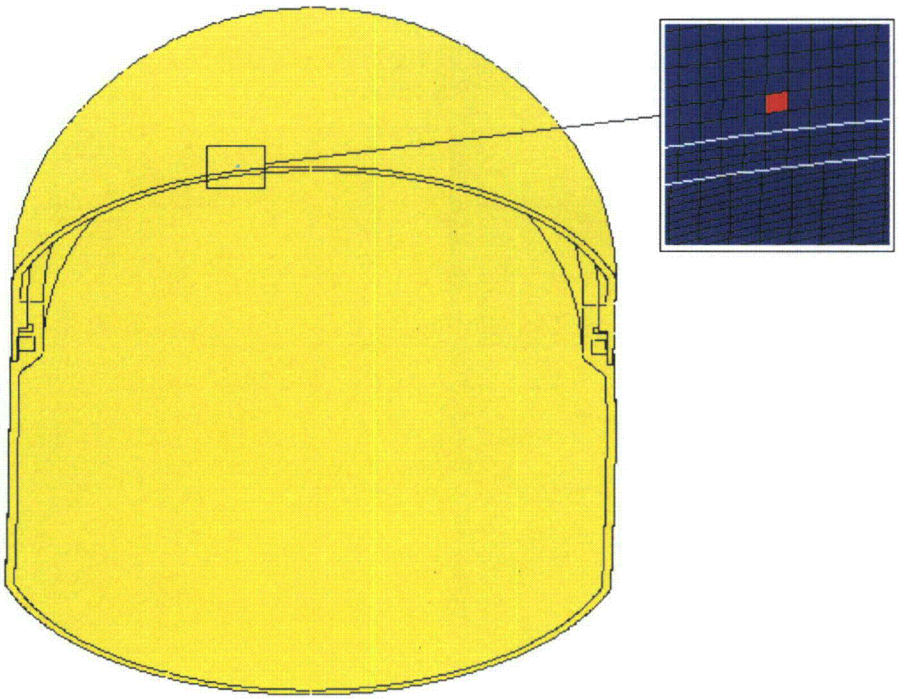

Figure 2-147. Plot of Elements Exceeding the Experimental Strain Locus for the 831-g, Plutonium Metal Hollow Cylinder, Far Side Position, Side Impact

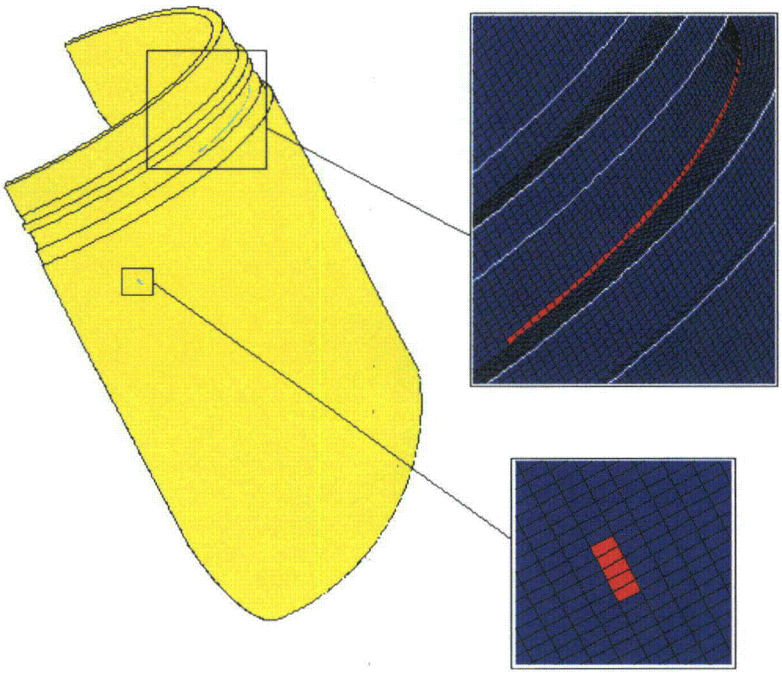

Figure 2-148. Plot of Elements Exceeding the Experimental Strain Locus for the 831-g, Plutonium Metal Hollow Cylinder, Far Side Position, Side Impact

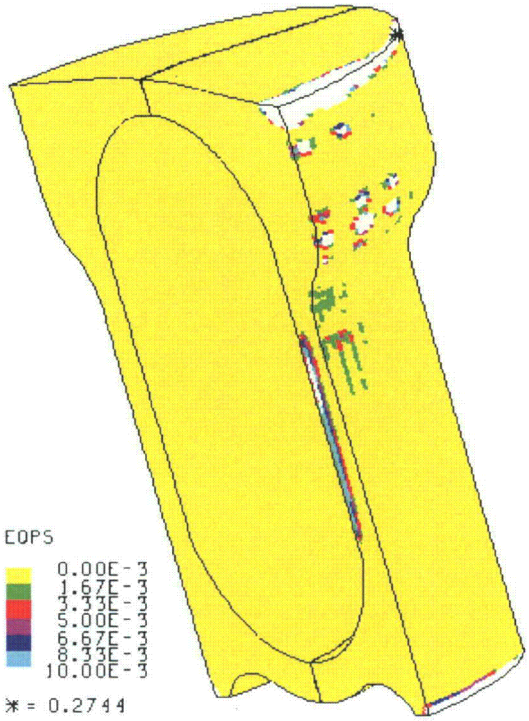

Figure 2-149. Plot of EQPS in the TB-1 for the 831-g, ER, Cylinder, Far Side Position, Side Impact

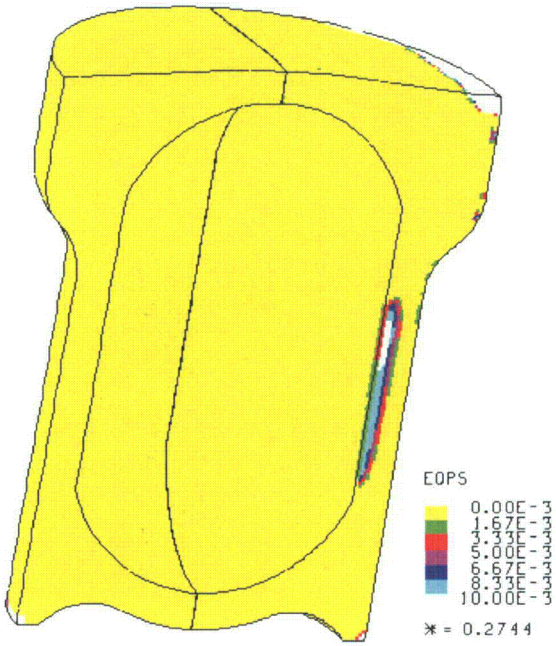

Figure 2-150. Plot of EQPS in the TB-1 for the 831-g, ER Cylinder, Far Side Position, Side Impact

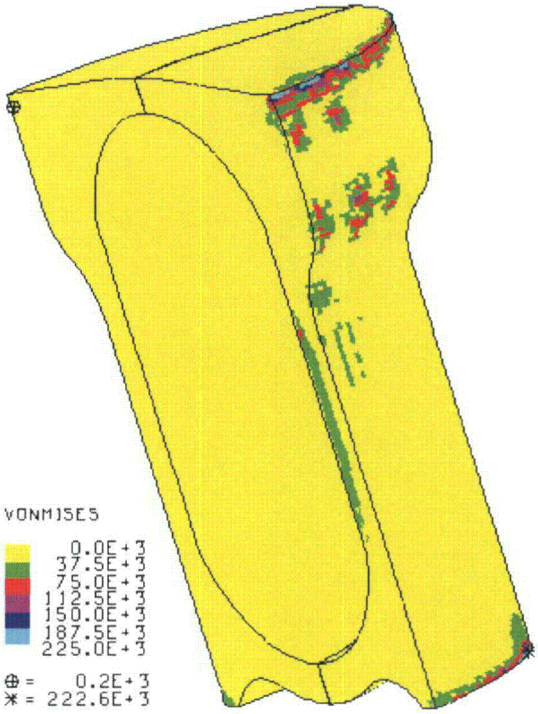

Figure 2-151. Plot of von Mises Stress in the TB-1 for the 831-g, ER Cylinder, Far Side Position, Side Impact

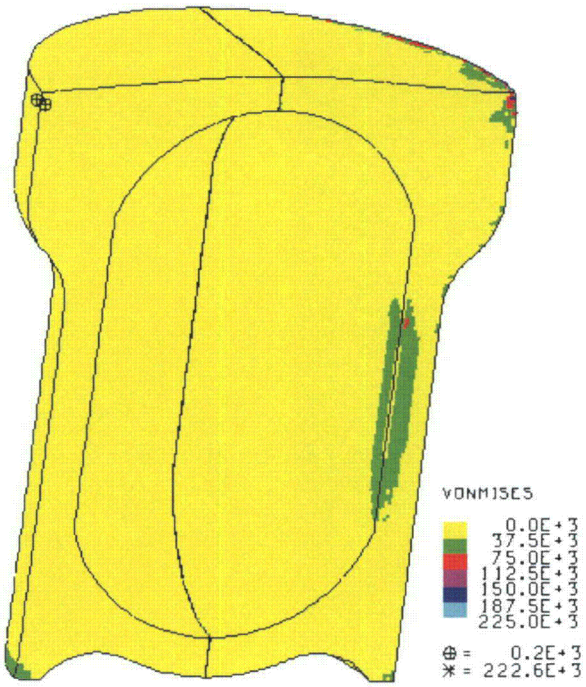

Figure 2-152. Plot of von Mises Stress in the TB-1 for the 831-g, ER, Cylinder, Far Side Position, Side Impact

2.12.5.4.6 Run 5 - 831-g Angled Plutonium Metal Hollow Cylinder Side Impact

The side impact model for the plutonium metal hollow cylinder, angled orientation, is shown in Figure 2-153. The cylinder is located at the far side of the T-Ampoule so that its net impact velocity with the side of the T-Ampoule is maximized, but also angled to present a sharp corner impact with the T-Ampoule surface. The post-impact deformation is shown in Figure 2-154 and its kinetic energy history in Figure 2-155. The plutonium metal hollow cylinder deforms moderately but maintains much of its original shape because of its conservatively "infinitely ductile" material constitutive model definition.

Average stress-triaxiality versus EQPS is shown in Figures 2-156 and 2-157 for the 91 elements extending beyond the tested Bao-Wierzbicki strain locus. All of these elements are at relatively high stress triaxiality and low EQPS. The Tearing Parameter values for these same 91 elements are shown in Figure 2-158, and all are still below the critical Tearing Parameter value of 1.012 for Ti-6Al-4V. These elements are highlighted in red Figure 2-159, but these elements are still below the critical value and do not indicate failure; T-Ampoule integrity is maintained.

Peak EQPS in the TB-1 vessel is shown in Figures 2-160 and 2-161 to be about 26.7%, although this peak is only in a highly localized outer corner region where there is a slight contact overclosure issue with the redwood overpack. Through-thickness plasticity is non-existent and the TB-1 integrity is maintained. The von Mises stresses (see Figures 2-162 and 2-163) peak at 221 ksi (due to the localized redwood contact), which is above the elevated-temperature minimum yield strength for the TB-1 of 141 ksi, but more importantly, through-thickness TB-1 stress values are less than 112.5 ksi, below yield.

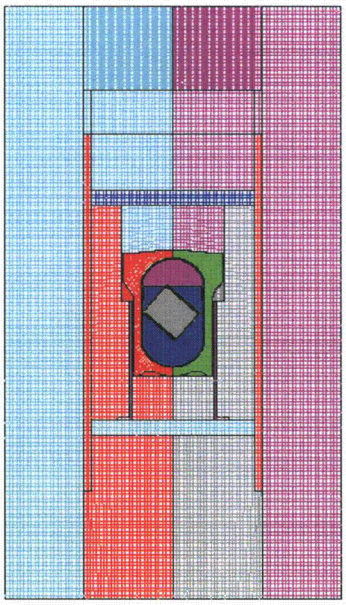

Figure 2-153. Finite Element Mesh for the 831-g, Angled, ER Cylinder, Far Side Position, Side Impact

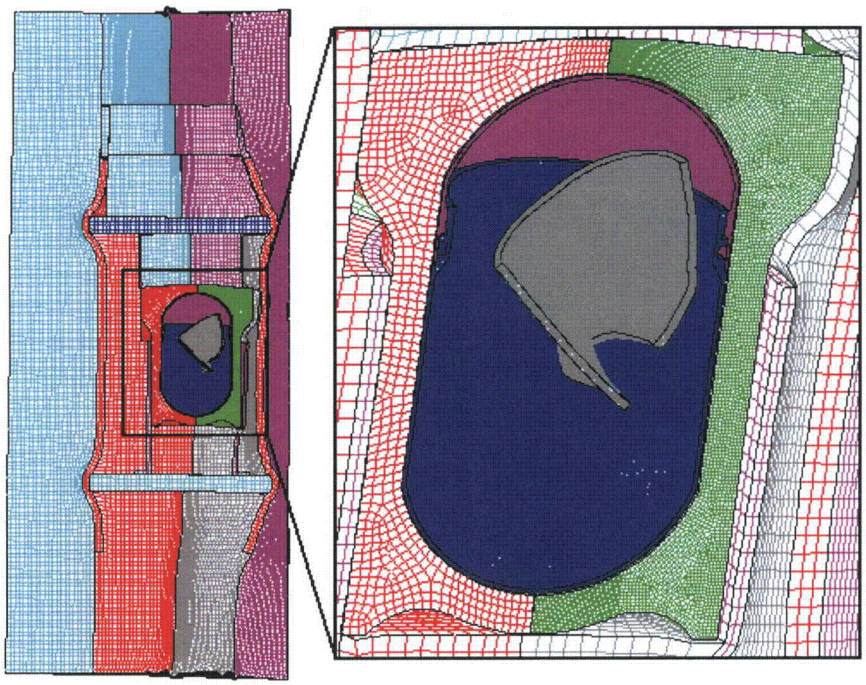

Figure 2-154. Finite Element Mesh for the 831-g, Angled, ER Cylinder, Far Side Position, Side Impact – Final Displacement

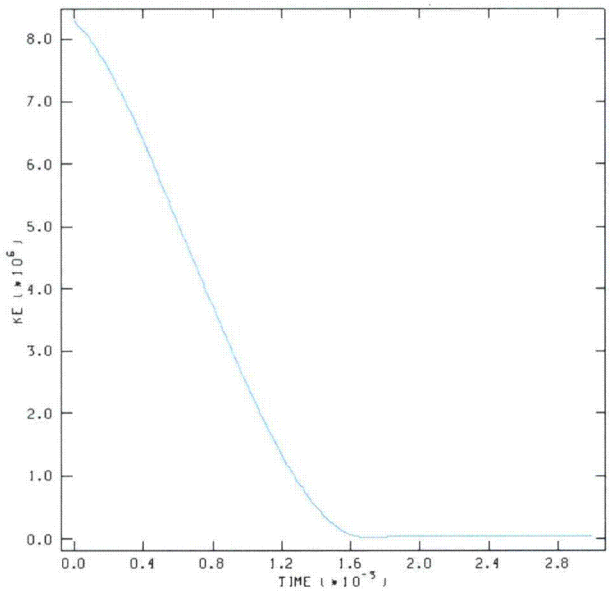

Figure 2-155. Kinetic Energy Time History for the 831-g, Angled, Plutonium Metal Hollow Cylinder, Far Side Position, Side Impact

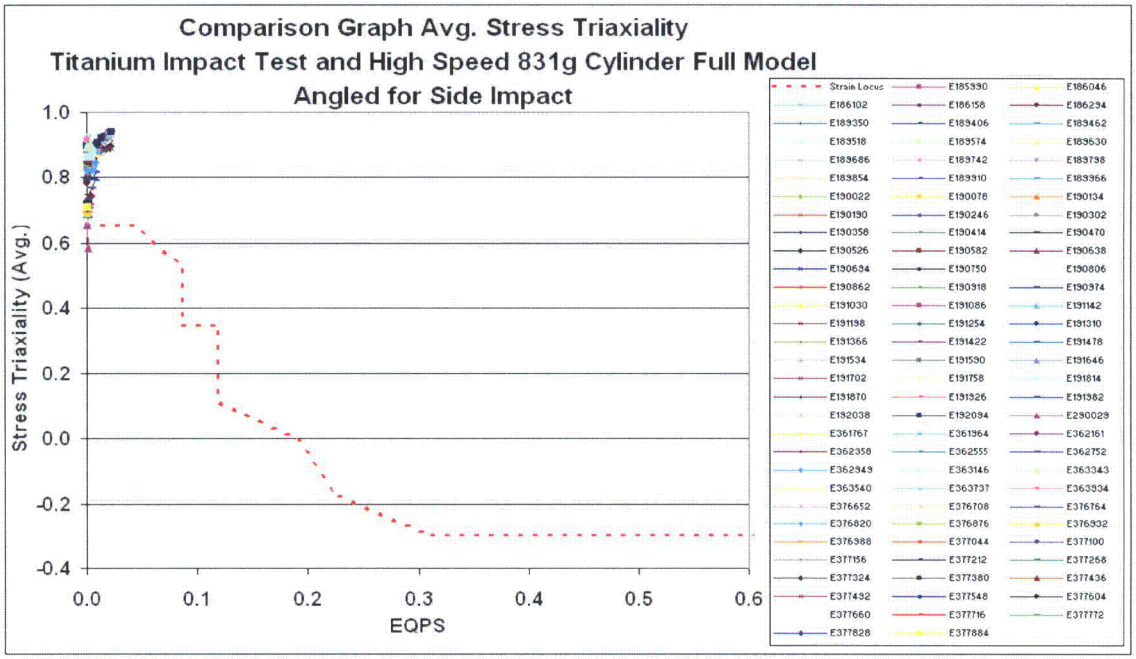

Figure 2-156. Graph of Average Stress Triaxiality versus EQPS of Elements Exceeding the Experimental Strain Locus for the 831-g, Angled, Plutonium Metal Hollow Cylinder, Far Side Position, Side Impact

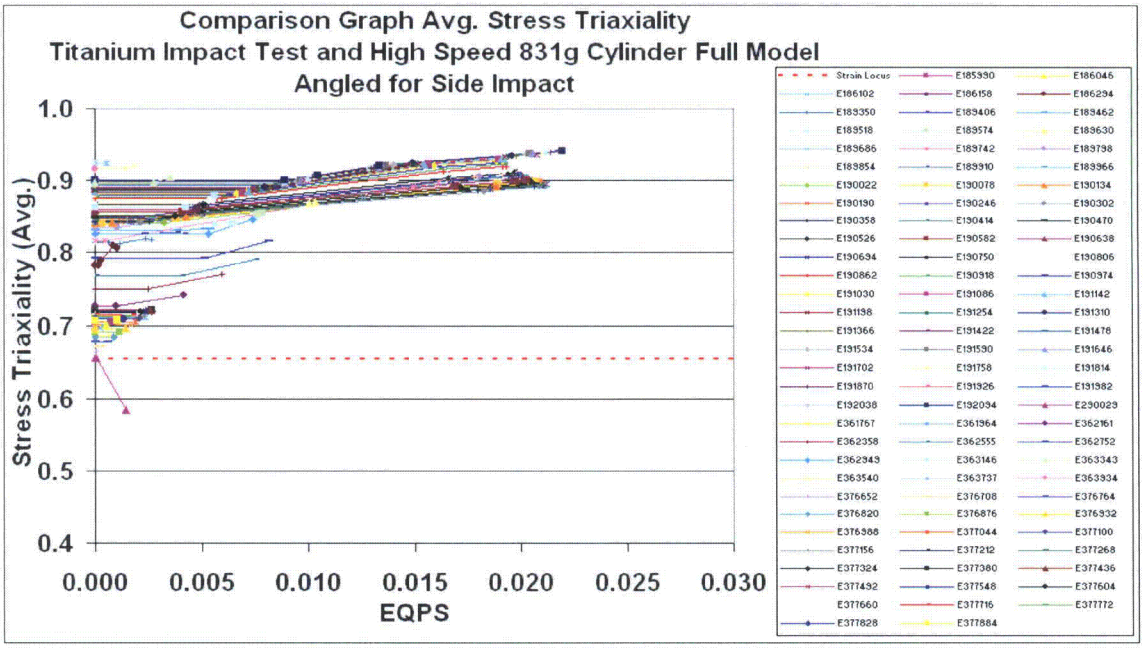

Figure 2-157. Graph of Average Stress Triaxiality versus EQPS of Elements Exceeding the Experimental Strain Locus (Zoomed In) for the 831-g, Angled, Plutonium Metal Hollow Cylinder, Far Side Position, Side Impact

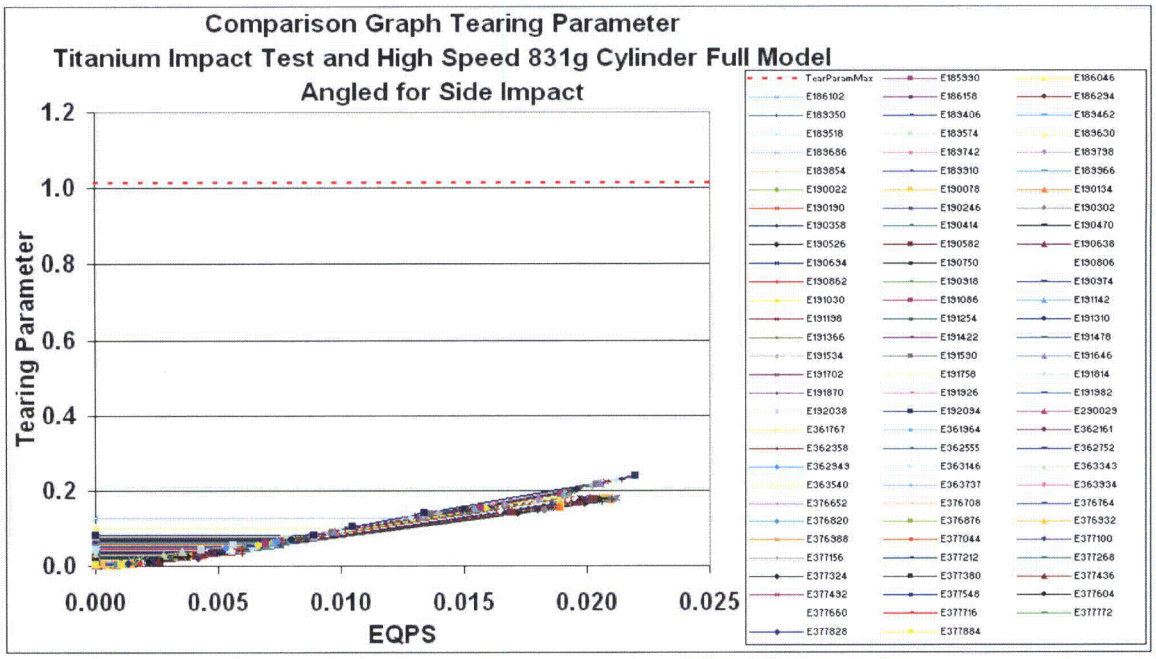

Figure 2-158. Graph of Tearing Parameter versus EQPS of Elements Exceeding the Experimental Strain Locus for the 831-g, Angled, Plutonium Metal Hollow Cylinder, Far Side Position, Side Impact

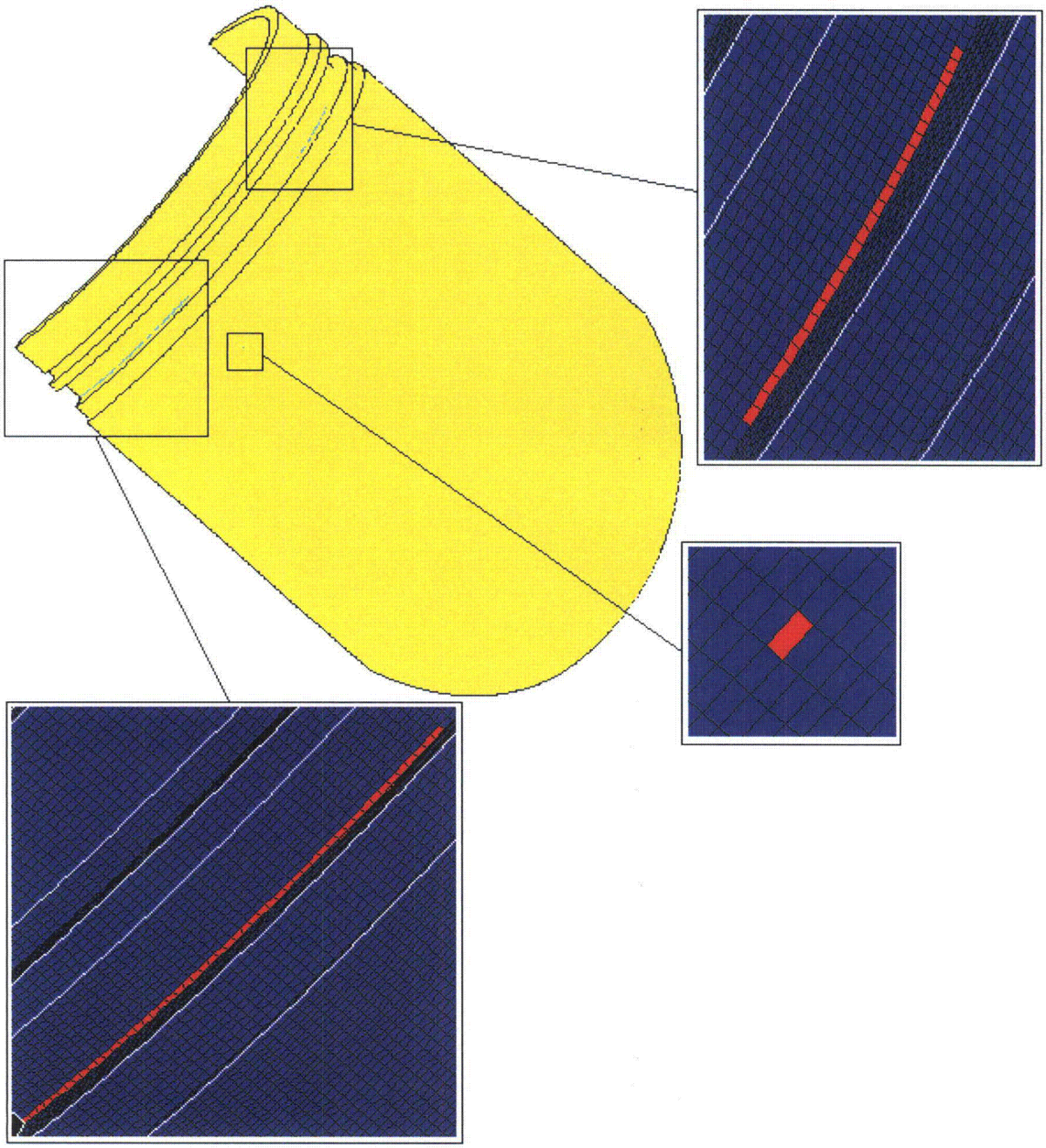

Figure 2-159. Plot of Elements Exceeding the Experimental Strain Locus for the 831-g, Angled, Plutonium Metal Hollow Cylinder, Far Side Position, Side Impact

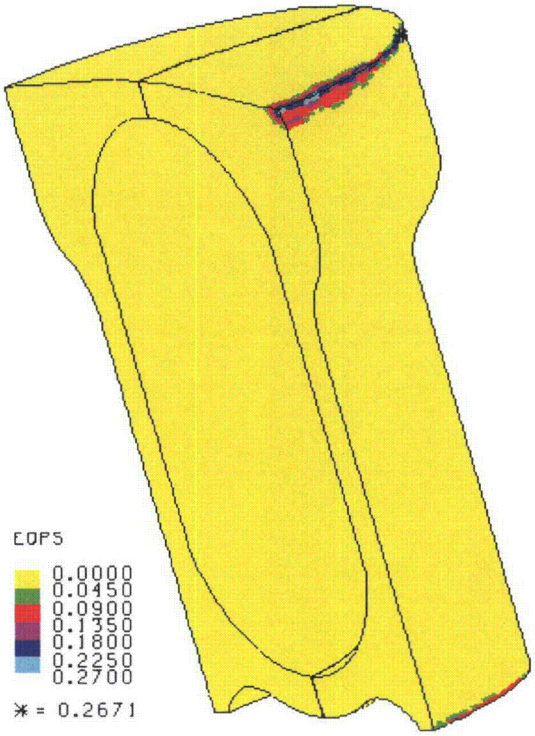

Figure 2-160. Plot of EQPS in the TB-1 for the 831-g, Angled, ER Cylinder, Far Side Position, Side Impact

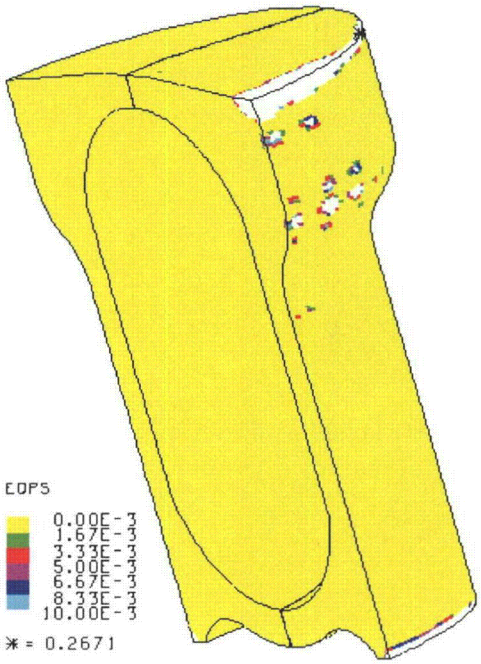

Figure 2-161. Plot of EQPS in the TB-1 for the 831-g, Angled, ER Cylinder, Far Side Position, Side Impact

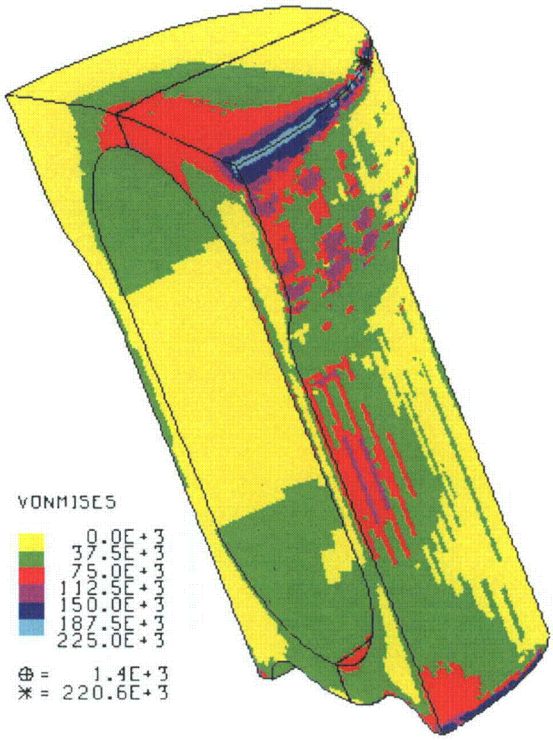

Figure 2-162. Plot of von Mises Stress in the TB-1 for the 831-g, Angled, Plutonium Metal Hollow Cylinder, Far Side Position, Side Impact

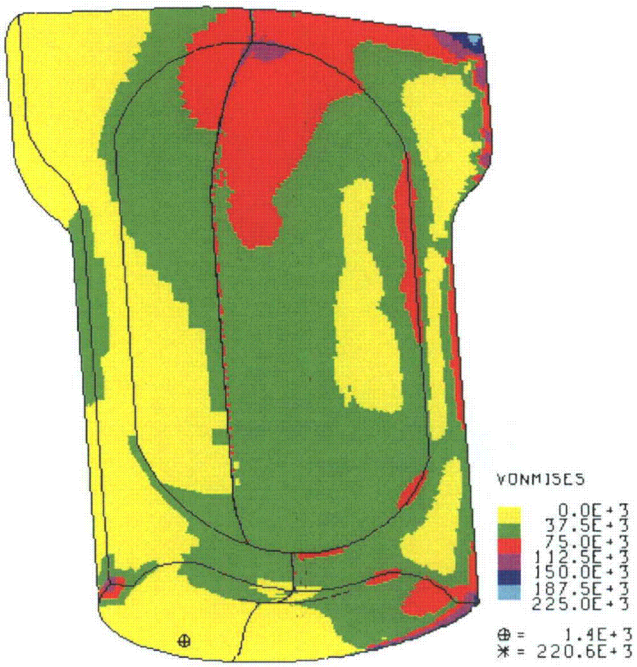

Figure 2-163. Plot of von Mises Stress in the TB-1 for the 831-g, Angled, Plutonium Metal Hollow Cylinder, Far Side Position, Side Impact

2.12.5.4.7 Run 6 - 731-g Plutonium Metal Hollow Cylinder Top Impact

The top end impact model for the slightly smaller (731 g) plutonium metal hollow cylinder, oriented axially (with the impact direction, as opposed to angled) is shown in Figure 2-164. Note that the cylinder is located at the bottom of the T-Ampoule so that its net impact velocity with the top of the T-Ampoule is maximized. The post-impact deformation is shown in Figure 2-165 and its kinetic energy history in Figure 2-166. This slightly shorter plutonium metal hollow cylinder still exhibits buckling, despite its conservatively "strongest shape" definition.

Equivalent Plastic Strain (EQPS) in the TB-1 vessel is shown in Figure 2-167 to be less than 2.7%, and only in some localized outer contact regions with the redwood overpack. The von Mises stresses (see Figures 2-168 and 2-169) peak at 148.5 ksi, is just above the elevated-temperature minimum yield strength for the TB-1 of 141 ksi, but more importantly, through-thickness TB-1 stress values are in the less-than-25 ksi range, below yield. The time at which the peak value of the von Mises stress occurs coincides with the peak value of the contact force (summed over the lid area). A plot of this force as a function of time is shown in Figure 2-170. A maximum contact load of 66,273 lbs is applied to the inner surface of the TB-1 lid during the impact. No T-Ampoule elements exceeded the tested B-W strain locus, and the peak Tearing Parameter value (see Table 2-11, run #6) of 0.1507 was below the critical Tearing Parameter value of 1.012 for Ti-6Al-4V. Note that the peak Tearing Parameter value for the T-Ampoule in this 731 g, plutonium metal hollow cylinder impact case is slightly larger than that of the 831 g cylinder impact, because the shorter plutonium metal hollow cylinder has a slightly higher net impact velocity with the T-Ampoule.

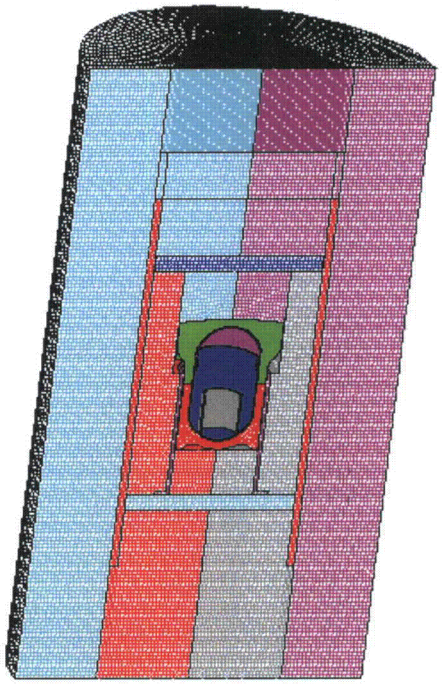

Figure 2-164. Finite Element Mesh for the 731-g, ER, Cylinder, Bottom Position, Top Impact

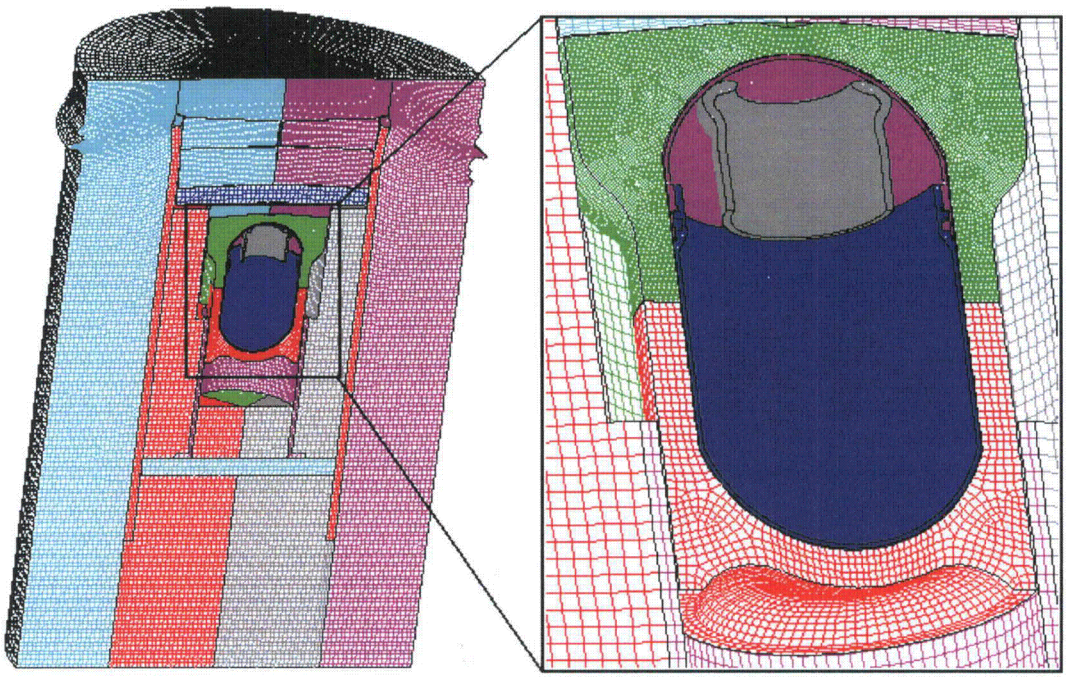

Figure 2-165. Finite Element Mesh for the 731-g, ER, Cylinder, Bottom Position, Top Impact – Final Displacement

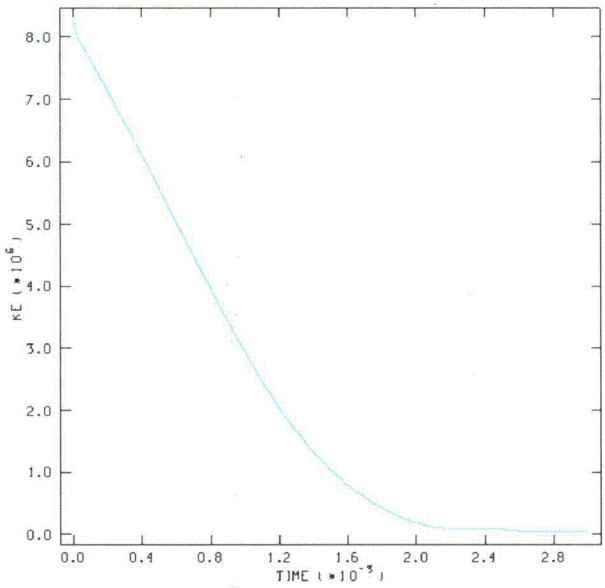

Figure 2-166. Kinetic Energy Time History for the 731-g, ER, Cylinder, Bottom Position, Top Impact

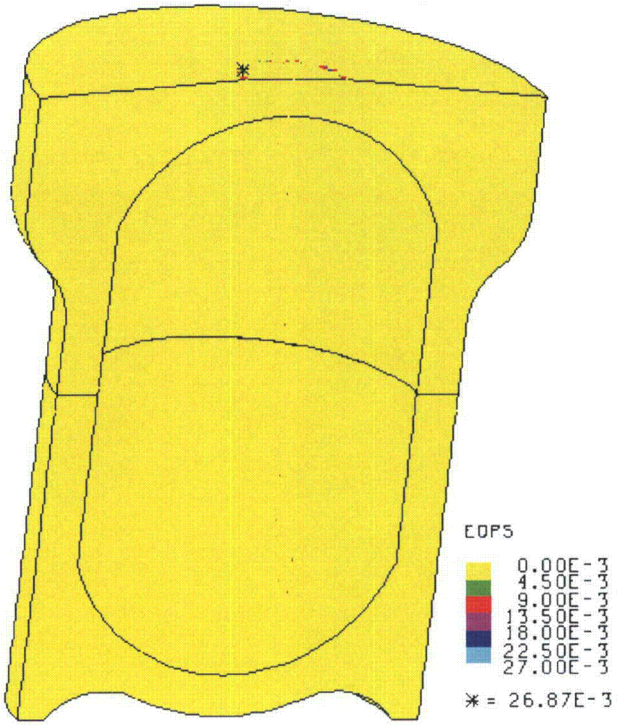

Figure 2-167. EQPS in the TB-1 for the 731-g, Plutonium Metal Hollow Cylinder, Bottom Position, Top Impact

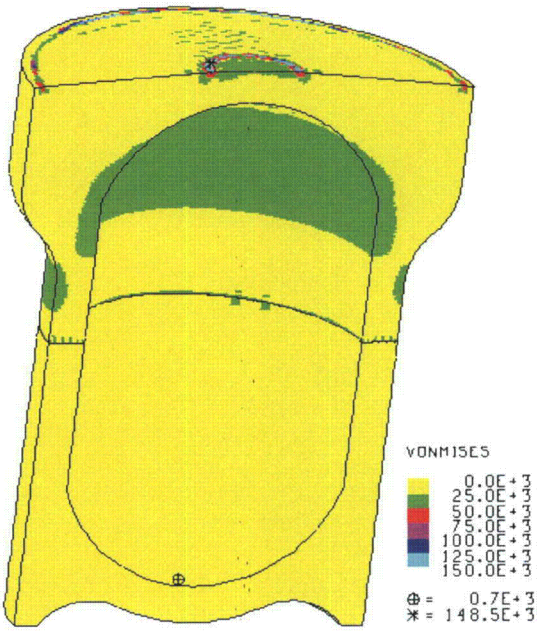

Figure 2-168. von Mises Stress in the TB-1 for the 731-g, ER, Cylinder, Bottom Position, Top Impact

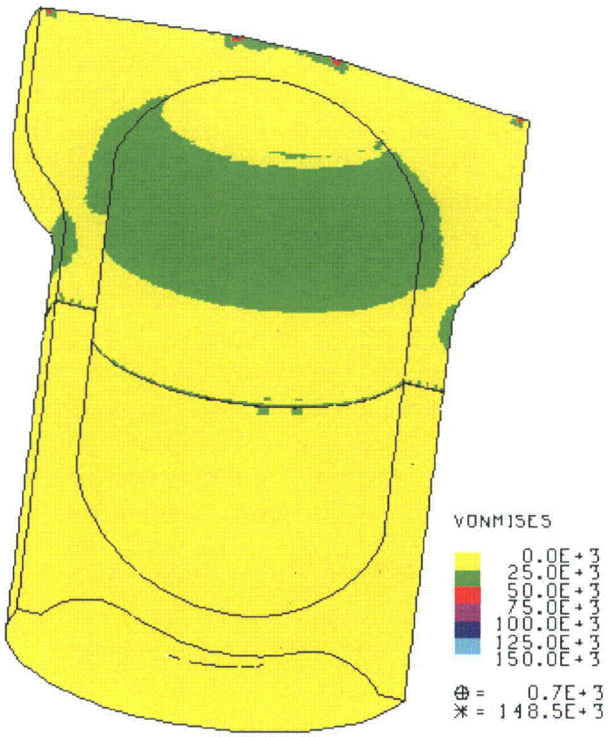

Figure 2-169. von Mises Stress in the TB-1 for the 731-g, ER, Cylinder, Bottom Position, Top Impact

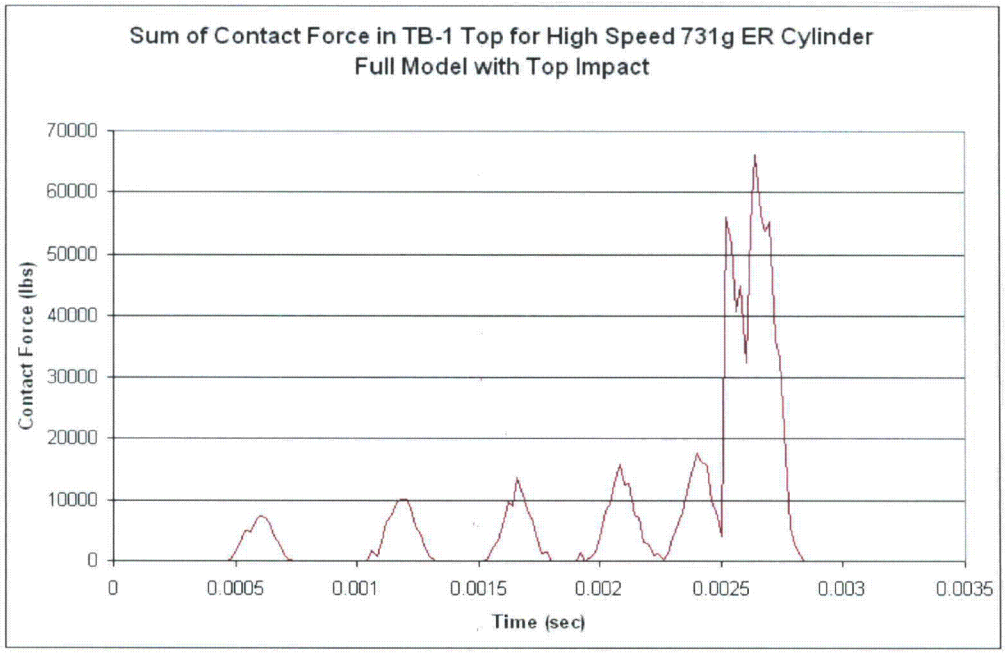

Figure 2-170. Contact Forces in the TB-1 for the 731-g, ER, Cylinder, Bottom Position, Top Impact

2.12.5.4.8 Run 7 - 731-g, Angled, Plutonium Metal Hollow Cylinder Top Impact

The top end impact model for the shorter 731 g plutonium metal hollow cylinder, oriented angled, is shown in Figure 2-171. The cylinder is located at the bottom of the T-Ampoule so that its net impact velocity with the top of the T-Ampoule is maximized. The post-impact deformation is shown in Figure 2-172 and its kinetic energy history in Figure 2-173. The plutonium metal hollow cylinder deforms but maintains much of its original shape because of its conservatively "infinitely ductile" material constitutive model definition (despite its alpha Pu being a relatively brittle material in reality).

Average stress-triaxiality versus EQPS is shown in Figures 2-174 and 2-175 for the 21 elements extending beyond the tested Bao-Wierzbicki strain locus. All of these elements are at high stress triaxiality and low EQPS. The Tearing Parameter values for these same 21 elements are shown in Figure 2-176, and all are below the critical Tearing Parameter value of 1.012 for Ti-6Al-4V. These elements are highlighted in red Figure 2-177, but note that these elements are still below the initiation of a ductile tear, thus T-Ampoule integrity is maintained.

Peak EQPS in the TB-1 vessel, shown in Figure 2-178, is about 2.4% and is only in some localized outer contact regions with the redwood overpack. The von Mises stresses (see Figures 2-179 and 2-180) peak at 148.5 ksi, is just above the elevated-temperature minimum yield strength for the TB-1 of 141 ksi, but more importantly, through-thickness TB-1 stress values are less than 25 ksi, below yield. The time at which the peak value of the von Mises stress occurs coincides with the peak value of the contact force (summed over the lid area). A plot of this force as a function of time is shown in Figure 2-181. A maximum contact load of 58,873 lbs is applied to the inner surface of the TB-1 during the impact.

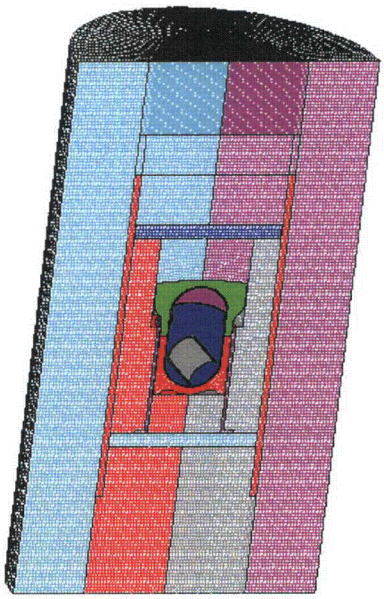

Figure 2-171. Finite Element Mesh for the 731-g, Angled, ER Cylinder, Bottom Position, Top Impact

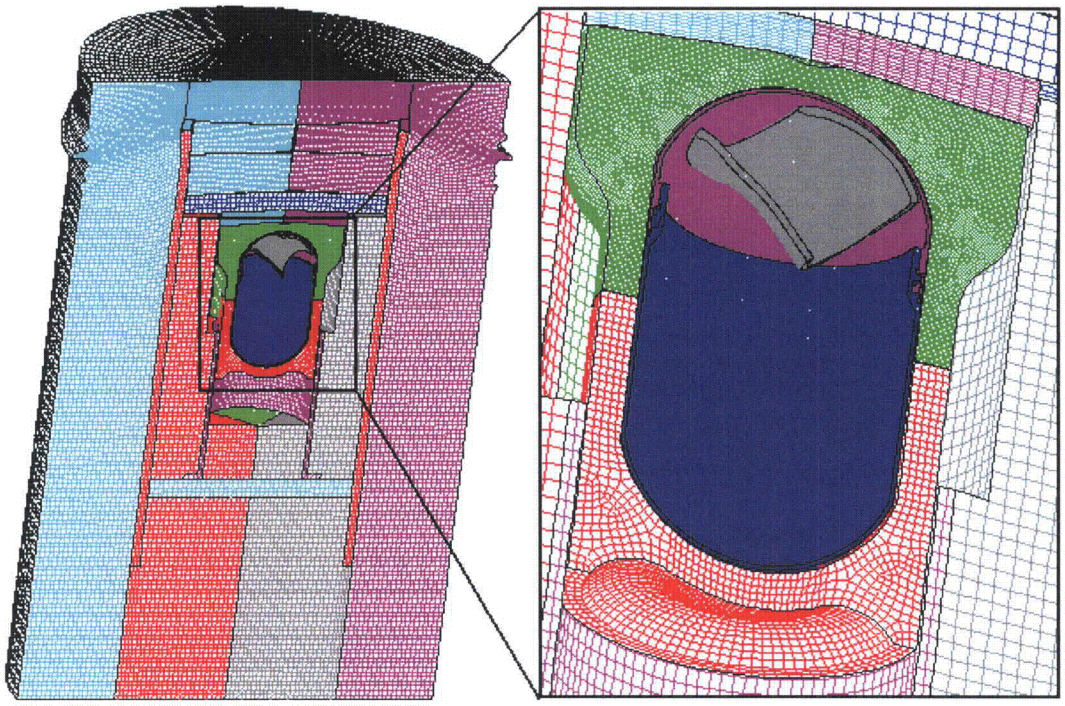

Figure 2-172. Finite Element Mesh for the 731-g, Angled, ER Cylinder, Bottom Position, Top Impact – Final Displacement

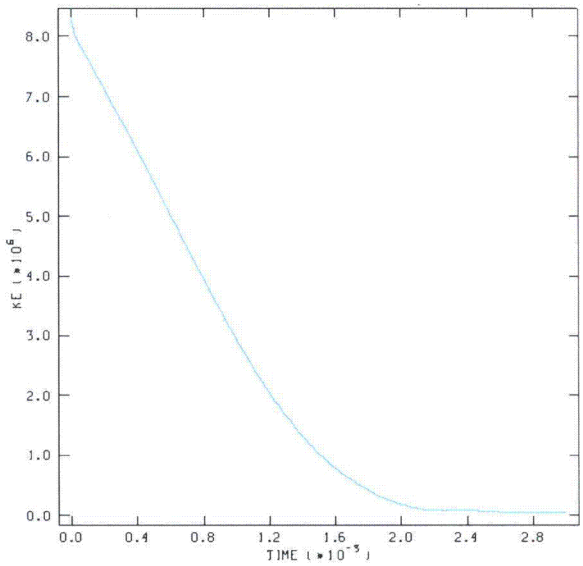

Figure 2-173. Kinetic Energy Time History for the 731-g, Angled, Plutonium Metal Hollow Cylinder, Bottom Position, Top Impact

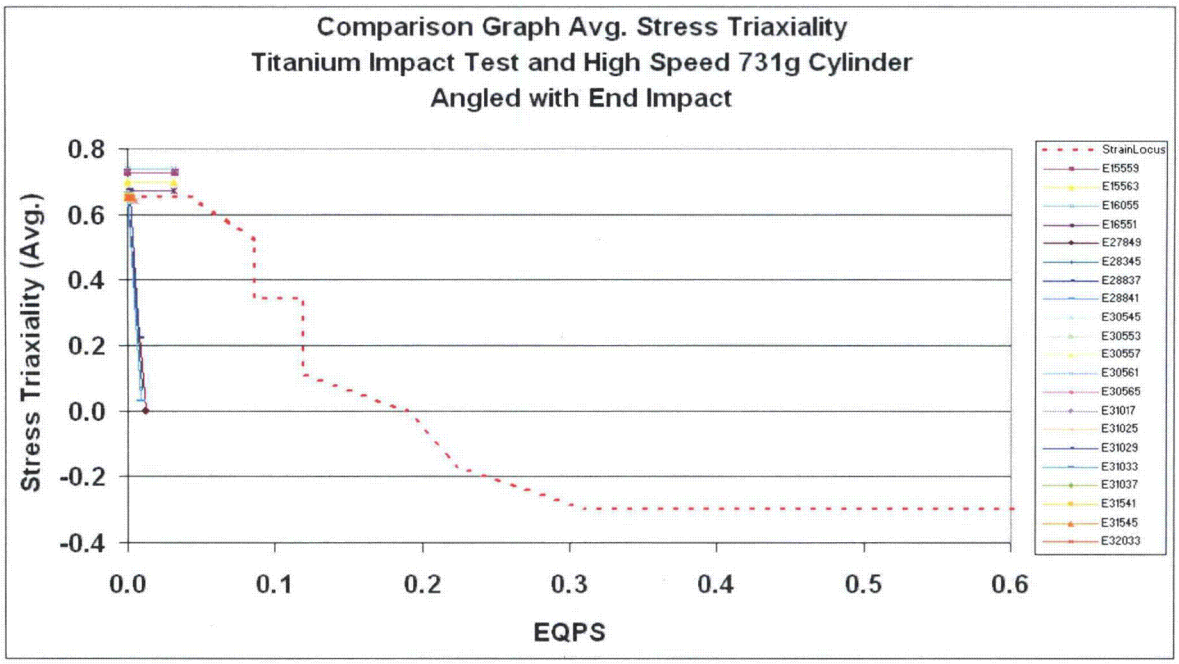

Figure 2-174. Graph of Average Stress Triaxiality versus EQPS of Elements Exceeding the Experimental Strain Locus for the 731-g, Angled, Plutonium Metal Hollow Cylinder, Bottom Position, Top Impact

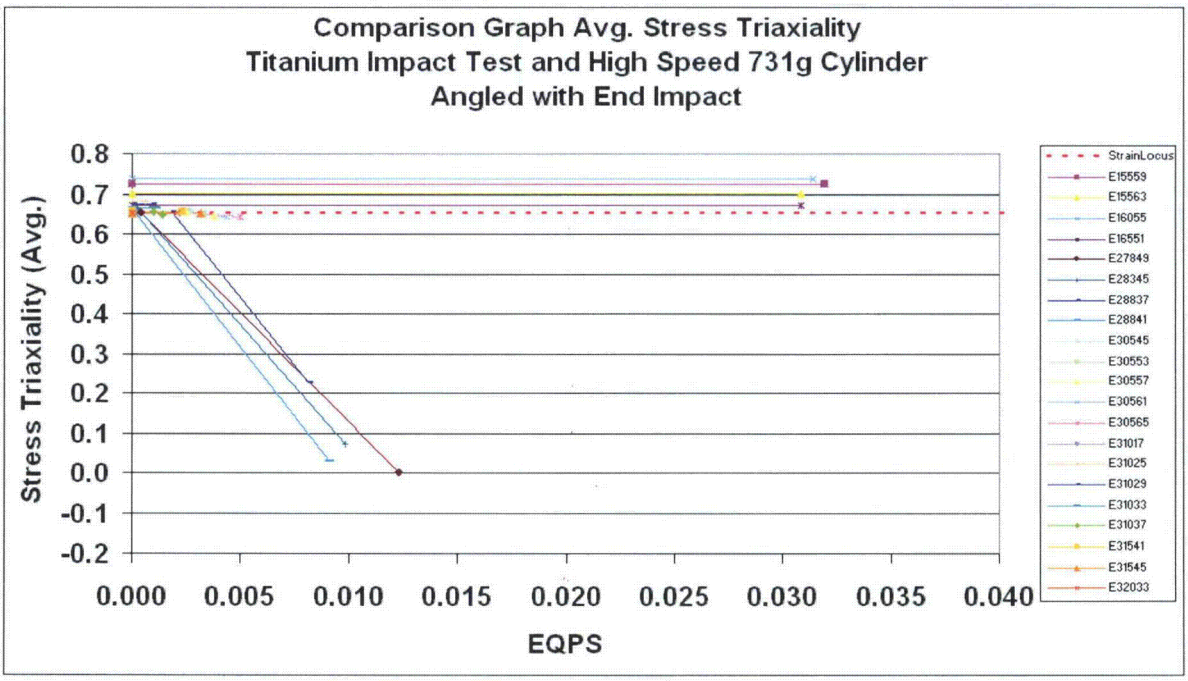

Figure 2-175. Graph of Average Stress Triaxiality versus EQPS of Elements Exceeding the Experimental Strain Locus (Zoomed In) for the 731-g, Angled, Plutonium Metal Hollow Cylinder, Bottom Position, Top Impact

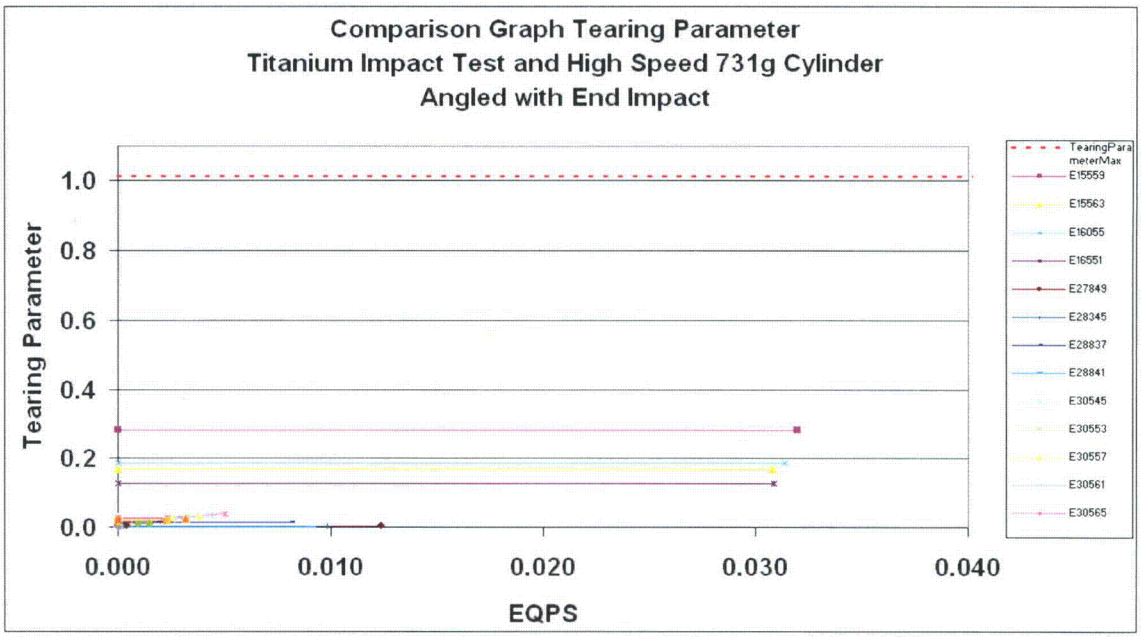

Figure 2-176. Graph of Tearing Parameter versus EQPS of Elements Exceeding the Experimental Strain Locus for the 731-g, Angled, Plutonium Metal Hollow Cylinder, Bottom Position, Top Impact

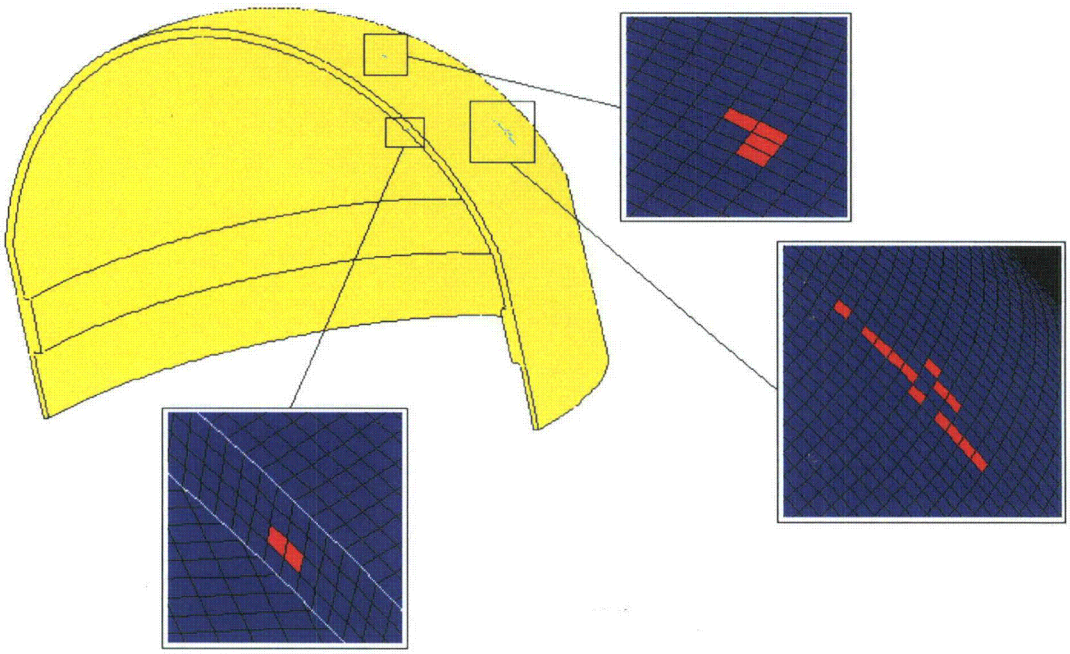

Figure 2-177. Plot of Elements Exceeding the Experimental Strain Locus for the 731-g, Angled, Plutonium Metal Hollow Cylinder, Bottom Position, Top Impact

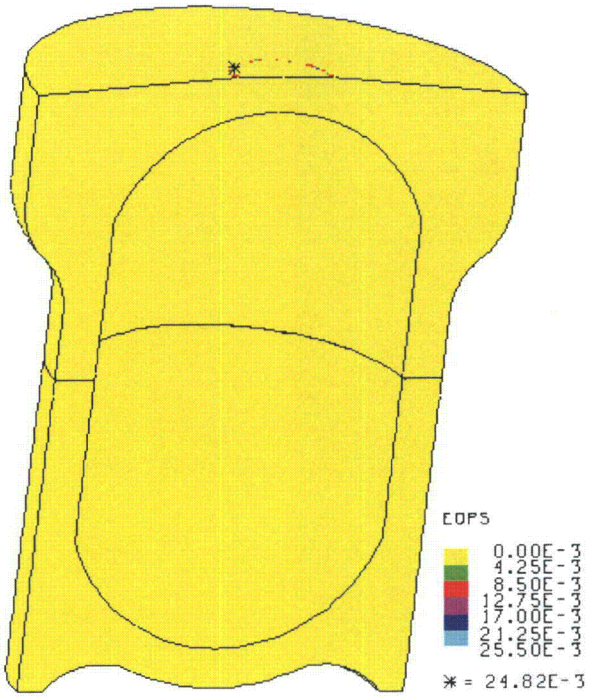

Figure 2-178. Plot of EQPS in the TB-1 for the 731-g, Angled, Plutonium Metal Hollow Cylinder, Bottom Position, Top Impact

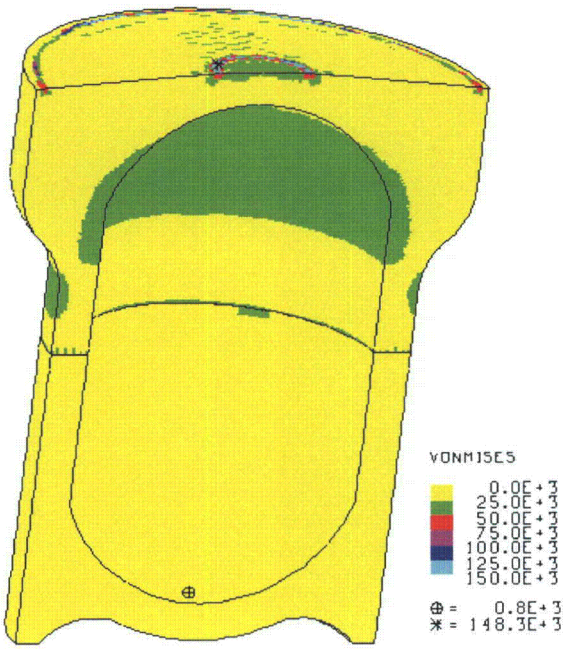

Figure 2-179. Plot of von Mises Stress for the 731-g, Angled, Plutonium Metal Hollow Cylinder, Bottom Position, Top Impact

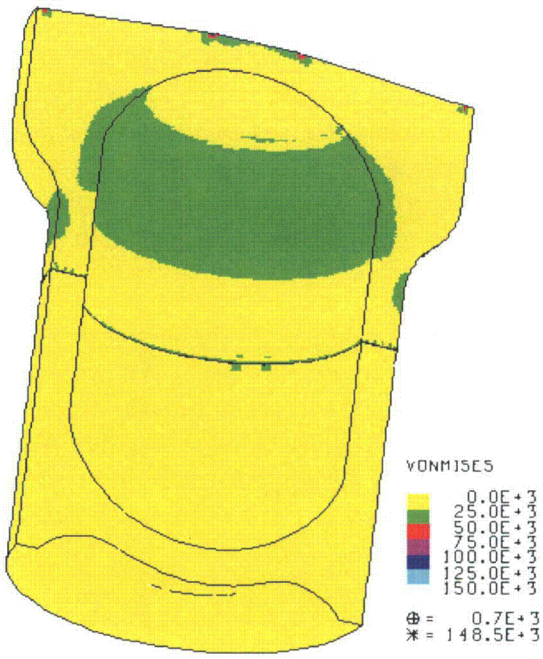

Figure 2-180. Plot of von Mises Stress for the 731-g, Angled, Plutonium Metal Hollow Cylinder, Bottom Position, Top Impact

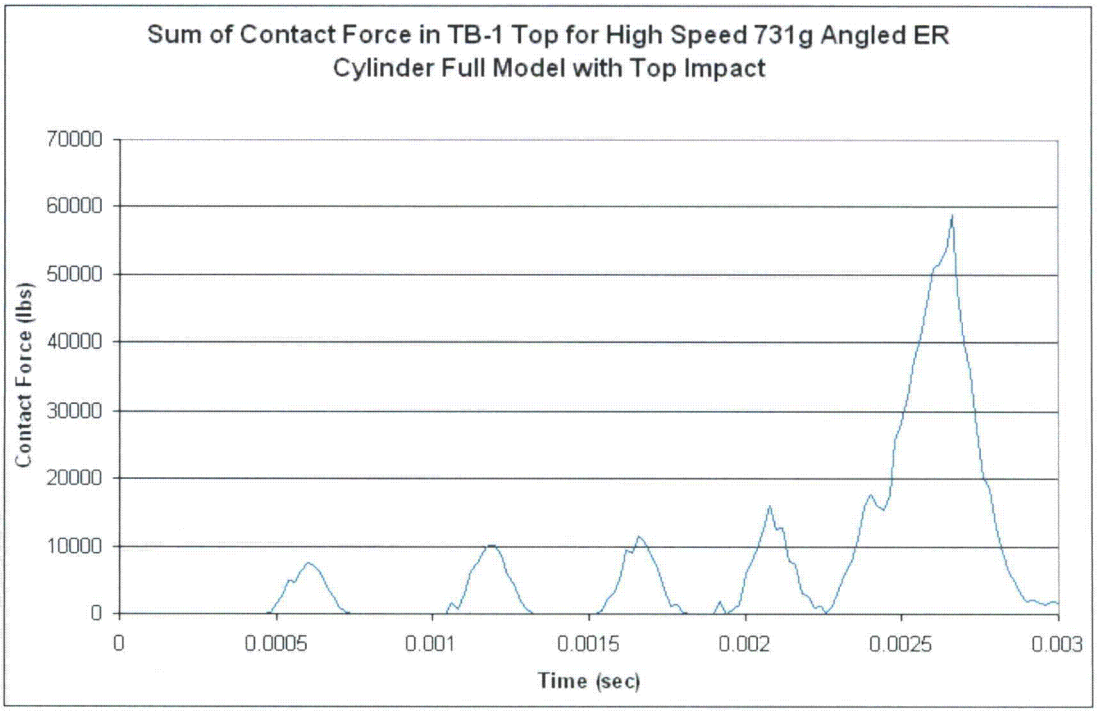

Figure 2-181. Plot of Contact Force for the 731-g, Angled, Plutonium Metal Hollow Cylinder, Bottom Position, Top Impact

2.12.5.4.9 Run 8 - 731-g Angled Plutonium Metal Hollow Cylinder CGOC Impact

The lid end CG-over-corner impact model for the shorter 731 g plutonium metal hollow cylinder is shown in Figure 2-182. The cylinder is located at the bottom of the T-Ampoule so that its net impact velocity with the top of the T-Ampoule is maximized. The post-impact deformation is shown in Figure 2-183 and its kinetic energy history in Figure 2-184. The plutonium metal hollow cylinder deforms slightly more than the previous case because of the slightly more side-impact-like orientation but maintains much of its original shape because of its conservatively "infinitely ductile" material constitutive model definition.

Average stress-triaxiality versus EQPS is shown in Figures 2-185 and 2-186 for the 84 elements extending beyond the tested Bao-Wierzbicki strain locus. All of these elements are at relatively high stress triaxiality and low EQPS. The Tearing Parameter values for these same 84 elements are shown in Figure 2-187 and all are still safely below the critical Tearing Parameter value of 1.012 for Ti-6Al-4V. These elements are highlighted in red in Figures 2-188 and 2-189 but these elements are still below the critical value, thus the T-Ampoule eutectic barrier integrity is maintained.

Peak EQPS in the TB-1 vessel is shown in Figure 2-190 to be about 28.5%, although this peak is only in a highly localized outer corner region where there is a slight contact over closure issue with the redwood overpack. Through-thickness plasticity is non-existent and the TB-1 integrity is maintained. The von Mises stress (see Figure 2-191) peak at 225 ksi (due to the localized redwood contact) is above the elevated-temperature minimum yield strength for the TB-1 of 141 ksi, but more importantly, through-thickness TB-1 stress values are less than 37.5 ksi, below yield.

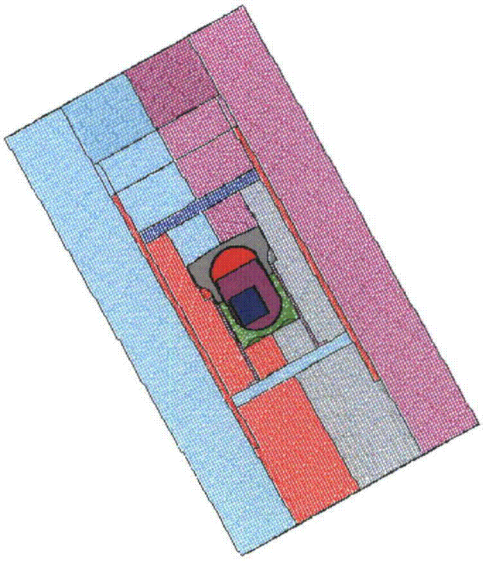

Figure 2-182. Finite Element Mesh for the 731-g, Angled, Plutonium Metal Hollow Cylinder, Bottom Position, CGOC Impact

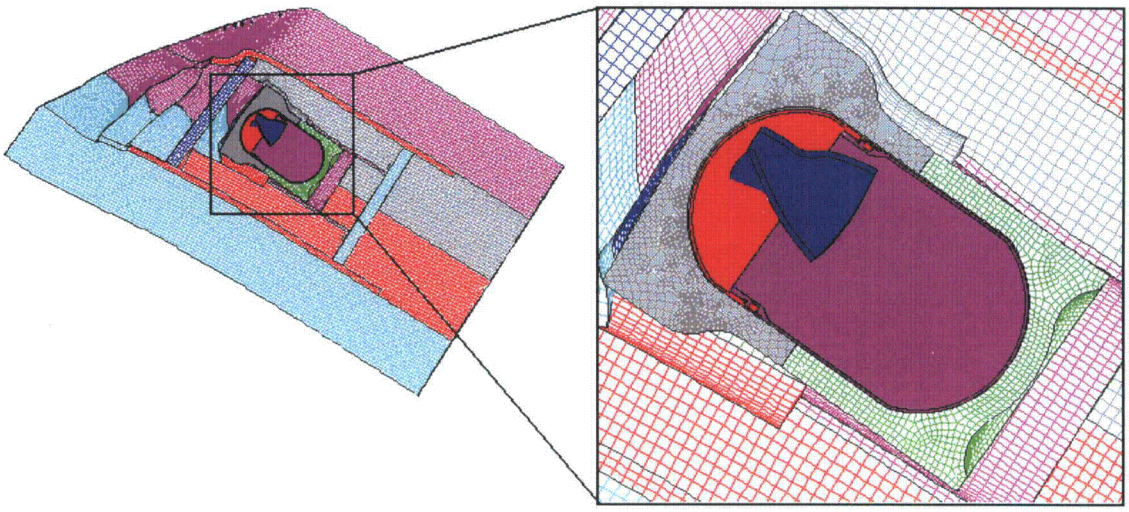

Figure 2-183. Finite Element Mesh for the 731-g, Angled, Plutonium Metal Hollow Cylinder, Bottom Position, CGOC Impact – Final Displacement

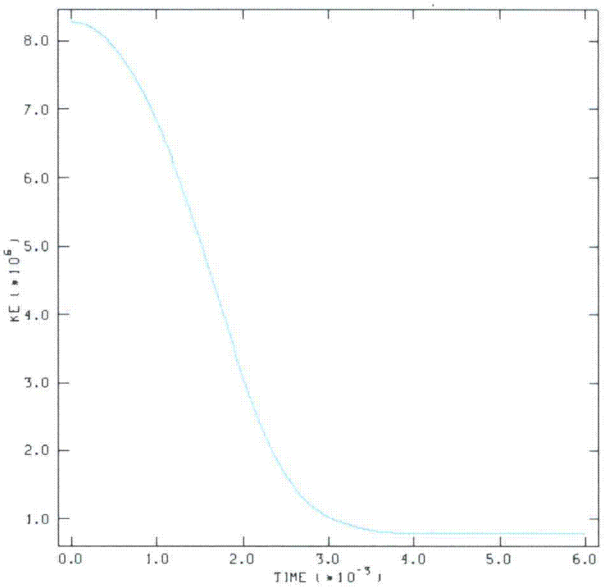

Figure 2-184. Kinetic Energy Time History for the 731-g, Angled, Plutonium Metal Hollow Cylinder, Bottom Position, CGOC Impact

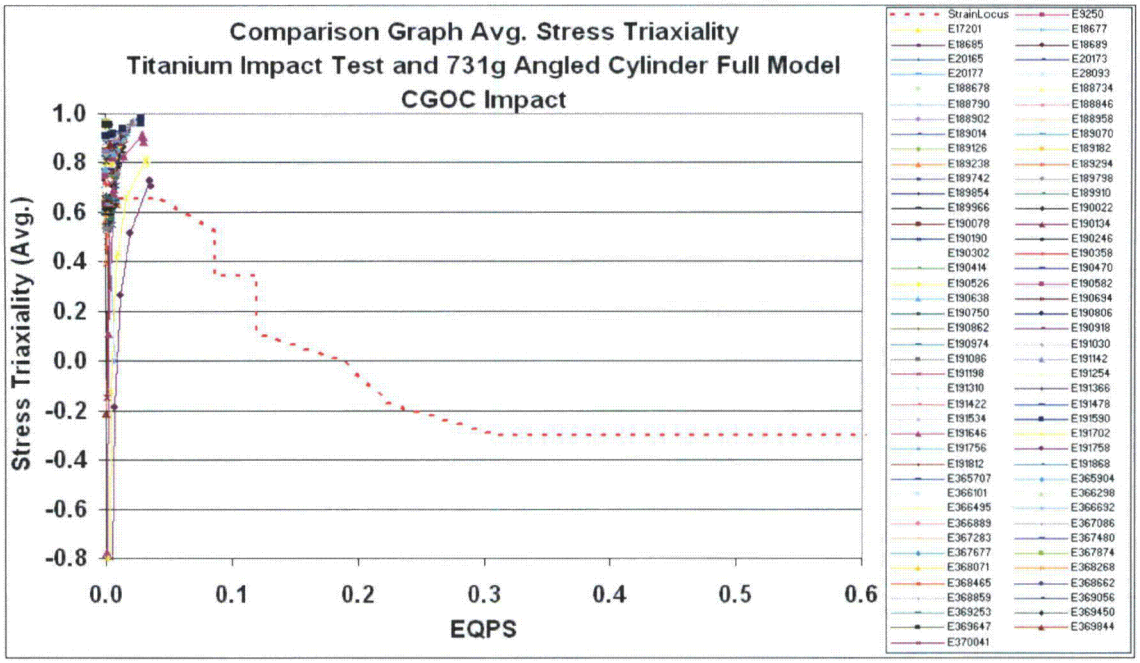

Figure 2-185. Graph of Average Stress Triaxiality versus EQPS of Elements Exceeding the Experimental Strain Locus for the 731-g, Angled, Plutonium Metal Hollow Cylinder, Bottom Position, CGOC Impact

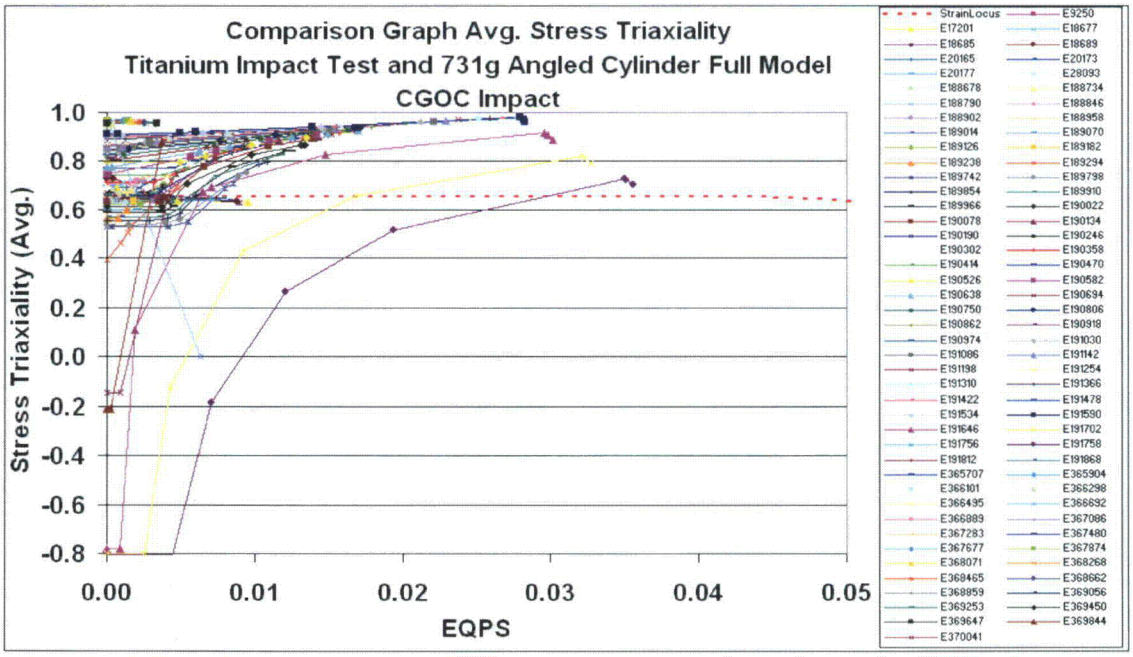

Figure 2-186. Graph of Average Stress Triaxiality versus EQPS of Elements Exceeding the Experimental Strain Locus (Zoomed In) for the 731-g, Angled, Plutonium Metal Hollow Cylinder, Bottom Position, CGOC Impact

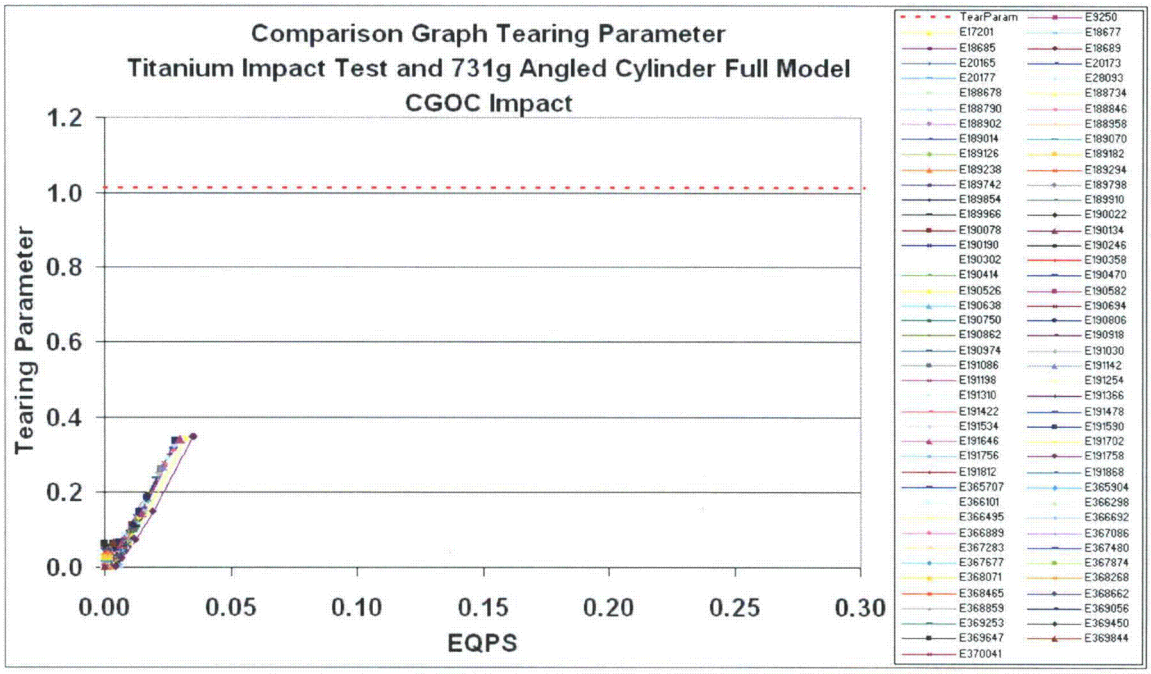

Figure 2-187. Graph of Tearing Parameter versus EQPS of Elements Exceeding the Experimental Strain Locus for the 731-g, Angled, Plutonium Metal Hollow Cylinder, Bottom Position, CGOC Impact

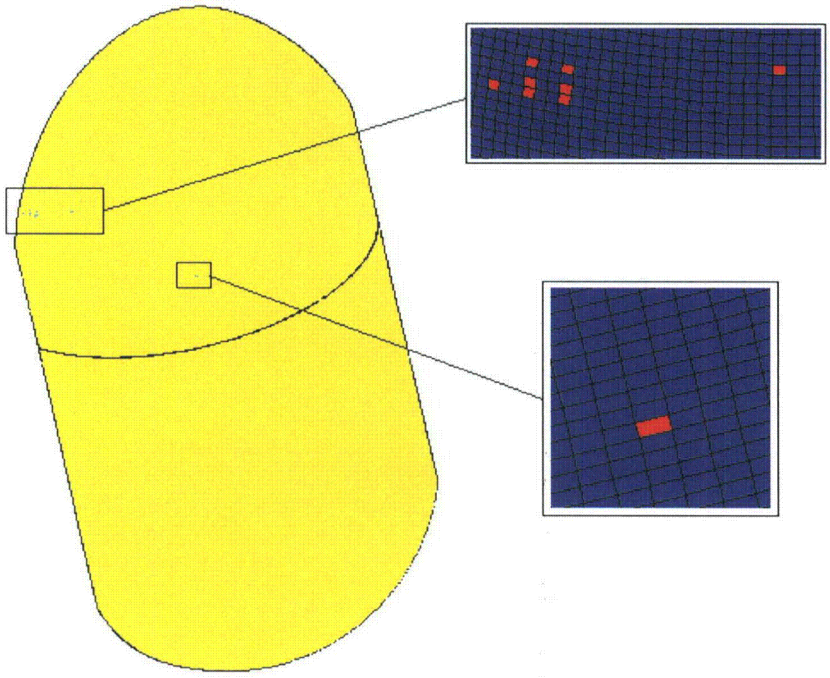

Figure 2-188. Plot of Elements Exceeding the Experimental Strain Locus for the 731-g, Angled, Plutonium Metal Hollow Cylinder, Bottom Position, CGOC Impact

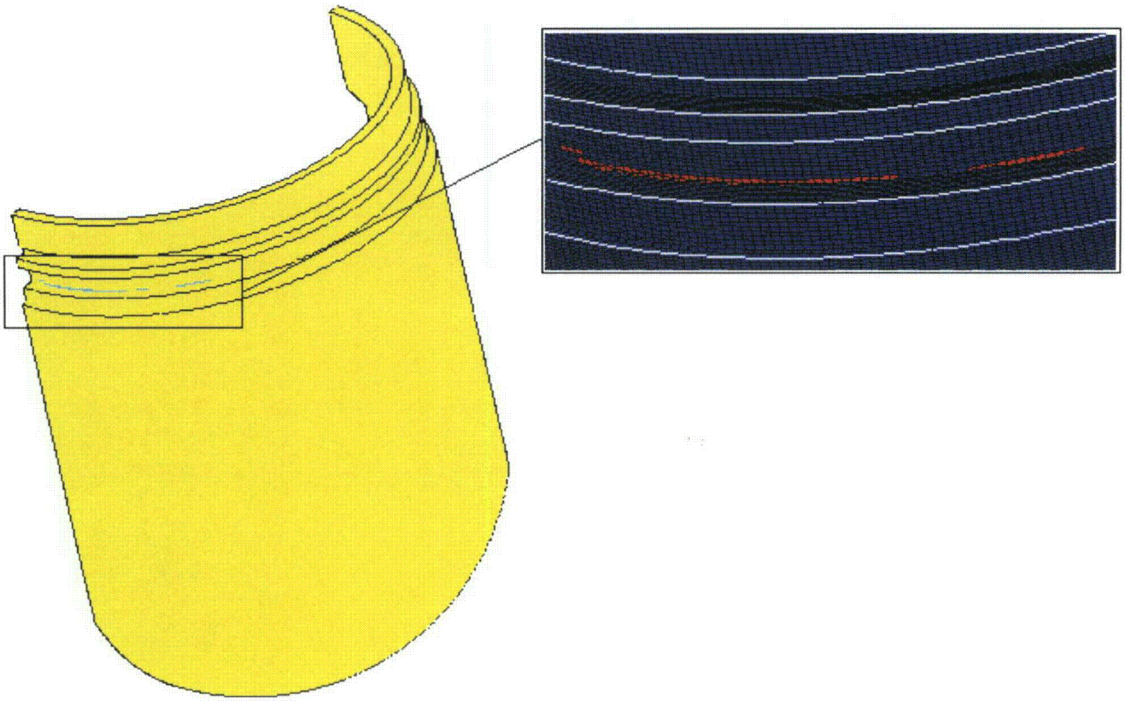

Figure 2-189. Plot of Elements Exceeding the Experimental Strain Locus for the 731-g, Angled, Plutonium Metal Hollow Cylinder, Bottom Position, CGOC Impact

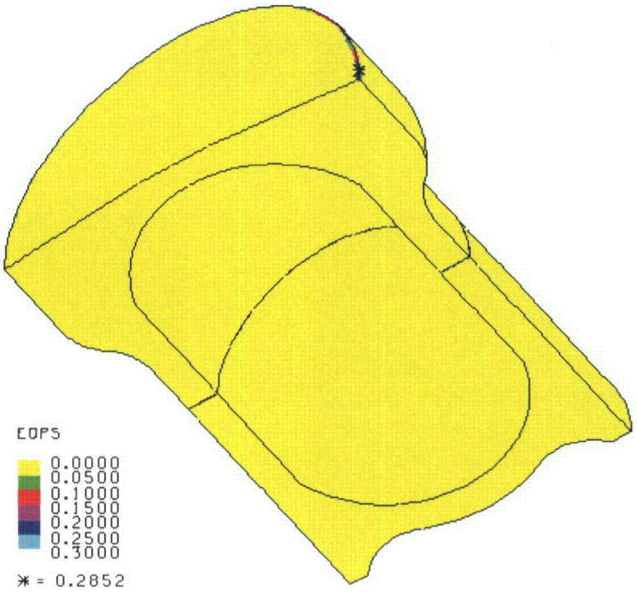

Figure 2-190. Plot of EQPS in the TB-1 for the 731-g, Angled, Plutonium Metal Hollow Cylinder, Bottom Position, CGOC Impact

Figure 2-191. Plot of von Mises Stress in the TB-1 for the 731-g, Angled, Plutonium Metal Hollow Cylinder, Bottom Position, CGOC Impact

2.12.5.4.10 Run 9 - 731-g Plutonium Metal Hollow Cylinder Side Impact

The side impact model for the shorter and lighter 731 g plutonium metal hollow cylinder is shown in Figure 2-192. The cylinder is located at the far side of the T-Ampoule so that its net impact velocity with the side of the T-Ampoule is maximized. The post-impact deformation is shown in Figure 2-193 and its kinetic energy history in Figure 2-194. The plutonium metal hollow cylinder deforms much more than the previous case because of its weaker side-impact-like orientation.

Average stress-triaxiality versus EQPS is shown in Figures 2-195 and 2-196 for the 63 elements extending beyond the tested Bao-Wierzbicki strain locus. All of these elements are at relatively high stress triaxiality and low EQPS. The Tearing Parameter values for these same 63 elements are shown in Figure 2-197 and all are still below the critical Tearing Parameter value of 1.012 for Ti-6Al-4V. These elements are highlighted in red Figure 2-198 but these elements are still below the critical value and do not indicate failure; T-Ampoule integrity is maintained.

Peak EQPS in the TB-1 vessel is shown in Figures 2-199 through 2-202 and is about 30%, although this peak is only in a highly localized outer corner region where there is a slight contact overclosure issue with the redwood overpack. A slight (<1% EQPS) dent is visible in Figure 2-202 from the internal impact of the plutonium metal hollow cylinder into the TB-1 wall (via the T-Ampoule). Through-thickness plasticity is non-existent and the TB-1 integrity is maintained. The von Mises stresses (see Figures 2-203 and 2-204) peak at 225 ksi (due to the localized redwood contact), above the elevated-temperature minimum yield strength for the TB-1

of 141 ksi, but more importantly, through-thickness TB-1 stress values are less than 80 ksi, below yield.

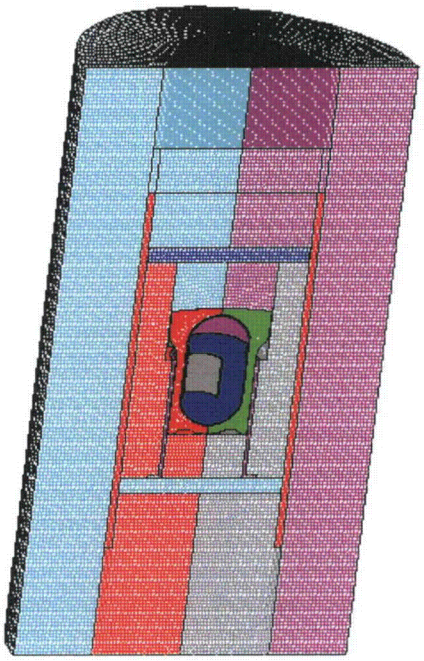

Figure 2-192. Finite Element Mesh for the 731-g, ER, Cylinder, Far Side Position, Side Impact

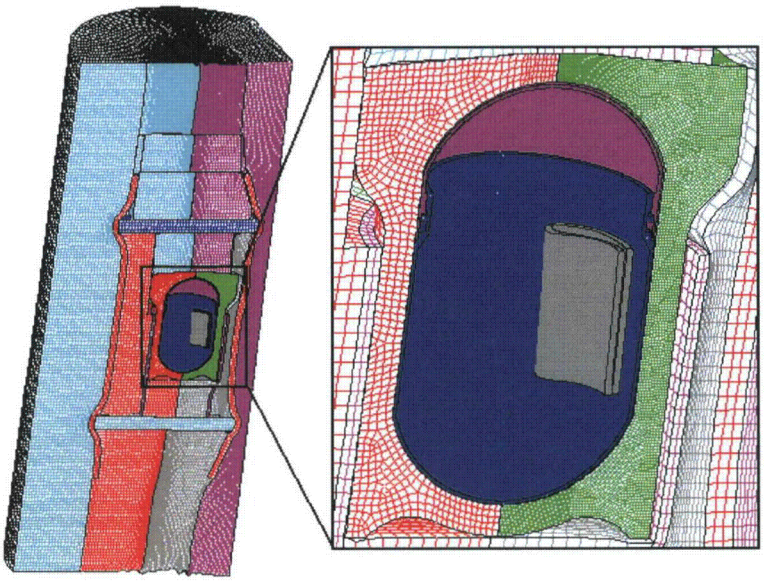

Figure 2-193. Finite Element Mesh for the 731-g, Plutonium Metal Hollow Cylinder, Far Side Position, Side Impact – Final Displacement

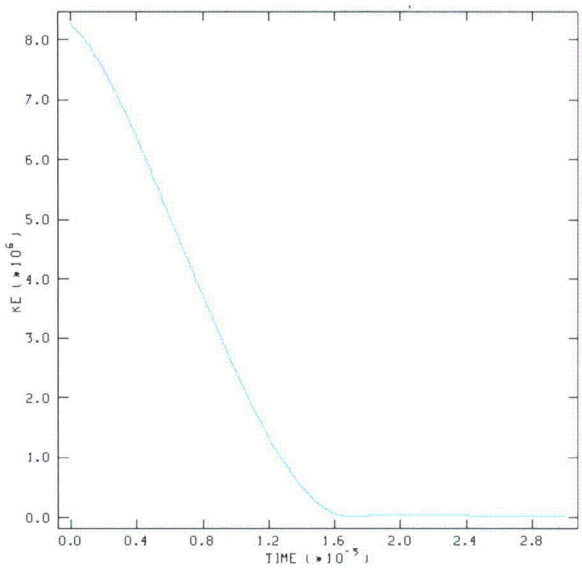

Figure 2-194. Kinetic Energy Time History for the 731-g, ER, Cylinder, Far Side Position, Side Impact

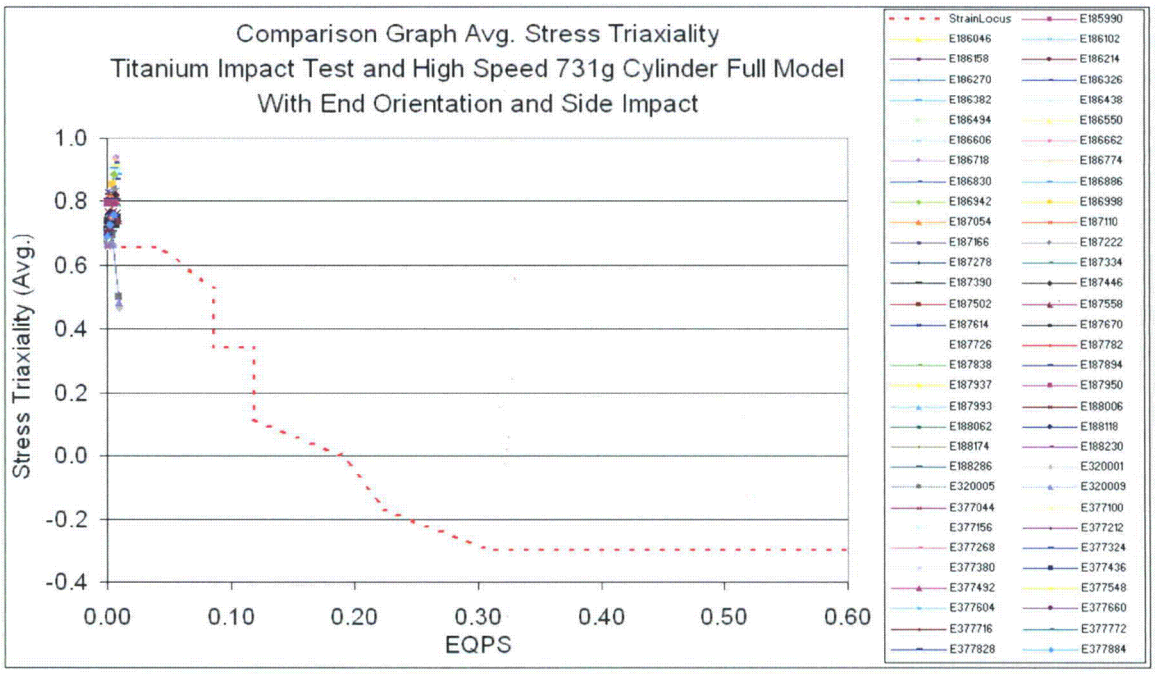

Figure 2-195. Graph of Average Stress Triaxiality versus EQPS of Elements Exceeding the Experimental Strain Locus for the 731-g, Plutonium Metal Hollow Cylinder, Far Side Position, Side Impact

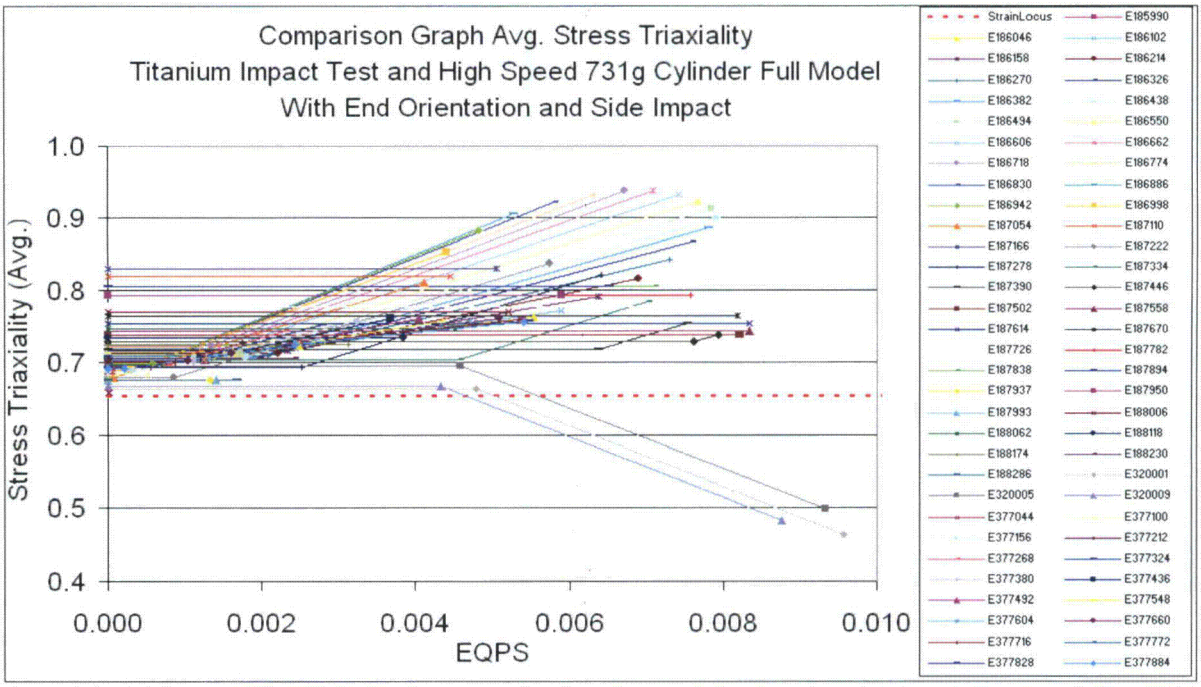

Figure 2-196. Graph of Average Stress Triaxiality versus EQPS of Elements Exceeding the Experimental Strain Locus (Zoomed In) for the 731-g, Plutonium Metal Hollow Cylinder, Far Side Position, Side Impact

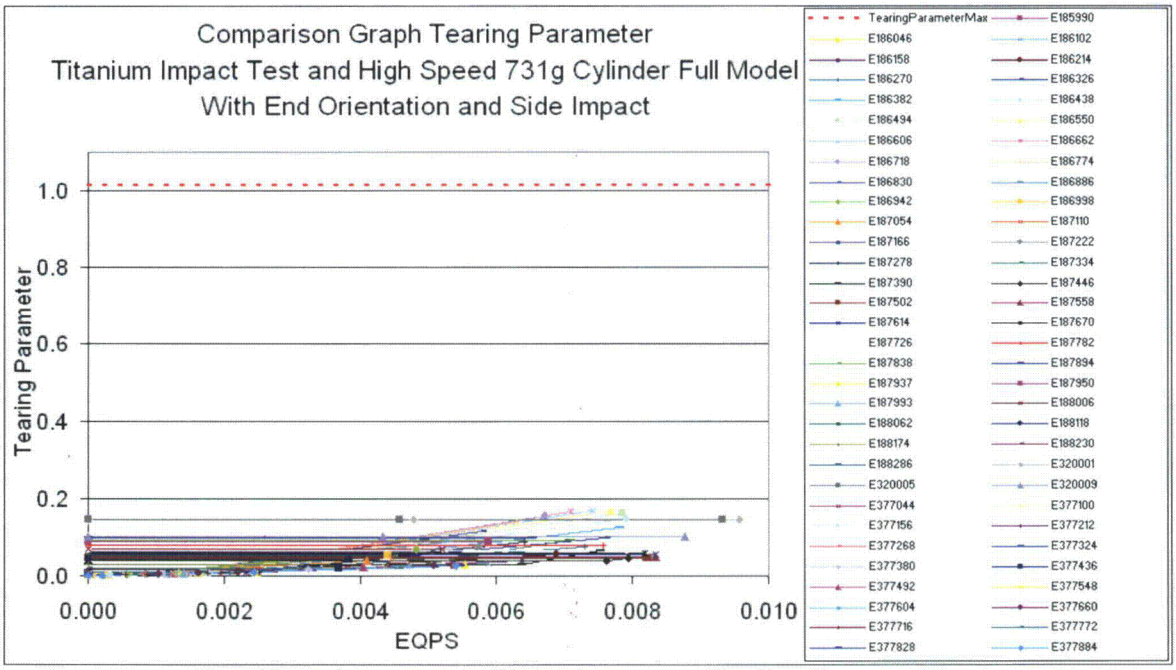

Figure 2-197. Graph of Tearing Parameter versus EQPS of Elements Exceeding the Experimental Strain Locus for the 731-g, Plutonium Metal Hollow Cylinder, Far Side Position, Side Impact

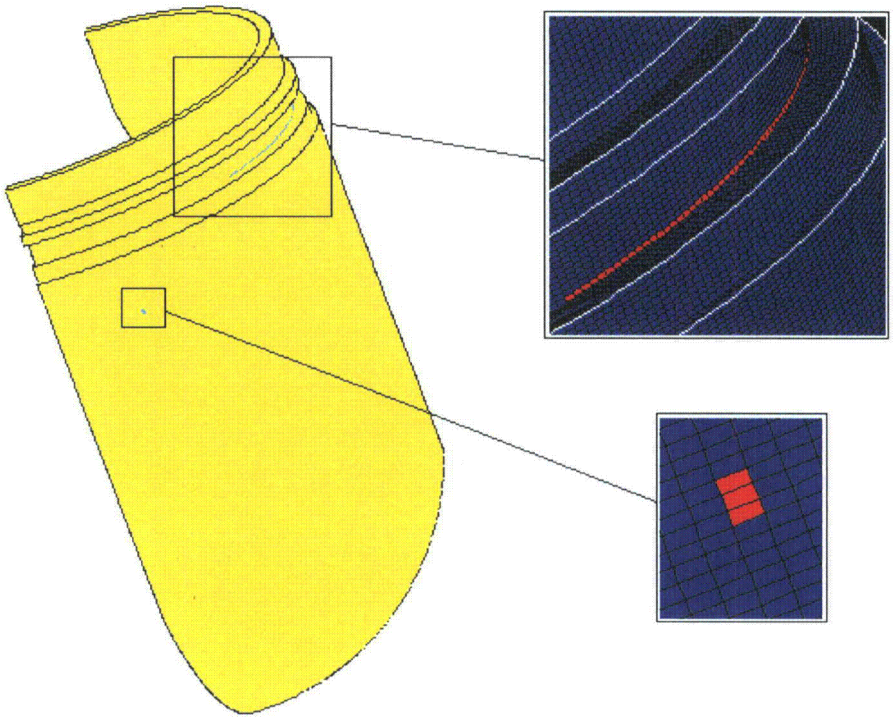

Figure 2-198. Plot of Elements Exceeding the Experimental Strain Locus for the 731-g, Plutonium Metal Hollow Cylinder, Far Side Position, Side Impact

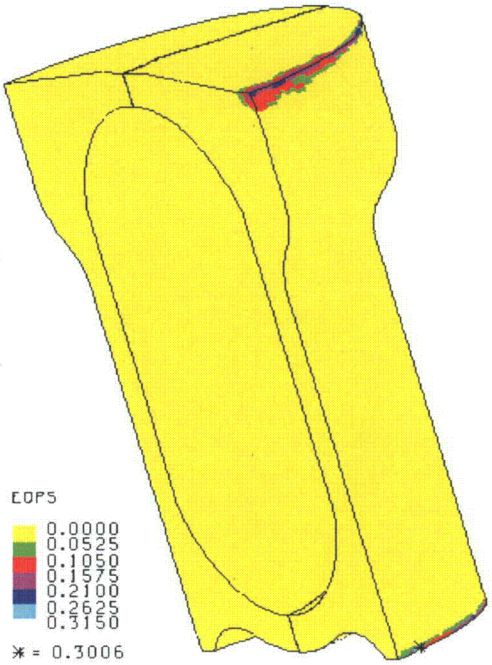

Figure 2-199. Plot of EQPS in the TB-1 for the 731-g, ER Cylinder, Far Side Position, Side Impact

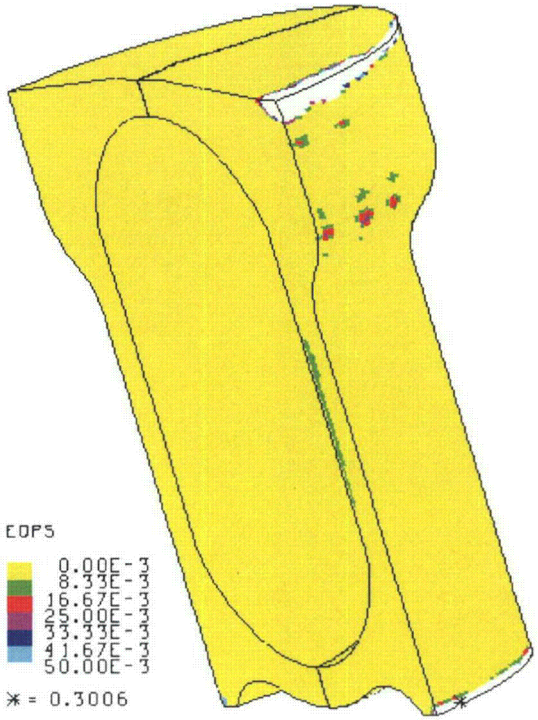

Figure 2-200. Plot of EQPS in the TB-1 for the 731-g, ER Cylinder, Far Side Position, Side Impact

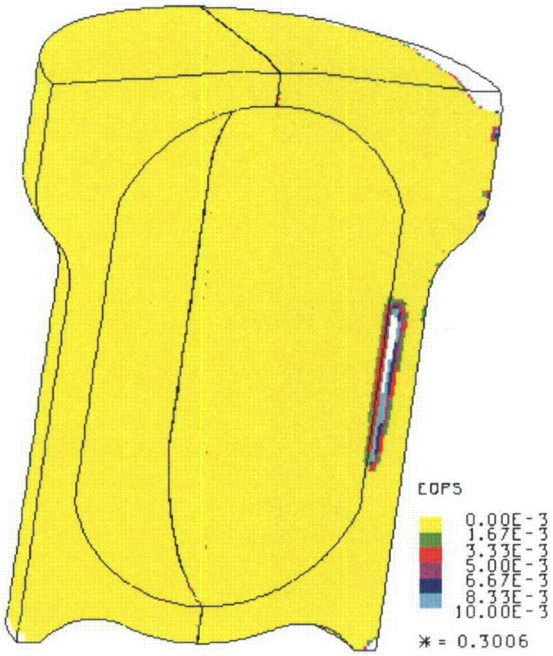

Figure 2-201. Plot of EQPS in the TB-1 for the 731-g, ER Cylinder, Far Side Position, Side Impact

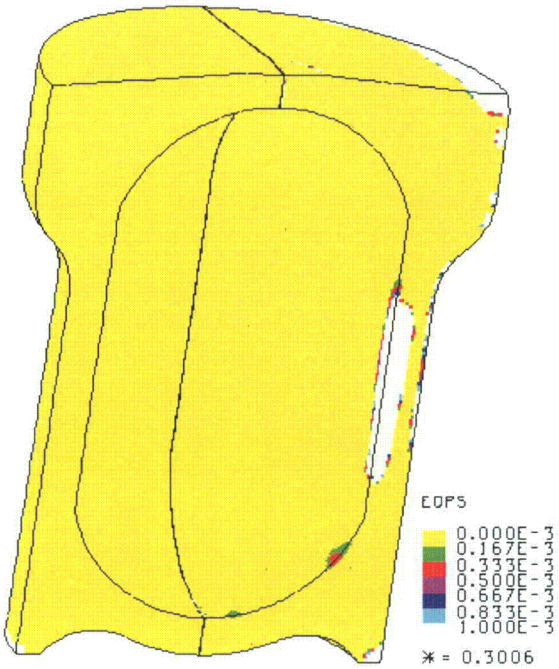

Figure 2-202. Plot of EQPS in the TB-1 for the 731-g, Plutonium Metal Hollow Cylinder, Far Side Position, Side Impact (Range Adjusted to Highlight Small Stains in the TB-1 Not Visible in Figure 2-201)

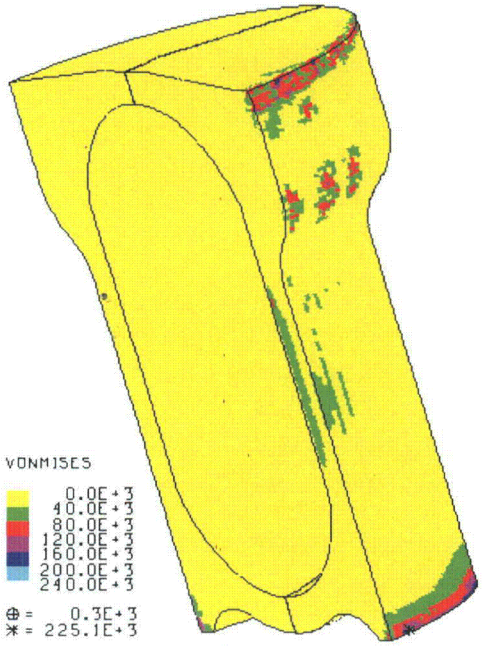

Figure 2-203. Plot of von Mises Stress in the TB-1 for the 731-g, Plutonium Metal Hollow Cylinder, Far Side Position, Side Impact

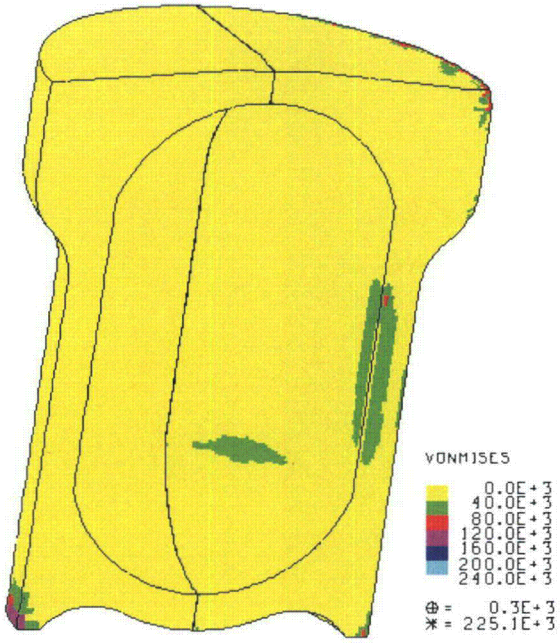

Figure 2-204. Plot of von Mises Stress in the TB-1 for the 731-g, Plutonium Metal Hollow Cylinder, Far Side Position, Side Impact (see Figure 2-203 Rotated to Show Internal Stresses)

2.12.5.4.11 Run 10 - 731-g Angled Plutonium Metal Hollow Cylinder Side Impact

The side impact model for the lighter, 731 g plutonium metal hollow cylinder, angled orientation, is shown in Figure 2-205. The cylinder is located at the far side of the T-Ampoule so that its net impact velocity with the side of the T-Ampoule is maximized, but also angled to present a sharp corner impact with the T-Ampoule surface. The post-impact deformation is shown in Figure 2-206 and its kinetic energy history in Figure 2-207. The plutonium metal hollow cylinder deforms moderately but maintains much of its original shape because of its conservatively "infinitely ductile" material constitutive model definition.

Average stress-triaxiality versus EQPS is shown in Figures 2-208 and 2-209 for the 94 elements extending beyond the tested Bao-Wierzbicki strain locus. All of these elements are at relatively high stress triaxiality and low EQPS. The Tearing Parameter values for these same 94 elements are shown in Figure 2-210 and all are still below the critical Tearing Parameter value of 1.012 for Ti-6Al-4V. These elements are highlighted in red Figure 2-211 but these elements are still below the critical value and do not indicate failure; T-Ampoule integrity is maintained.

Peak EQPS in the TB-1 vessel is shown in Figures 2-212 and 2-213 and is about 27.6%, although this peak is only in a highly localized outer corner region where there is a slight contact over closure issue with the redwood overpack. Through-thickness plasticity is non-existent and the TB-1 integrity is maintained. The von Mises stresses (see Figures 2-214 and 2-215) peak at 224 ksi (due to the localized redwood contact), above the elevated-temperature minimum yield strength for the TB-1 of 141 ksi, but more importantly, through-thickness TB-1 stress values are less than 112.5 ksi, below yield.

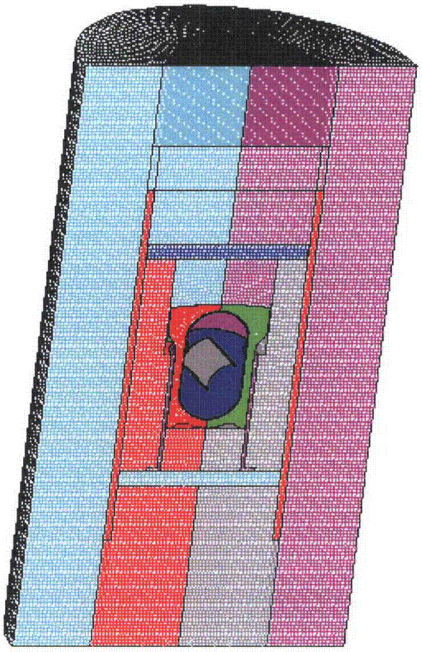

Figure 2-205. Finite Element Mesh for the 731-g, Angled, ER Cylinder, Far Side Position, Side Impact

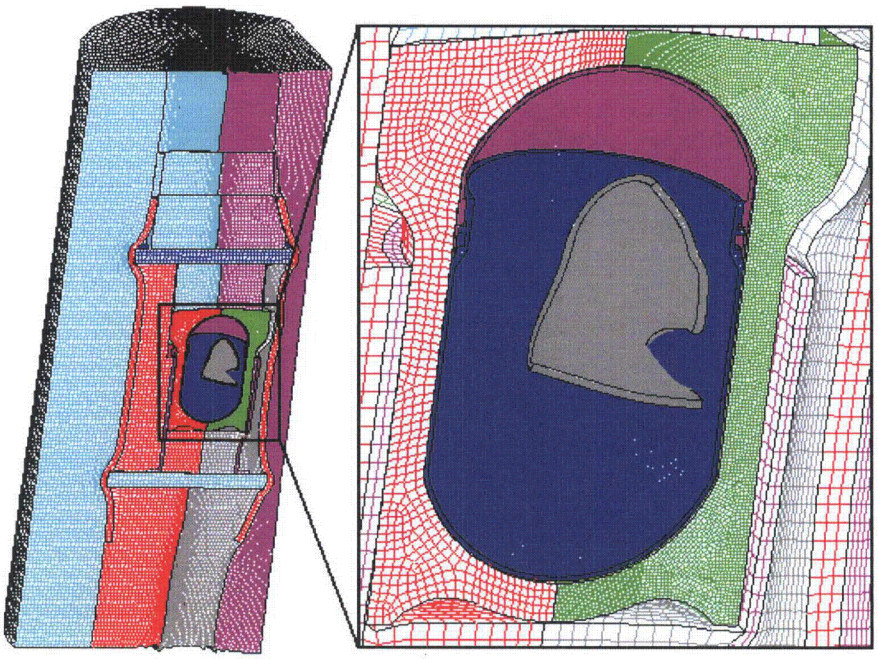

Figure 2-206. Finite Element Mesh for the 731-g, Angled, ER Cylinder, Far Side Position, Side Impact – Final Displacement

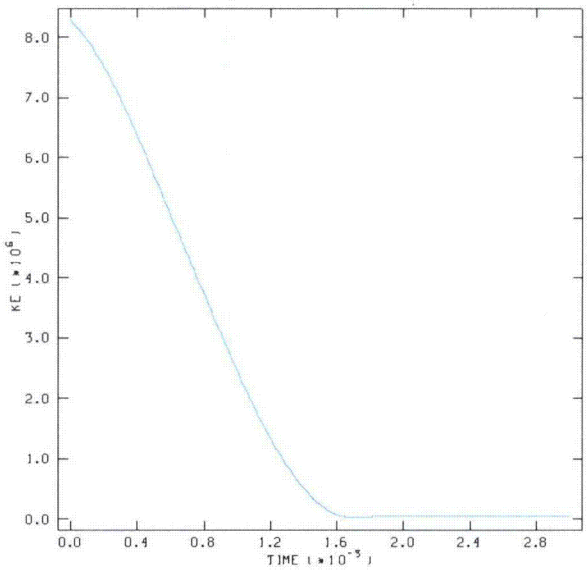

Figure 2-207. Kinetic Energy Time History for the 731-g, Angled, Plutonium Metal Hollow Cylinder, Far Side Position, Side Impact

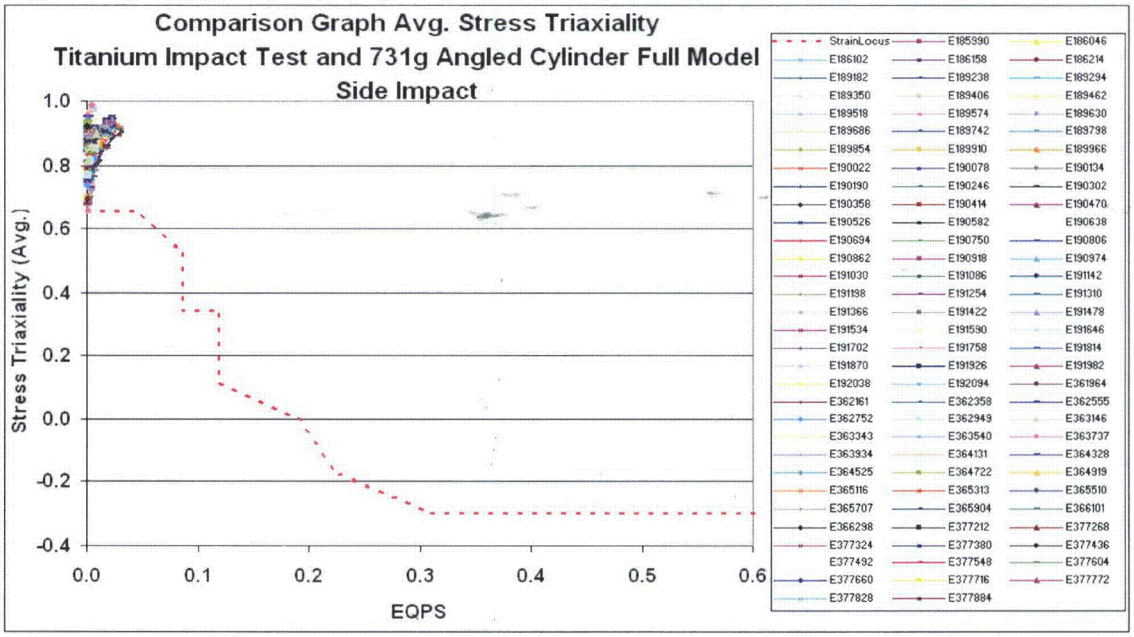

Figure 2-208. Graph of Average Stress Triaxiality versus EQPS of Elements Exceeding the Experimental Strain Locus for the 731-g, Angled, Plutonium Metal Hollow Cylinder, Far Side Position, Side Impact

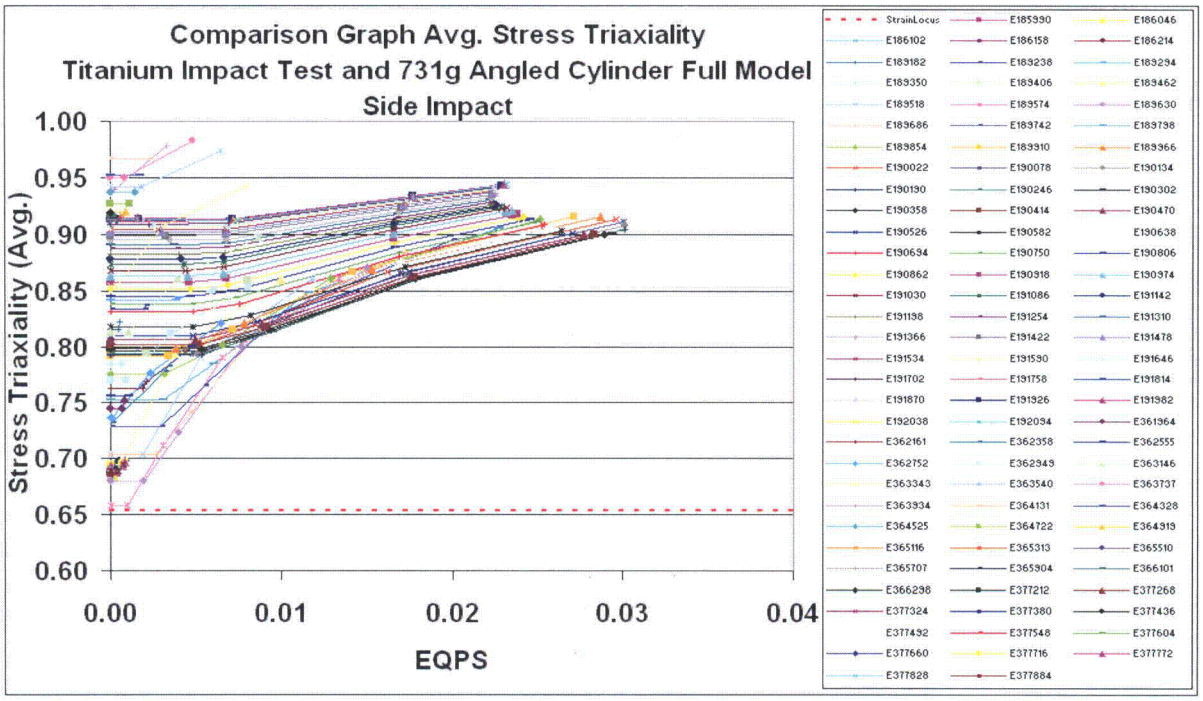

Figure 2-209. Graph of Average Stress Triaxiality versus EQPS of Elements Exceeding the Experimental Strain Locus (Zoomed In) for the 731-g, Angled, Plutonium Metal Hollow Cylinder, Far Side Position, Side Impact

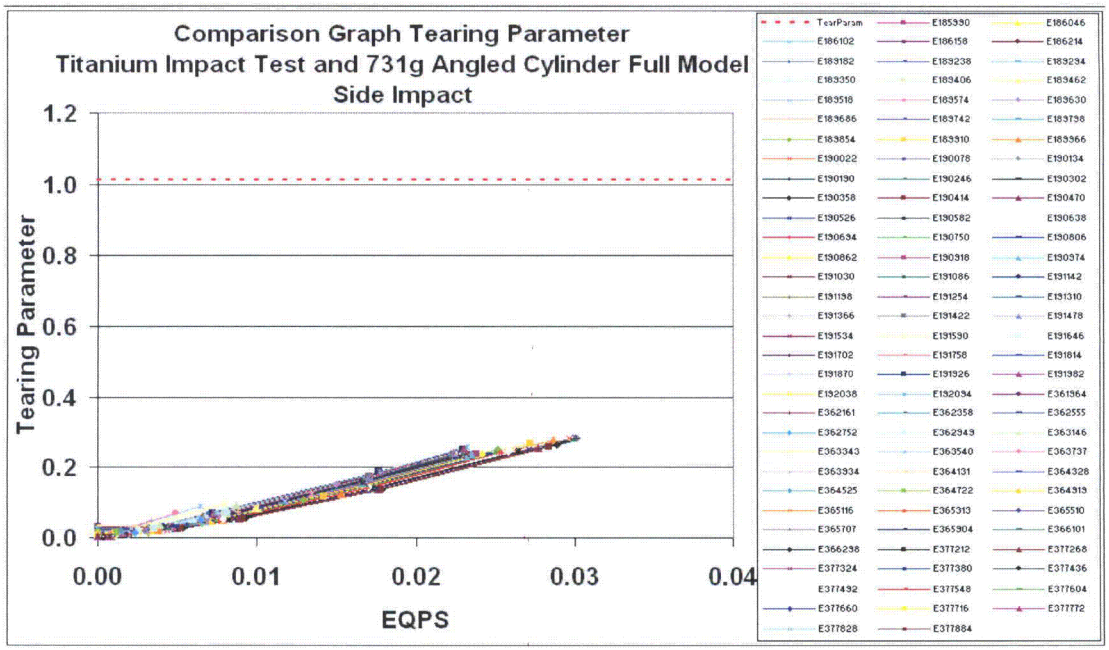

Figure 2-210. Graph of Tearing Parameter versus EQPS of Elements Exceeding the Experimental Strain Locus for the 731-g, Angled, Plutonium Metal Hollow Cylinder, Far Side Position, Side Impact

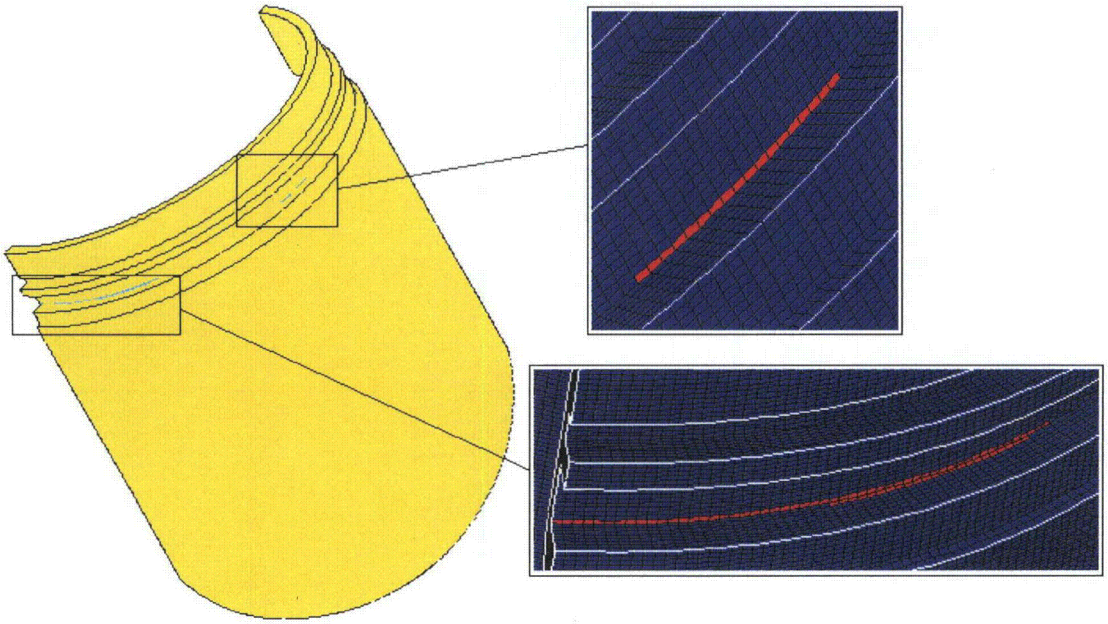

Figure 2-211. Plot of Elements Exceeding the Experimental Strain Locus for the 731-g, Angled, Plutonium Metal Hollow Cylinder, Far Side Position, Side Impact

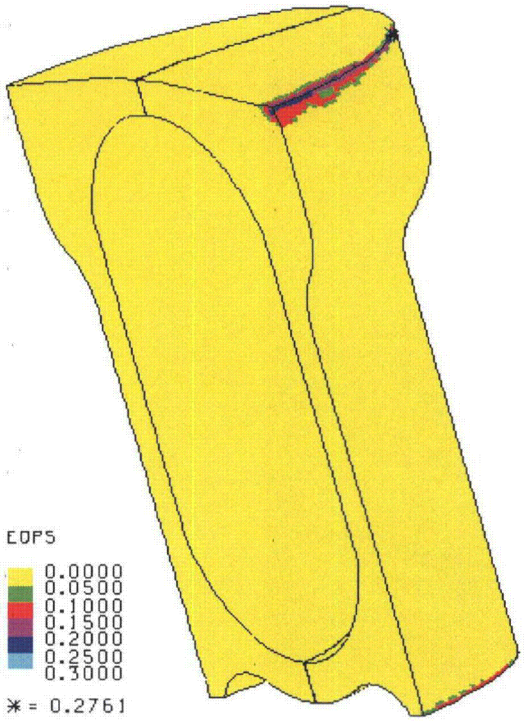

Figure 2-212. Plot of EQPS in the TB-1 for the 731-g, Angled, Plutonium Metal Hollow Cylinder, Far Side Position, Side Impact

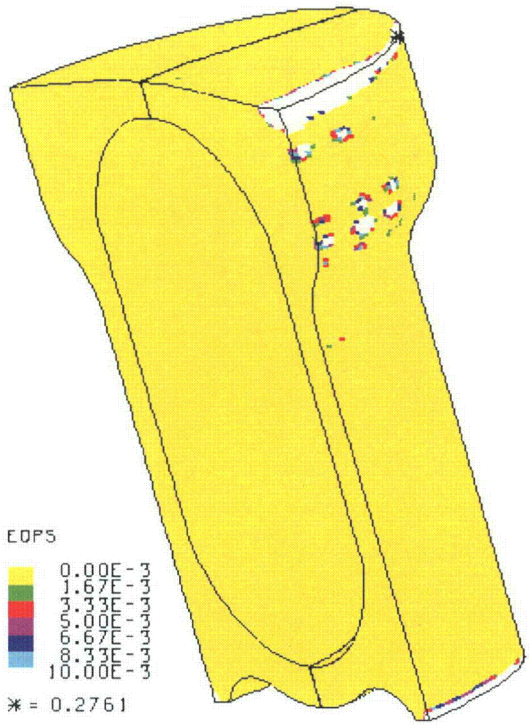

Figure 2-213. Plot of EQPS in the TB-1 for the 731-g, Angled, Plutonium Metal Hollow Cylinder, Far Side Position, Side Impact

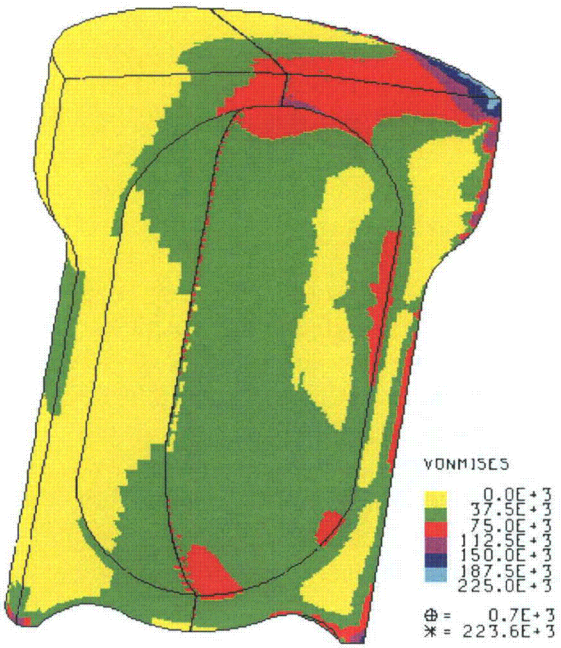

Figure 2-214. Plot of von Mises Stress in the TB-1 for the 731-g, Angled, Plutonium Metal Hollow Cylinder, Far Side Position, Side Impact

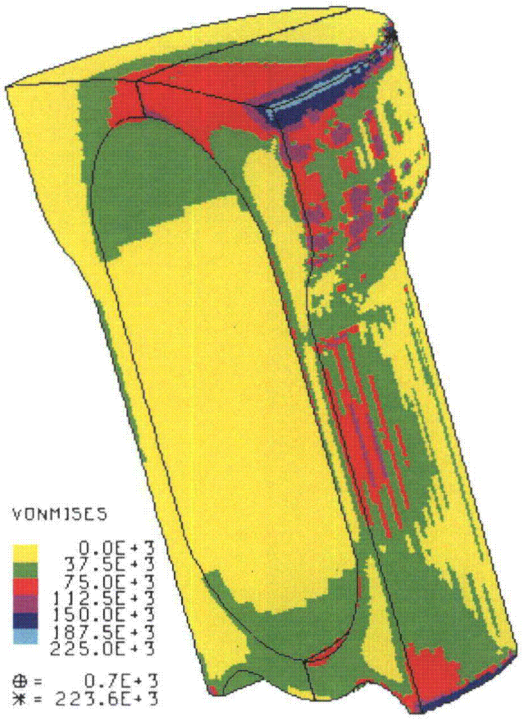

Figure 2-215. Plot of von Mises Stress in the TB-1 for the 731-g, Angled, Plutonium Metal Hollow Cylinder, Far Side Position, Side Impact

2.12.5.5 Sample Container Analyses

Seventeen separate sample container high speed impact analyses were conducted. The SC-1 (3 per cradle) sample containers can each contain 174 g solid cylinders of delta Pu or 60 g solid cylinders of Pu/Be composite. The larger SC-2 sample containers (2 per cradle) can contain 338 g solid cylinders of delta Pu each. Pu/Be composite payload is maximized using 3 SC-1 sample containers, so that case was analyzed as the bounding condition. There are several inherent conservatisms in the models:

1. In the sample containers, the tantalum foil used to package the cylinders inside the T-Ampoule is not modeled. The small quantity of energy it would absorb, and load spreading it would provide, is conservatively ignored. The sample container body is initially positioned with the Ti-6Al-4V support structure (inner cradle) and was shown in the NCT analyses to be unaltered after 4 ft. drops.

2. Although the plutonium contents are positioned using tantalum foil, no credit is taken for positioning the cylinder inside the sample container. Each analysis is run with the cylinder inside the ampoule positioned in a location farthest from the impact surface.

3. The Pu material is modeled using a power-law hardening constitutive model without fracture. The plutonium content of the sample containers is modeled as delta-plutonium, with material properties derived from Hecker and Stevens.[3] This material is very ductile; in order to maximize the energy and impulse load applied to the T-Ampoule wall, the

cylinder is modeled as a continuously hardened material model that does not fracture. Heavier alpha Pu density was assumed for the delta Pu to further decrease the cylinder size and increase its net impact velocity (for higher loads).

4. The beryllium composite material is modeled using a power-law hardening constitutive model without fracture. The Be composite content of the sample containers is conservatively modeled as delta-plutonium density (heavier and more compact than Be), yet higher material strength properties of Be. This material is very ductile; in order to maximize the energy and impulse load applied to the T-Ampoule wall, the cylinder is modeled as a continuously hardened material model that does not fracture. Heavier delta Pu density was assumed for the Be composite to further decrease the cylinder size and increase its net impact velocity (for higher loads).

5. The Be composite solid cylinders are always analyzed with their local orientation in a CG-over-corner fashion, so that their sharpest corner is presented to the SC wall and the T-Ampoule wall. This is not necessary for the much softer delta Pu cylinders.

6. The Pu and Be composite solid cylinders were dimensioned to represent the bounding configuration in terms of weight and size. They were sized to represent the worst-case for both impacting mass (maximizing the kinetic energy that needs to be absorbed by the T-Ampoule) and differential impact velocity between the cylinders and T-Ampoule.

7. The deformation of the sample container body does absorb a significant quantity of energy. To prevent the sample container body from absorbing an unrealistic quantity of energy, the Tearing Parameter failure criterion was implemented to limit the plastic deformation of the sample container and allow it to fracture. The fracture criterion, based on the work of Wellman,[4] was chosen for several reasons. First, the criterion works well for material in the high stress triaxiality region, which is the region where large bending stresses in the ampoule shell will lie. Second, the failure model has been implemented in the PRONTO-3D finite element code. Finally, the failure parameter can be determined from a tensile test model. Details of this model are presented in Section ~~2.12.3.7.~~ 2.12.3.8.

2.12.5.5.1 Run 11 - SC-1, Top Impact, Pu Contents

The top end impact model for each SC-1 with delta Pu contents is shown in Figure 2-216. Note that each Pu cylinder is located at the bottom of each SC-1 so that its net impact velocity with the top of the T-Ampoule is maximized. The post-impact deformation is shown in Figure 2-217 and its kinetic energy history in Figure 2-218. Note the similar degree of overpack crush up as compared to the certification test end impact in Figure 2-12, despite the slightly reduced impact velocity of 422 ft/sec versus the tested 445 ft/sec. The top SC-1 is crushed from the subsequent impacts of lower SC-1's, and its Pu contents nearly penetrate its upper wall, which directly impacts the T-Ampoule.

Equivalent Plastic Strain (EQPS) in the TB-1 containment vessel is shown, in Figure 2-219, to be less than 7.5% and exists only in some localized outer contact regions with the redwood overpack. The von Mises stresses (see Figure 2-220) peak at 147.1 ksi is just above the elevated-temperature minimum yield strength for the TB-1 of 141 ksi but more importantly, through-

thickness TB-1 stress values are in the less-than-27.5 ksi range, below yield. The time at which

the peak value of the von Mises stress occurs coincides with the peak value of the contact force (summed over the lid area). A plot of this force as a function of time is shown in Figure 2-221. A maximum contact load of 27,874 lbs is applied to the inner surface of the TB-1 lid during the impact. No T-Ampoule elements exceeded the tested B-W strain locus and the peak Tearing Parameter value (see Table 2-11, run #11) of 0.0319 was below the critical Tearing Parameter value of 1.012 for Ti-6Al-4V.

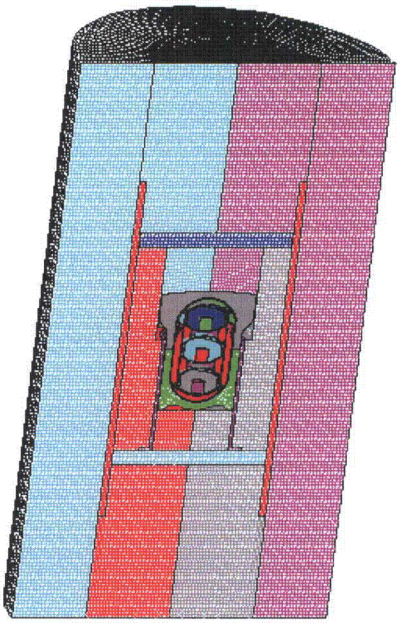

Figure 2-216. Finite Element Mesh for the SC-1, Pu Contents, End Impact

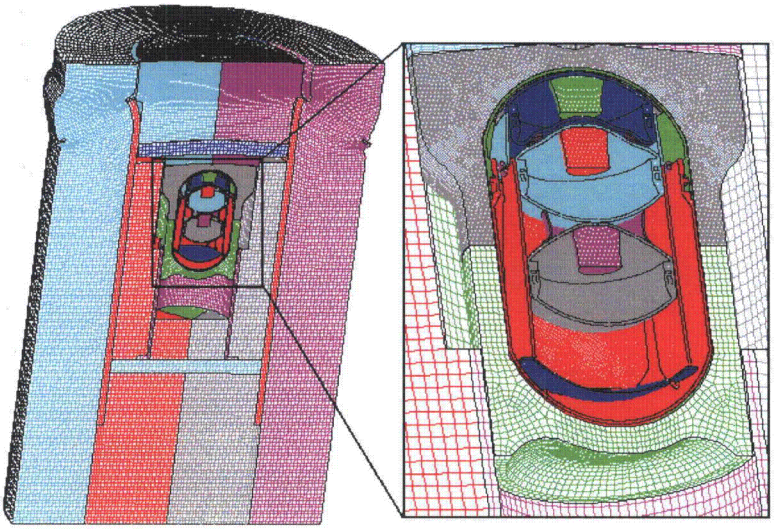

Figure 2-217. Finite Element Mesh for the SC-1, Pu Contents, End Impact – Final Displacement

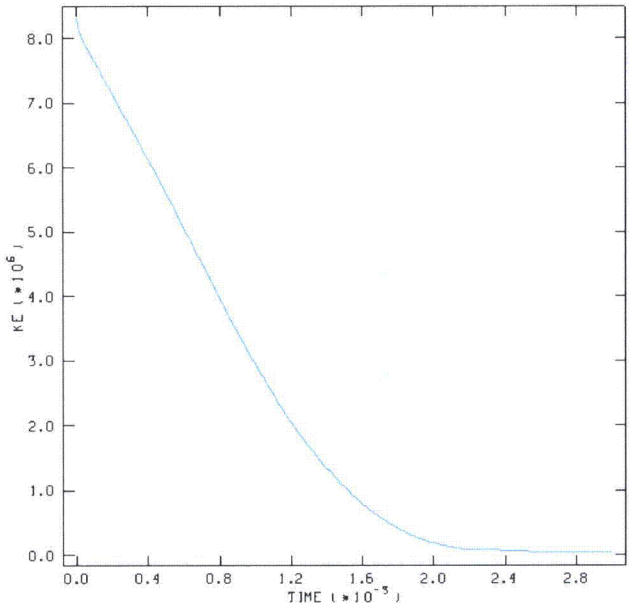

Figure 2-218. Kinetic Energy Time History for the SC-1, Pu Contents, End Impact

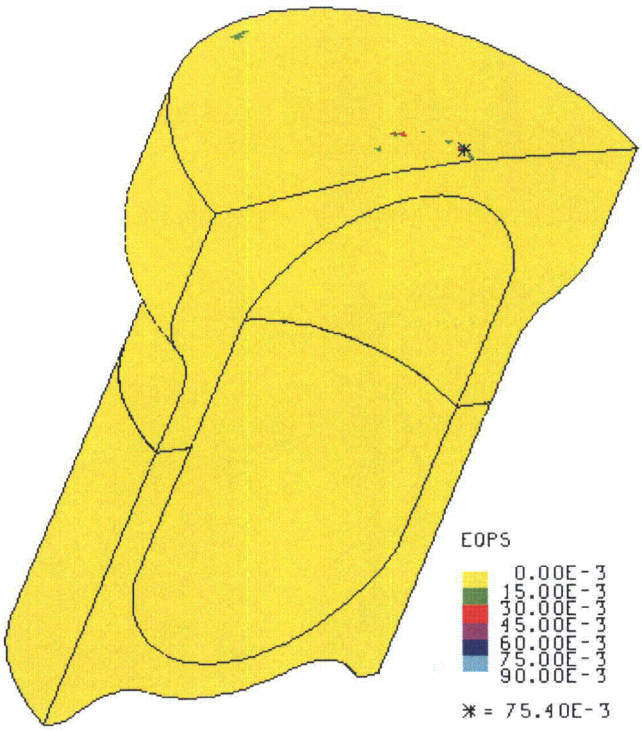

Figure 2-219. Plot of EQPS in the TB-1 for the SC-1, Pu Contents, End Impact

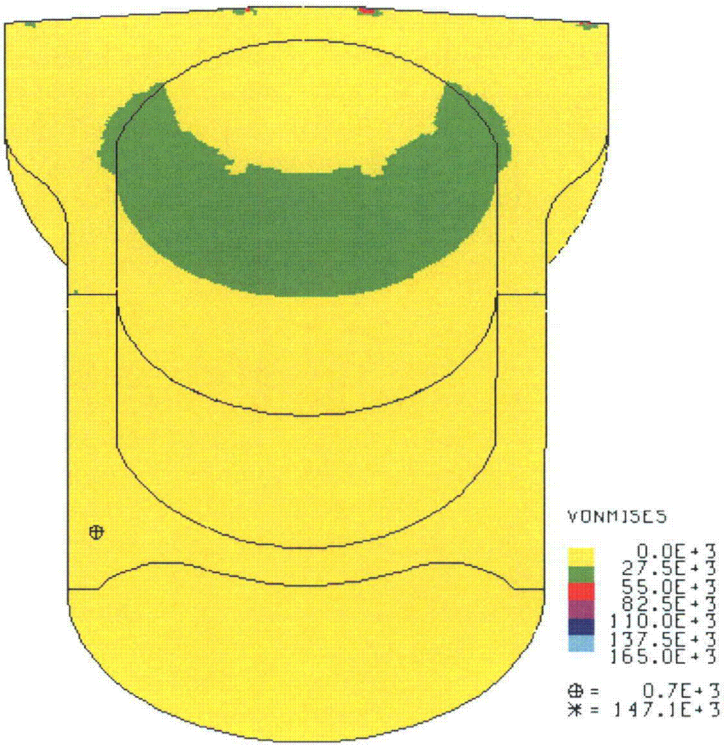

Figure 2-220. Plot of von Mises Stress in the TB-1 for the SC-1, Pu Contents, End Impact

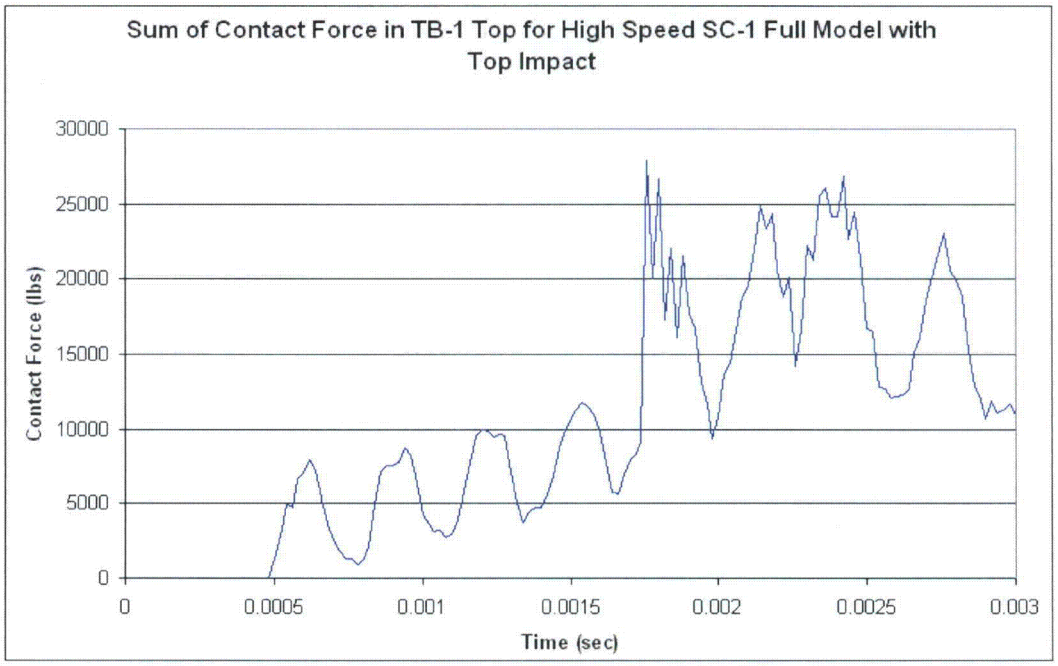

Figure 2-221. Plot of Contact Force in the TB-1 for the SC-1, Pu Contents, End Impact

2.12.5.5.2 Run 12 - SC-1 Sample Container, Side Impact, Support Structure 0°, Pu Contents

The side impact model for each SC-1 with delta Pu contents (cradle rotated 0 degrees) is shown in Figure 2-222. Note that each Pu cylinder is located at the far left side of each SC-1 so that its net impact velocity with the right side of the T-Ampoule is maximized. The post-impact deformation is shown in Figure 2-223 and its kinetic energy history in Figure 2-224. Note the similar degree of overpack crush up as compared to the certification test side impact in Figure 2-15, despite the slightly reduced impact velocity of 422 ft/sec versus the tested 445 ft/sec. The Pu contents penetrate each of the SC-1 side walls and directly impact the T-Ampoule.

Average stress-triaxiality versus EQPS is shown in Figure 2-225 for the 52 elements extending beyond the tested Bao-Wierzbicki strain locus. All of these elements are outside the B-W locus, for a variety of stress triaxialities, although most of the 580,000 T-Ampoule elements are inside the B-W locus. The Tearing Parameter values for these same 52 elements are shown in Figure 2-226 and all are below the critical Tearing Parameter value of 1.012 for Ti-6Al-4V. These elements are highlighted in red in Figures 2-227, 2-228, and 2-229, but note that these elements are still below the initiation of a ductile tear and thus T-Ampoule integrity is maintained.

Equivalent Plastic Strain (EQPS) in the TB-1 vessel is shown in Figures 2-230, 2-231, 2-232, and 2-233 to be less than 45% but only in some localized outer contact regions with the redwood overpack (contact modeling artifact). The EQPS due to internal denting of the upper SC-1 is shown in Figure 2-232 to be less than 0.01%, which is essentially elastic. The von Mises stresses (see Figure 2-234) peak at 273.5 ksi, above the elevated-temperature minimum yield strength for the TB-1 of 141 ksi but more importantly, through-thickness TB-1 stress values are in the less-than-47.5 ksi range, below yield.

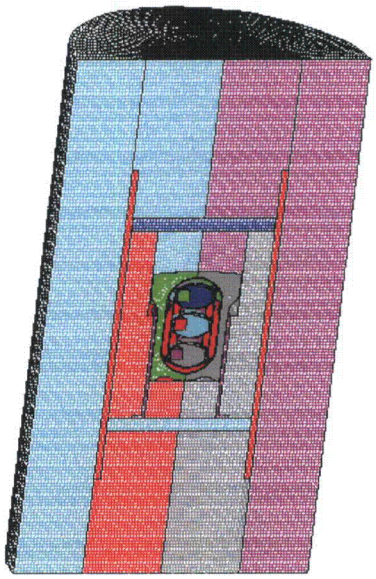

Figure 2-222. Finite Element Mesh for the SC-1, Pu Contents, Side Impact, 0° Support Structure

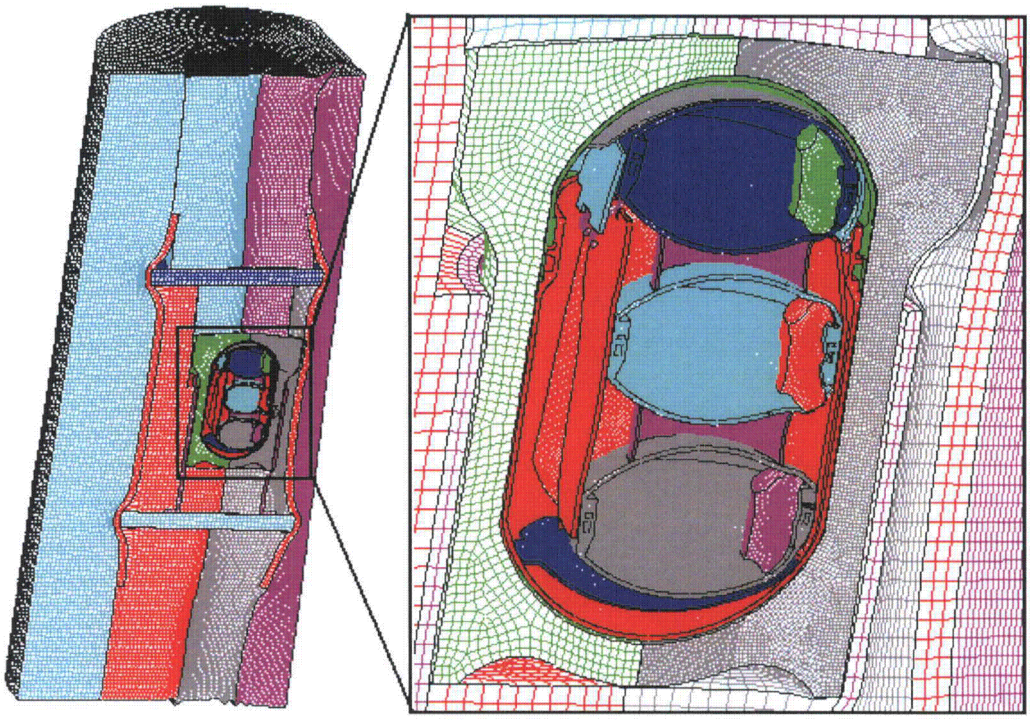

Figure 2-223. Finite Element Mesh for the SC-1, Pu Contents, Side Impact, 0° Support Structure – Final Displacement

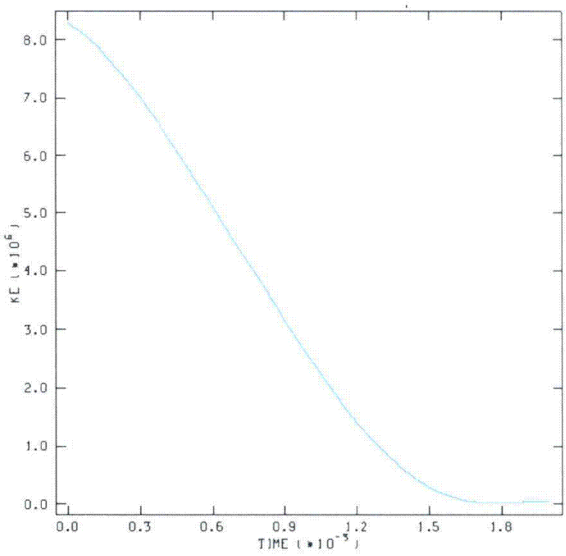

Figure 2-224. Kinetic Energy Time History for the SC-1, Pu Contents, Side Impact, 0° Support Structure

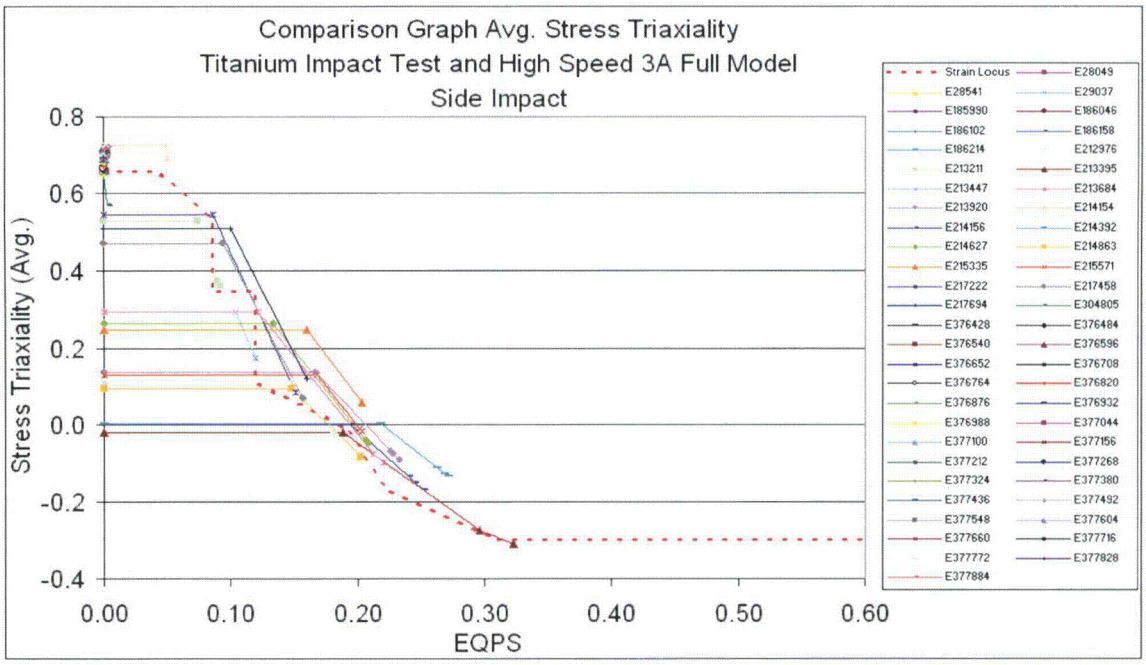

Figure 2-225. Graph of Average Stress Triaxiality versus EQPS of Elements Exceeding the Experimental Strain Locus for the SC-1, Pu Contents, Side Impact, 0° Support Structure

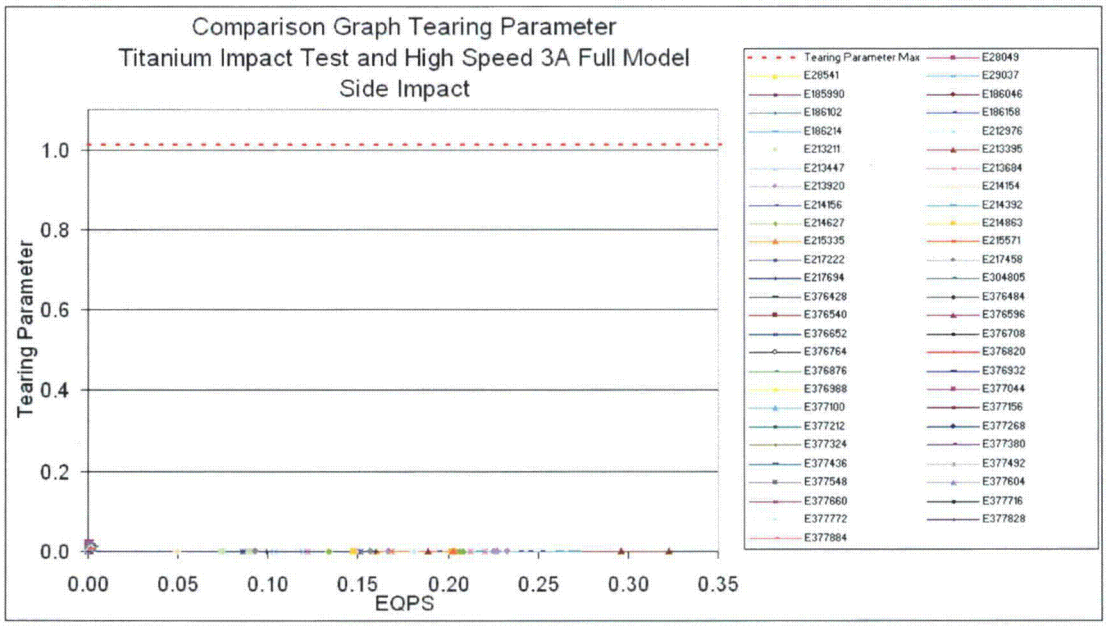

Figure 2-226. Graph of Tearing Parameter versus EQPS of Elements Exceeding the Experimental Strain Locus for the SC-1, Pu Contents, Side Impact, 0° Support Structure

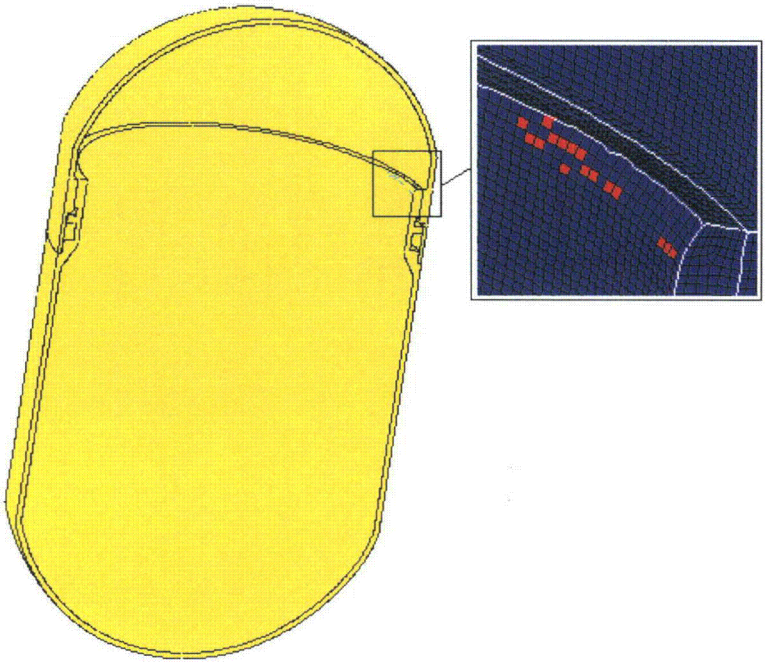

Figure 2-227. Plot of Elements Exceeding the Experimental Strain Locus for the SC-1, Pu Contents, Side Impact, 0° Support Structure

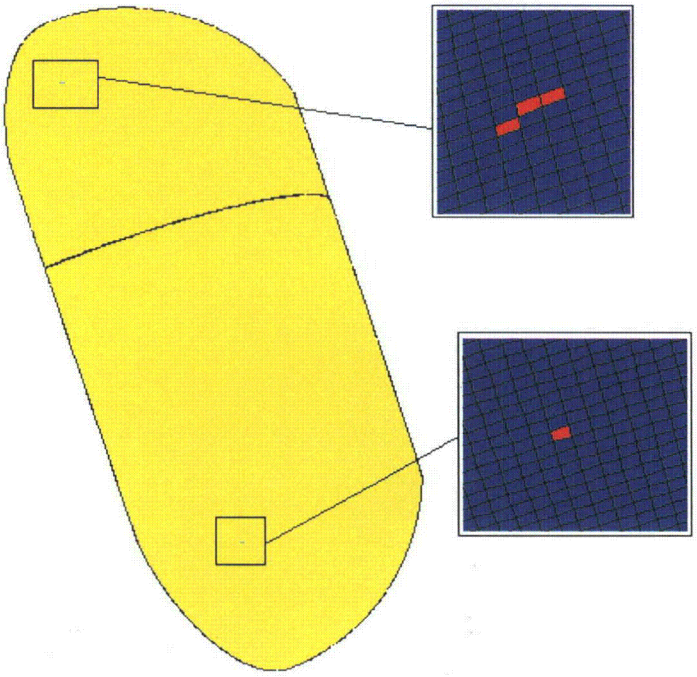

Figure 2-228. Plot of Elements Exceeding the Experimental Strain Locus for the SC-1, Pu Contents, Side Impact, 0° Support Structure

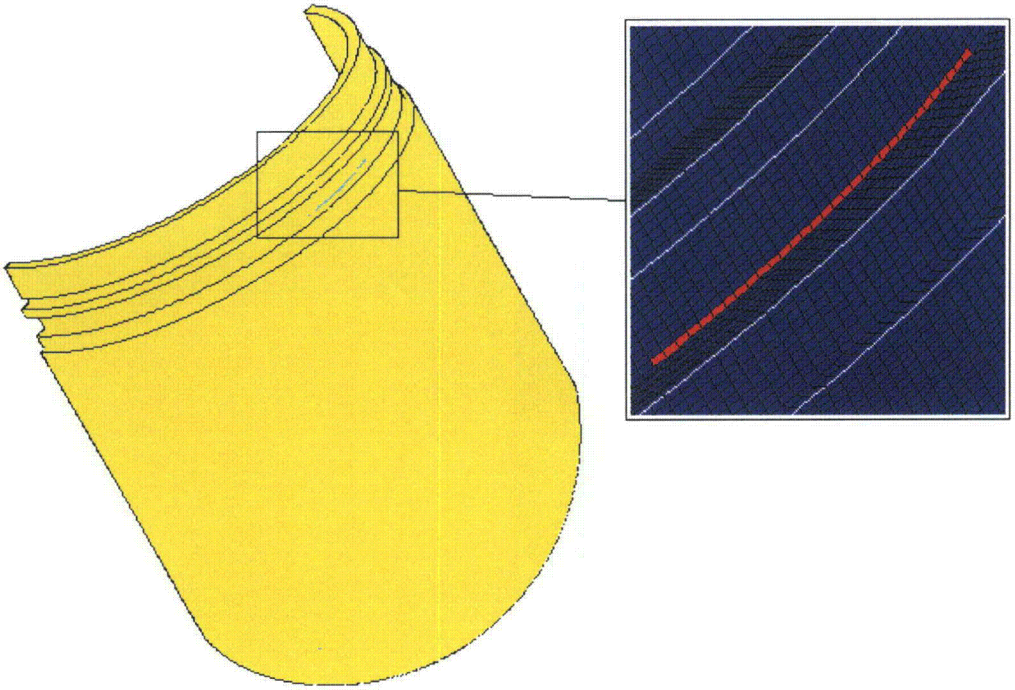

Figure 2-229. Plot of Elements Exceeding the Experimental Strain Locus for the SC-1, Pu Contents, Side Impact, 0° Support Structure

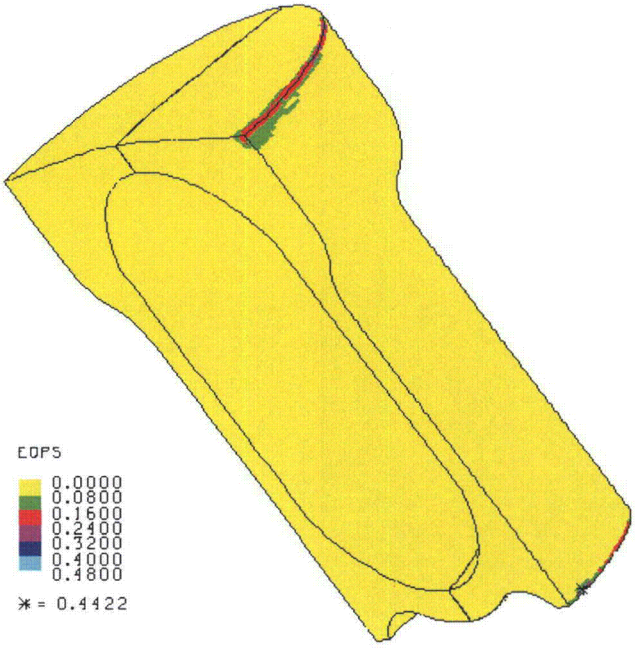

Figure 2-230. Plot of EQPS in the TB-1 for the SC-1, Pu Contents, Side Impact, 0° Support Structure

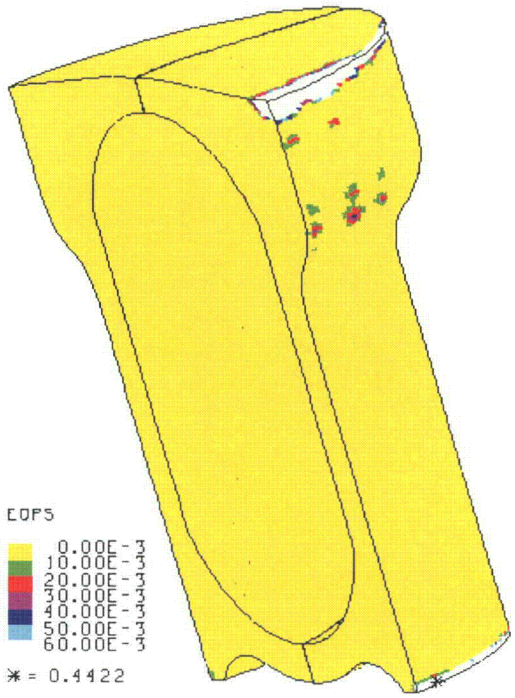

Figure 2-231. Plot of EQPS in the TB-1 for the SC-1, Pu Contents, Side Impact, 0° Support Structure

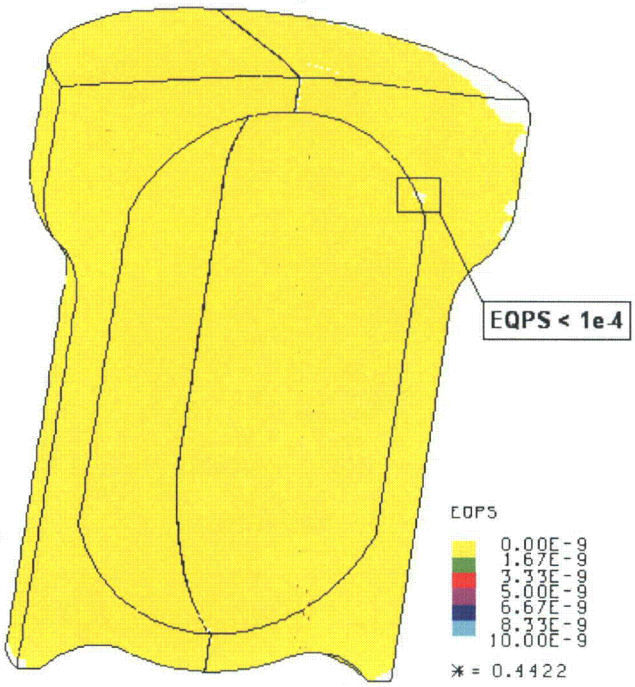

Figure 2-232. Plot of EQPS in the TB-1 for the SC-1, Pu Contents, Side Impact, 0° Support Structure

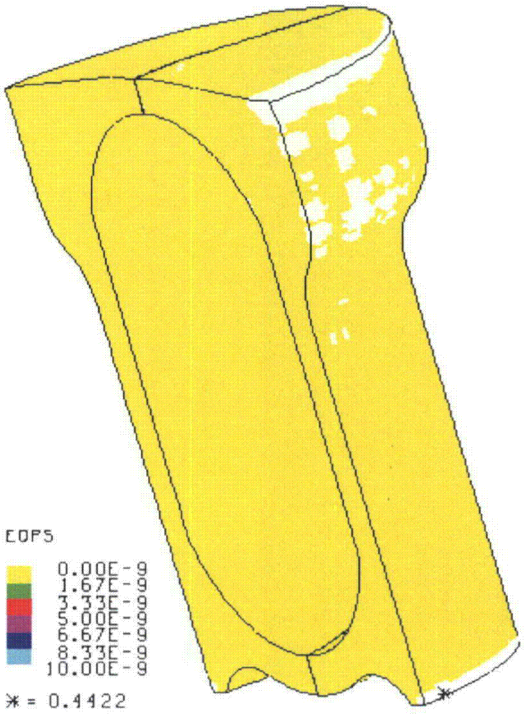

Figure 2-233. Plot of EQPS in the TB-1 for the SC-1, Pu Contents, Side Impact, 0° Support Structure

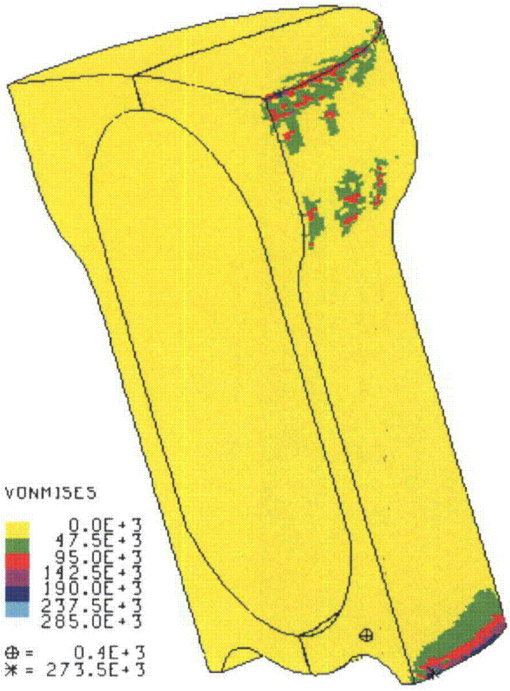

Figure 2-234. Plot of von Mises Stress in the TB-1 for the SC-1, Pu Contents, Side Impact, 0° Support Structure

2.12.5.5.3 Run 13 – SC-1, Side Impact, Support Structure 45°, Pu Contents

The side impact model for each SC-1 with delta Pu contents (cradle rotated 45 degrees to evaluate effect of sharp edges being pinched) is shown in Figure 2-235. Each Pu cylinder is located at the far left side of each SC-1 so that its net impact velocity with the right side of the T-Ampoule is maximized. The post-impact deformation is shown in Figure 2-236 and its kinetic energy history in Figure 2-237 indicating the container has begun to bounce and thus, peak loading has already occurred. In side impacts, the Pu contents penetrate each of the SC-1 side walls and directly impact the T-Ampoule.

Average stress-triaxiality versus EQPS is shown in Figure 2-238 for the 7 elements extending beyond the tested Bao-Wierzbicki strain locus. All of these elements are outside the B-W locus, for a variety of stress triaxialities, although most of the 580,000 T-Ampoule elements are inside the B-W locus. The Tearing Parameter values for these same 7 elements are shown in Figure 2-239, and all are below the critical Tearing Parameter value of 1.012 for Ti-6Al-4V. These elements are highlighted in red in Figures 2-240 and 2-241. Some localized crease-like deformations in Figure 2-240 are indicative of a slight contact issue, but these red elements (and all ~580,000 T-Ampoule elements) are still below the initiation of a ductile tear and thus, T-Ampoule integrity is maintained.

Equivalent Plastic Strain (EQPS) in the TB-1 vessel is shown in Figures 2-242 through 2-245 to be less than 31% but only in some localized outer contact regions with the redwood overpack. The EQPS due to internal denting of the upper SC-1 is shown in Figure 2-243 to be less than 0.017%, which is essentially elastic. The von Mises stresses (see Figure 2-246) peak at 230 ksi is above the elevated-temperature minimum yield strength for the TB-1 of 141 ksi but more importantly, through-thickness TB-1 stress values are in the less-than-120 ksi range, which is below yielding.

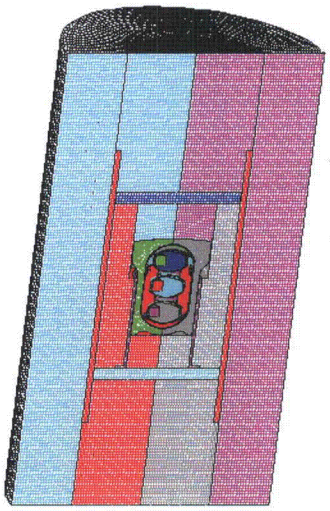

Figure 2-235. Finite Element Mesh for the SC-1, Pu Contents, Side Impact, 45° Support Structure

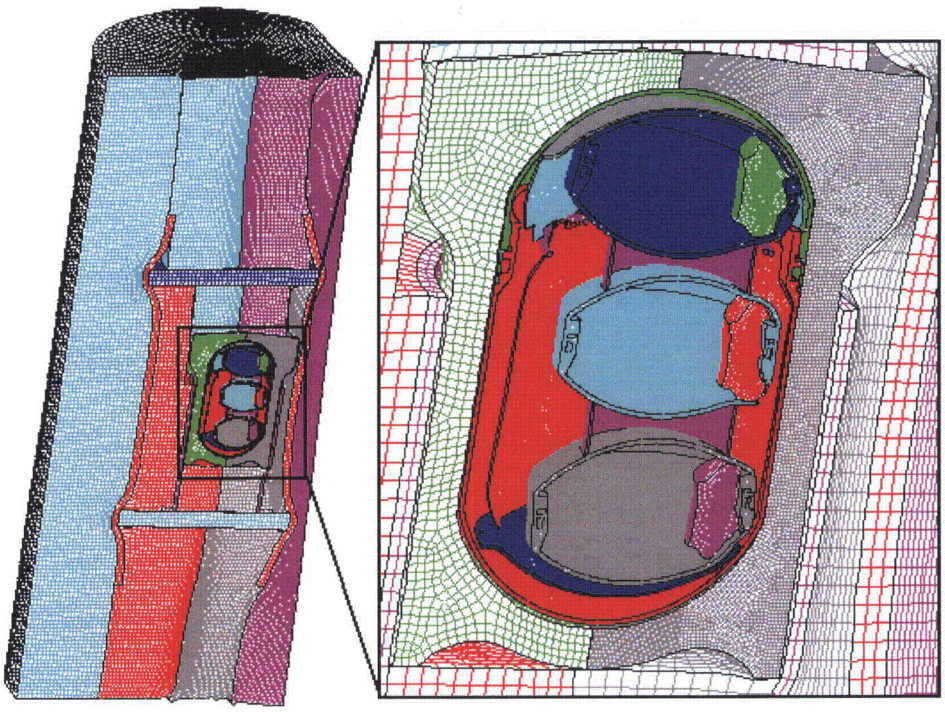

Figure 2-236. Finite Element Mesh for the SC-1, Pu Contents, Side Impact, 45° Support Structure – Final Displacement

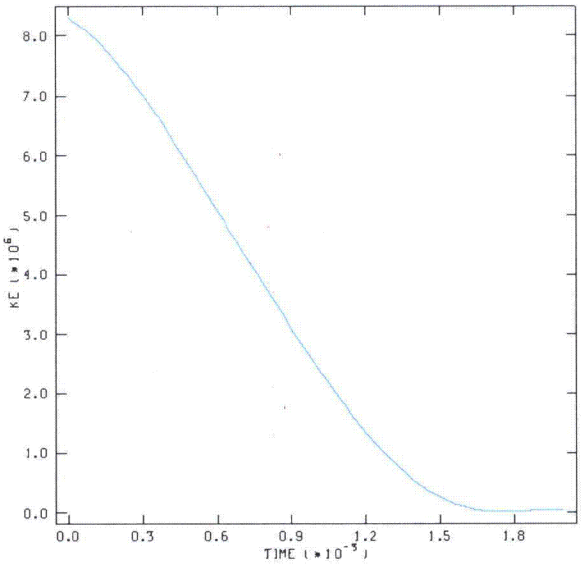

Figure 2-237. Kinetic Energy Time History for the SC-1, Pu Contents, Side Impact, 45° Support Structure

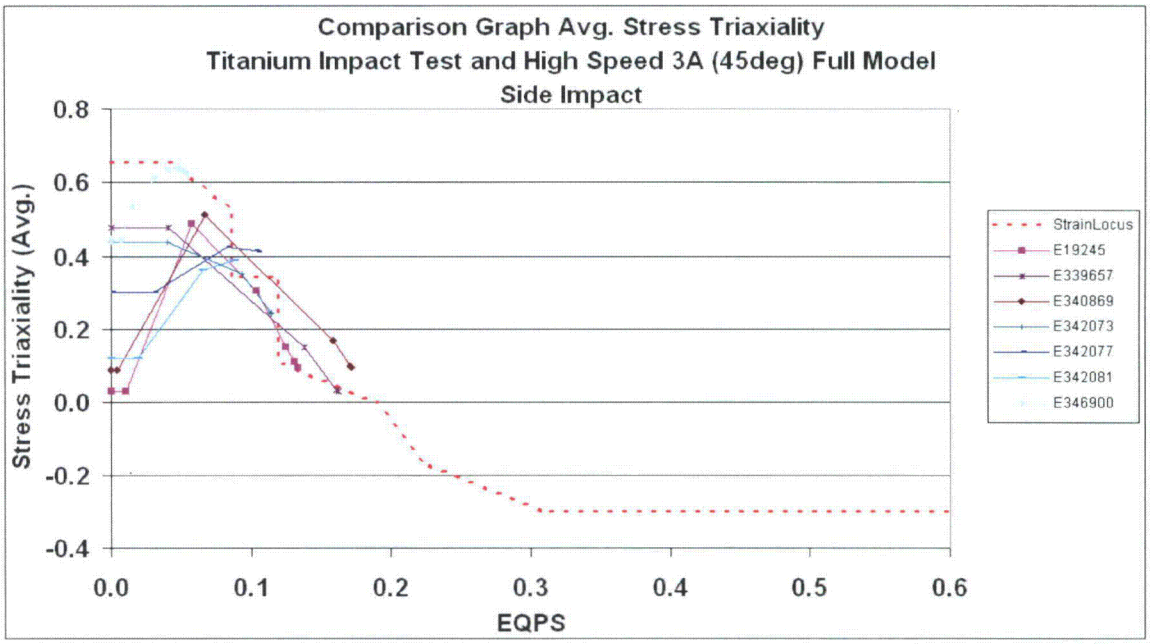

Figure 2-238. Graph of Average Stress Triaxiality versus EQPS of Elements Exceeding the Experimental Strain Locus for the SC-1, Pu Contents, Side Impact, 45° Support Structure

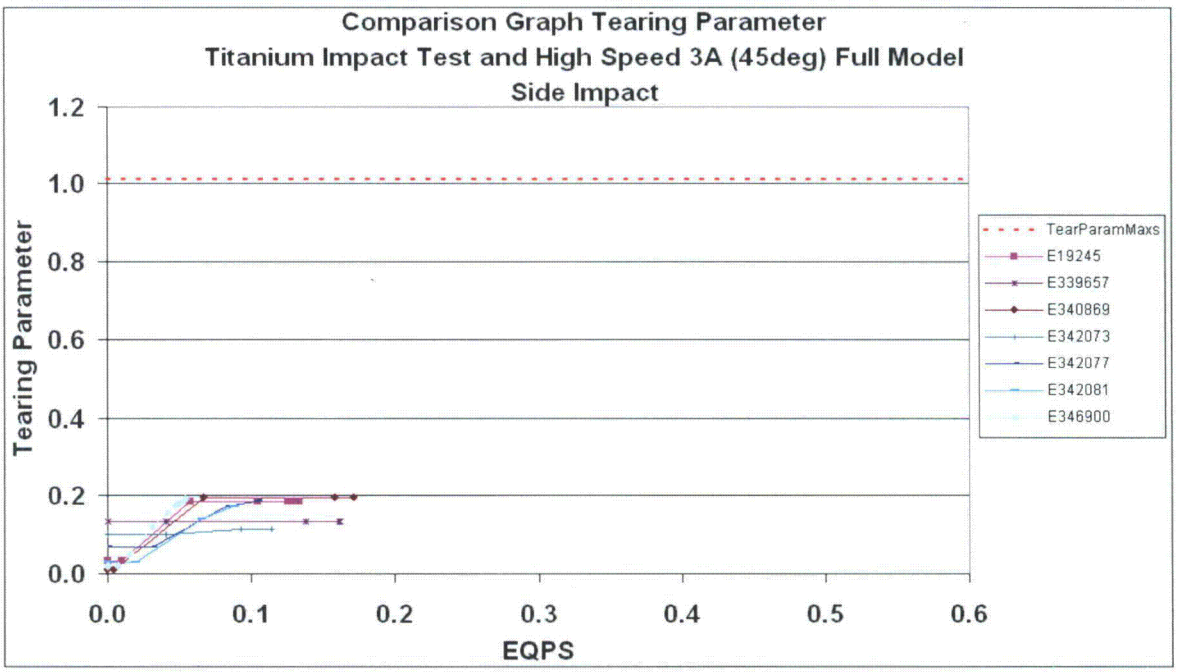

Figure 2-239. Graph of Tearing Parameter versus EQPS of Elements Exceeding the Experimental Strain Locus for the SC-1, Pu Contents, Side Impact, 45° Support Structure

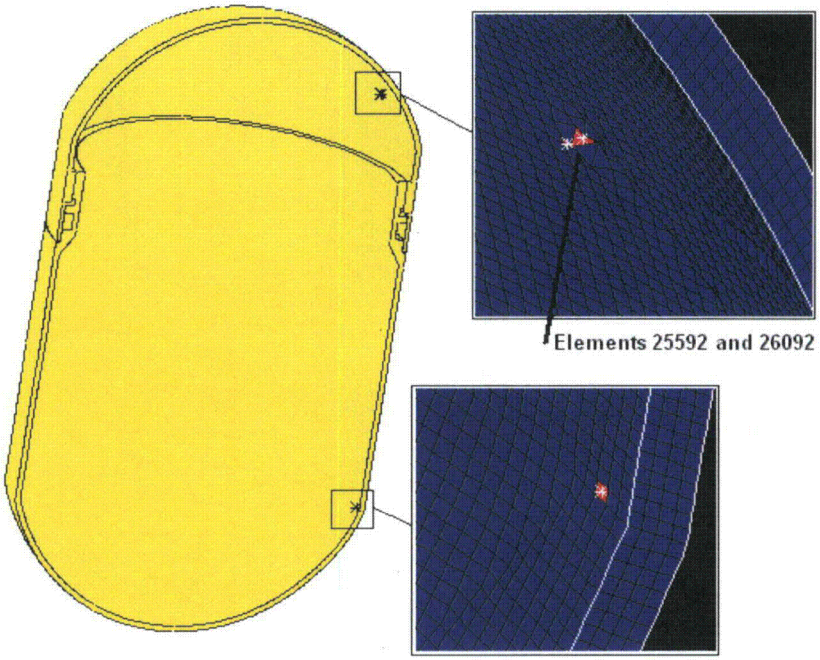

Figure 2-240. Plot of Elements Exceeding the Experimental Strain Locus for the SC-1, Pu Contents, Side Impact, 45° Support Structure

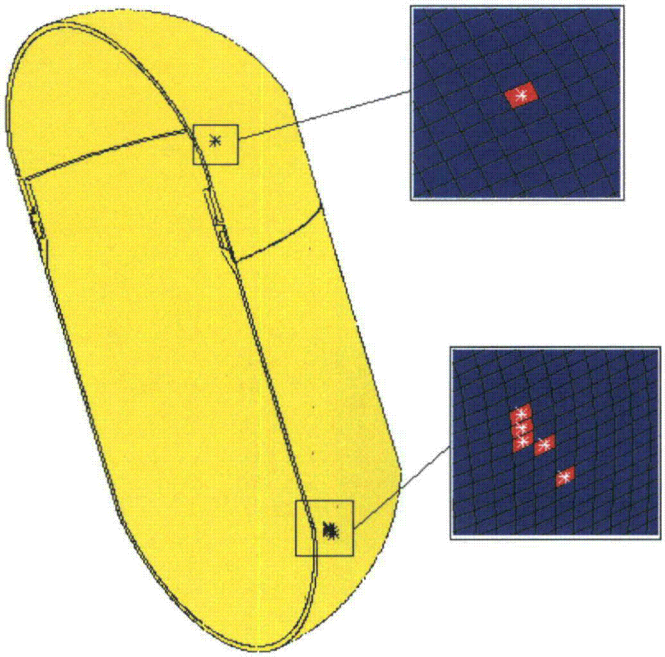

Figure 2-241. Plot of Elements Exceeding the Experimental Strain Locus for the SC-1, Pu Contents, Side Impact, 45° Support Structure

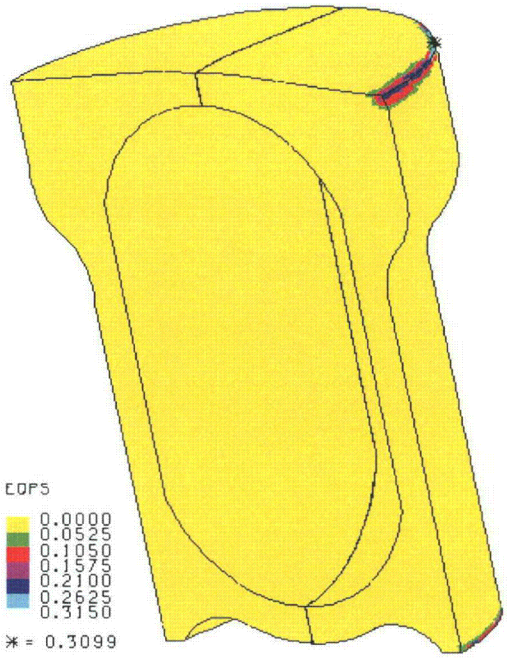

Figure 2-242. Plot of EQPS in the TB-1 for the SC-1, Pu Contents, Side Impact, 45° Support Structure

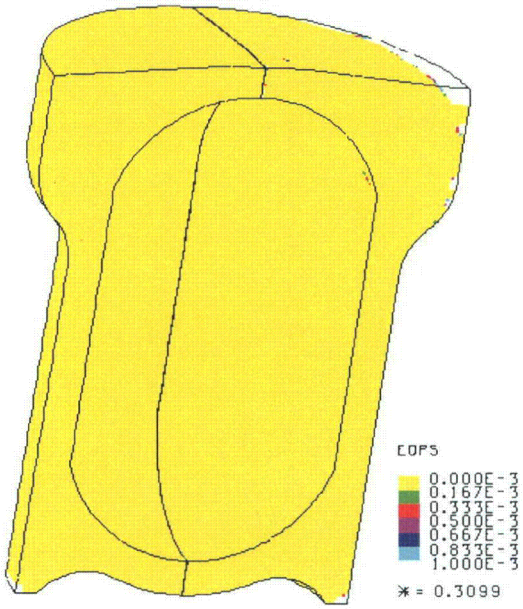

Figure 2-243. Plot of EQPS in the TB-1 for the SC-1, Pu Contents, Side Impact, 45° Support Structure

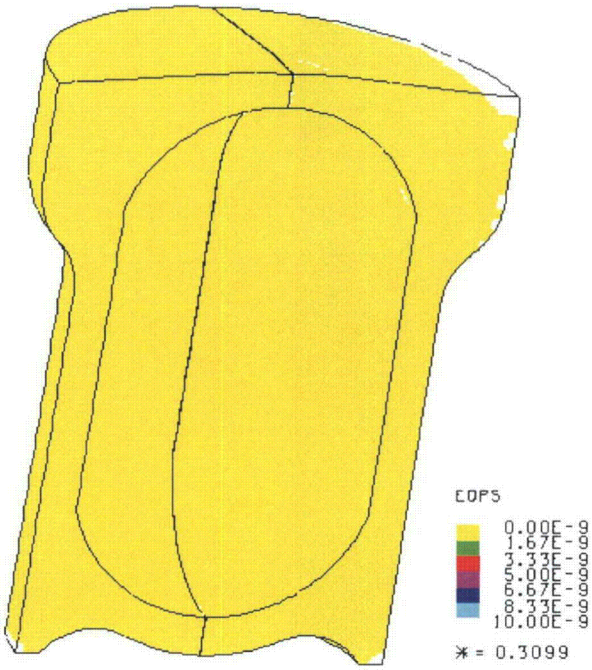

Figure 2-244. Plot of EQPS in the TB-1 for the SC-1, Pu Contents, Side Impact, 45° Support Structure

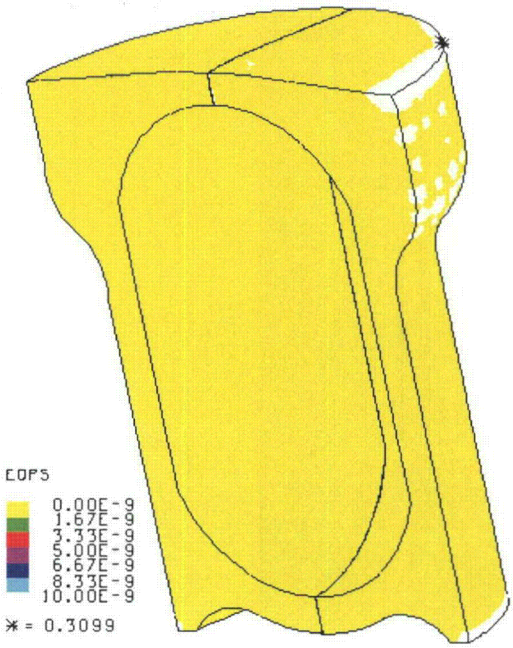

Figure 2-245. Plot of EQPS in the TB-1 for the SC-1, Pu Contents, Side Impact, 45° Support Structure

Figure 2-246. Plot of von Mises Stress in the TB-1 for the SC-1, Pu Contents, Side Impact, 45° Support Structure

2.12.5.5.4 Run 14 – SC-1, CGOC Impact, Pu Contents, Support Structure 0°

The lid end CG-over-corner impact model for each SC-1 with delta Pu contents (cradle rotated 0 degrees) is shown in Figure 2-247. Each Pu cylinder is located at the rotated bottom of each SC-1 so that its net impact velocity with the top of the T-Ampoule is maximized. The post-impact deformation is shown in Figure 2-248 and its kinetic energy history in Figure 2-249. Note the similar degree of overpack crush up as compared to the certification test corner impact in Figure 2-18, despite the slightly reduced impact velocity of 422 ft/sec versus the tested 445 ft/sec. The Pu cylinder contents remain largely confined within each SC-1, although significant localized deformation of the SC-1 has occurred.

Equivalent Plastic Strain (EQPS) in the TB-1 vessel is shown in Figures 2-250 and 2-251 to peak at about 27% but only in some localized outer contact regions with the redwood overpack. The von Mises stresses (see Figure 2-252) peak at 163.1 ksi is just above the elevated-temperature minimum yield strength for the TB-1 of 141 ksi but more importantly, through-thickness TB-1 stress values are in the less-than-25 ksi range, below yield. The time at which the peak value of the von Mises stress occurs coincides with the peak value of the contact force (summed over the lid area). A plot of this force as a function of time is shown in Figure 2-253. A maximum contact load of 14,225 lbs is applied to the inner surface of the TB-1 lid during the impact. No T-Ampoule elements exceeded the tested B-W strain locus and the peak Tearing Parameter value (see Table 2-11, run #14) of 0.0935 was below the critical Tearing Parameter value of 1.012 for Ti-6Al-4V.

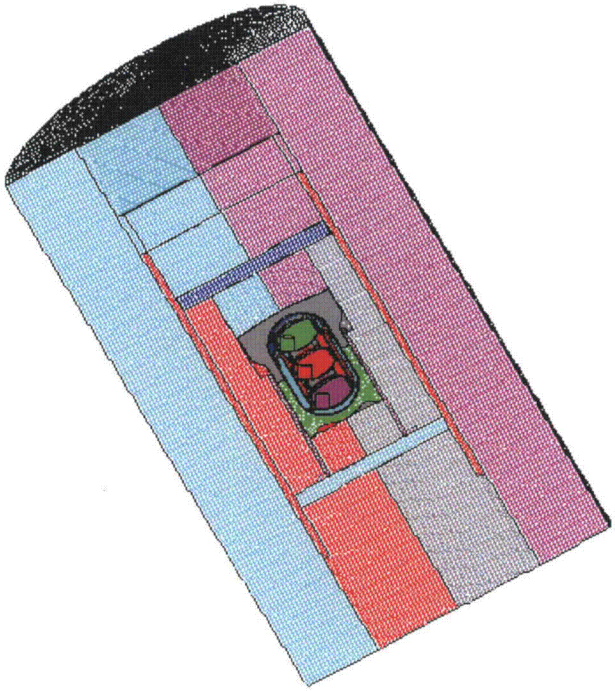

Figure 2-247. Finite Element Mesh for the SC-1, Pu Contents, CGOC Impact, 0° Support Structure

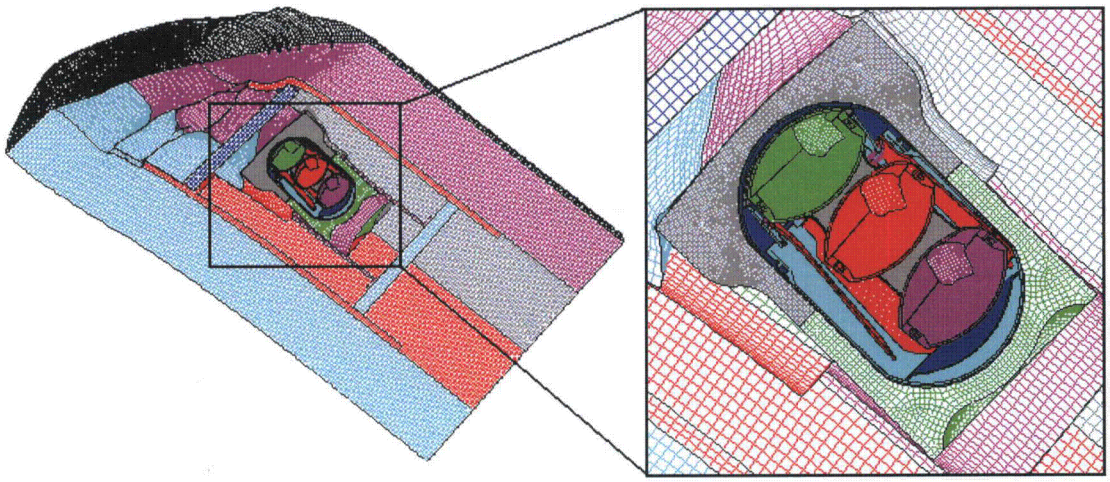

Figure 2-248. Finite Element Mesh for the SC-1, Pu Contents, CGOC Impact, 0° Support Structure – Final Displacement

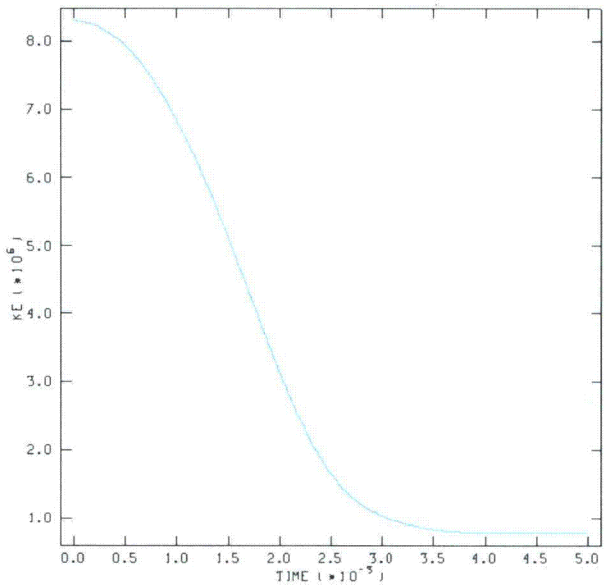

Figure 2-249. Kinetic Energy Time History for the SC-1, Pu Contents, CGOC Impact, 0° Support Structure

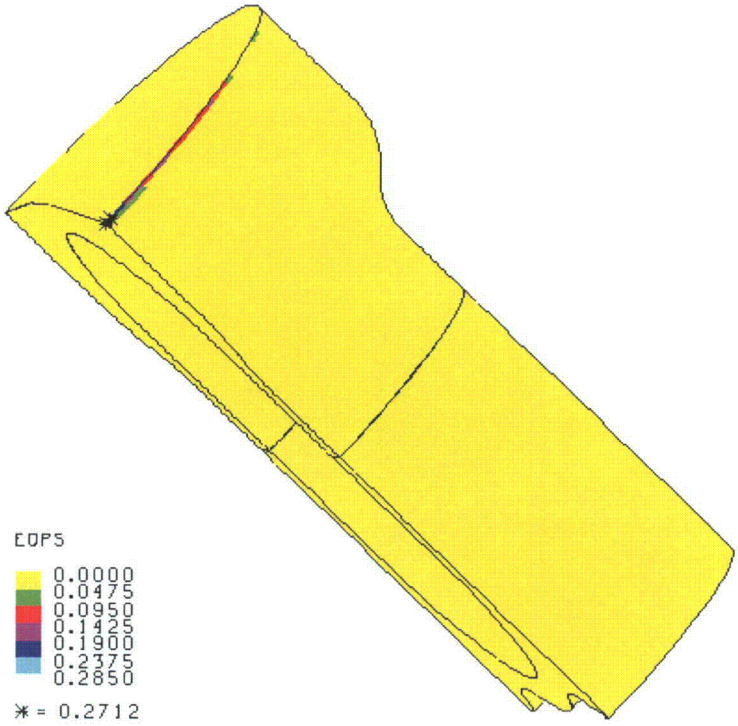

Figure 2-250. Plot of EQPS in the TB-1 for the SC-1, Pu Contents, CGOC Impact, 0° Support Structure

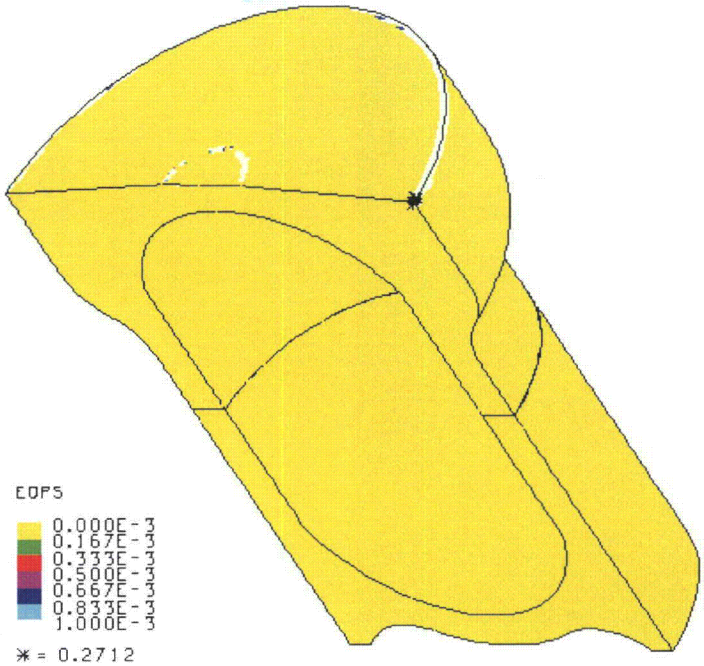

Figure 2-251. Plot of EQPS in the TB-1 for the SC-1, Pu Contents, CGOC Impact, 0° Support Structure

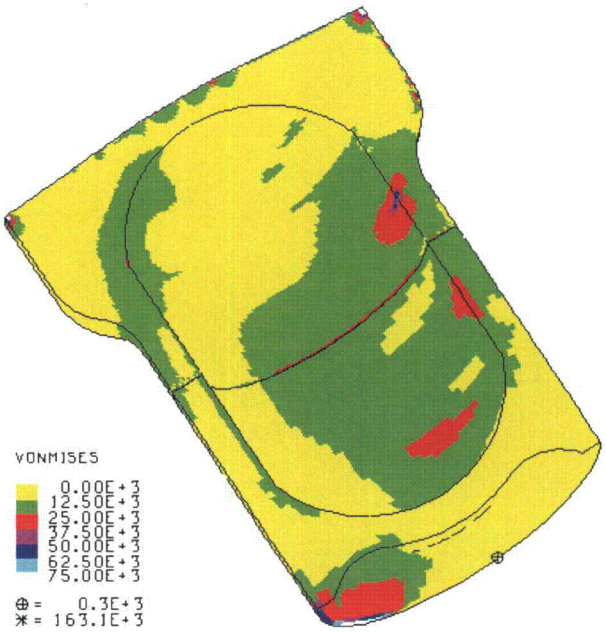

Figure 2-252. Plot of von Mises Stress in the TB-1 for the SC-1, Pu Contents, CGOC Impact, 0° Support Structure

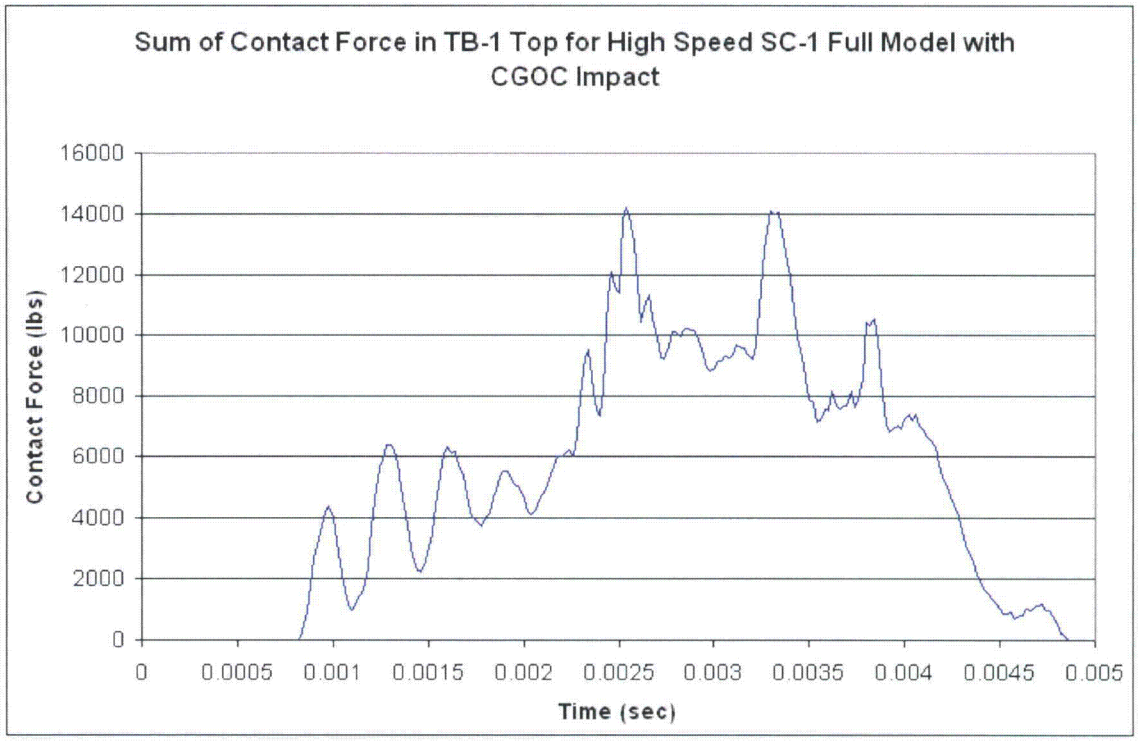

Figure 2-253. Plot of Contact Force in the TB-1 for the SC-1, Pu Contents, CGOC Impact, 0° Support Structure

2.12.5.5.5 Run 15 – SC-1, CGOC Impact, Pu Contents, Support Structure 45°

The lid end CG-over-corner impact model for each SC-1 with delta Pu contents (cradle rotated 45 degrees) is shown in Figure 2-254. Each Pu cylinder is located at the rotated bottom of each SC-1 so that its net impact velocity with the top of the T-Ampoule is maximized. The post-impact deformation is shown in Figure 2-255 and its kinetic energy history in Figure 2-256. The Pu cylinder contents remain largely confined within each SC-1, although significant localized deformation of the SC-1 has occurred.

Equivalent Plastic Strain (EQPS) in the TB-1 vessel is shown in Figures 2-257 and 2-258 to peak at about 21% but only in some localized outer contact regions with the redwood overpack. The von Mises stresses (see Figure 2-259) peak locally due to redwood contacts at 230 ksi, above the elevated-temperature minimum yield strength for the TB-1 of 141 ksi but more importantly, through-thickness TB-1 stress values are in the 80 ksi range, which is below yield. The time at which the peak value of the von Mises stress occurs coincides with the peak value of the contact force (summed over the lid area). A plot of this force as a function of time is shown in Figure 2-260. A maximum contact load of less than 15,613 lbs is applied to the inner surface of the TB-1 lid during the impact. No T-Ampoule elements exceeded the tested B-W strain locus, and the peak Tearing Parameter value (see Table 2-11, run #15) of 0.3061 was below the critical Tearing Parameter value of 1.012 for Ti-6Al-4V; thus T-Ampoule integrity was maintained.

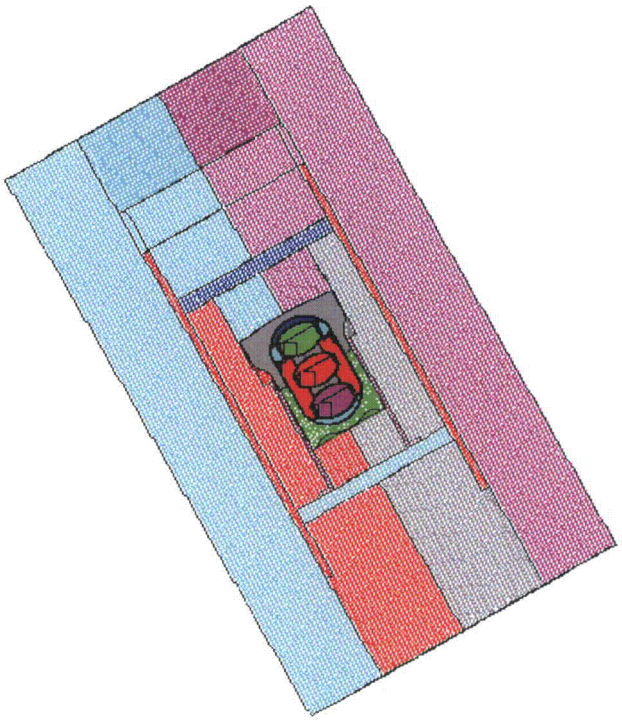

Figure 2-254. Finite Element Mesh for the SC-1, Pu Contents, CGOC Impact, 45° Support Structure

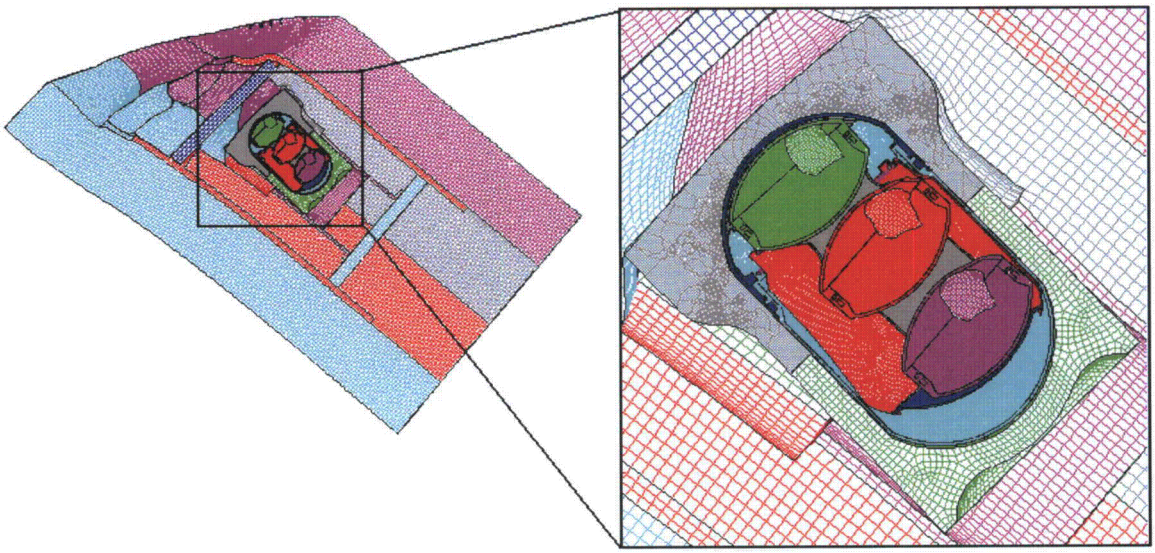

Figure 2-255. Finite Element Mesh for the SC-1, Pu Contents, CGOC Impact, 45° Support Structure – Final Displacement

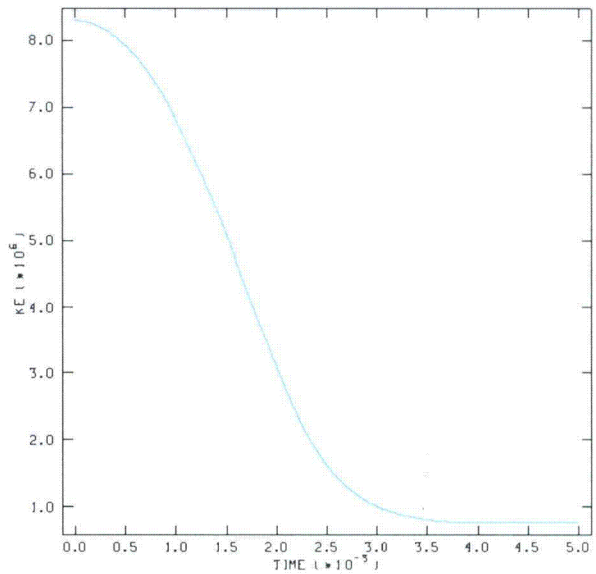

Figure 2-256. Kinetic Energy Time History for the SC-1, Pu Contents, CGOC Impact, 45° Support Structure

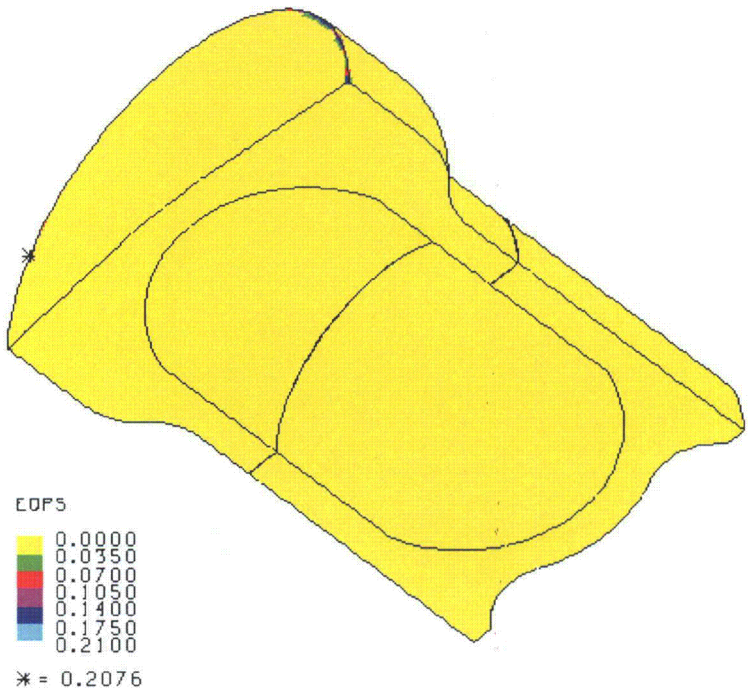

Figure 2-257. Plot of EQPS in the TB-1 for the SC-1, Pu Contents, CGOC Impact, 45° Support Structure

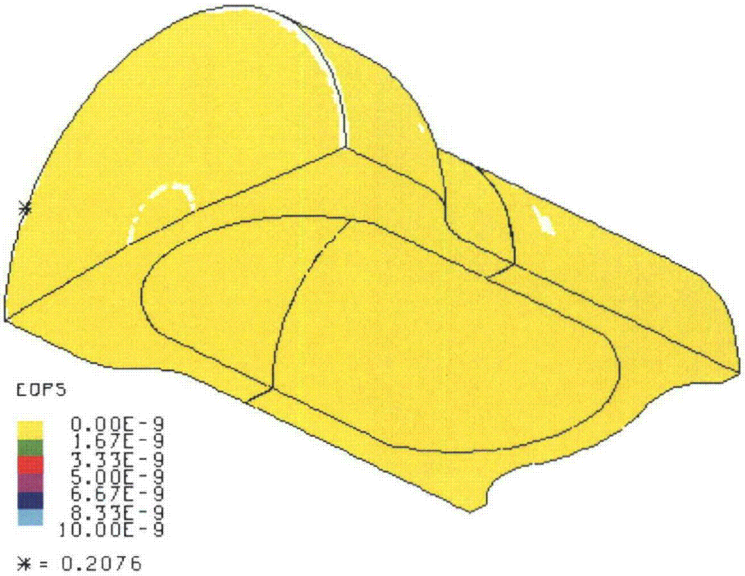

Figure 2-258. Plot of EQPS in the TB-1 for the SC-1, Pu Contents, CGOC Impact, 45° Support Structure

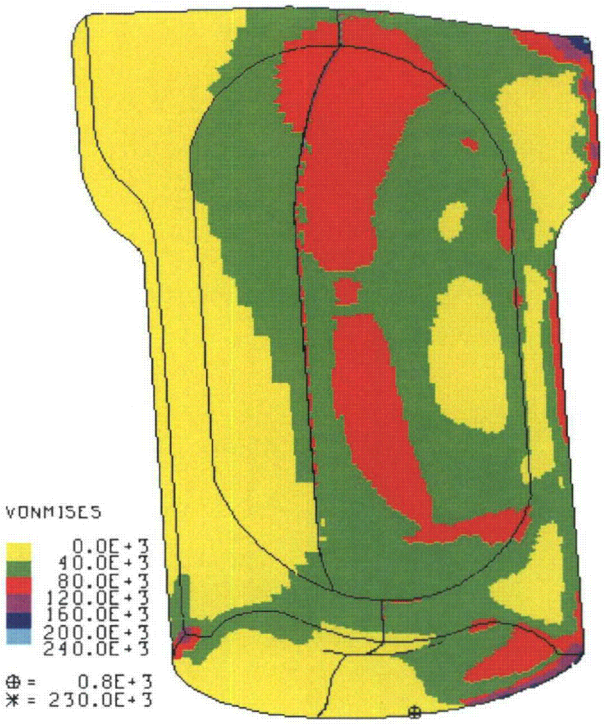

Figure 2-259. Plot of von Mises Stress in the TB-1 for the SC-1, Pu Contents, CGOC Impact, 45° Support Structure

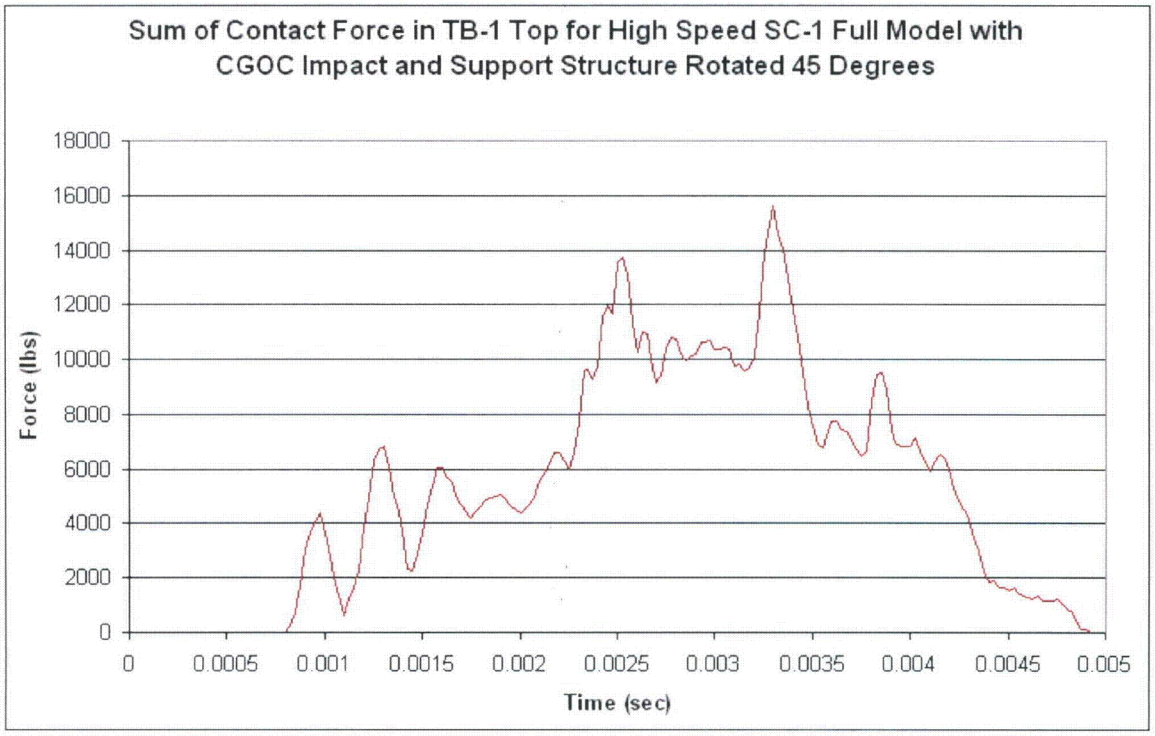

Figure 2-260. Plot of Contact Forces in the TB-1 for the SC-1, Pu Contents, CGOC Impact, 45° Support Structure

2.12.5.5.6 Run 16 - SC-2, Top Impact, Support Structure 0°

The top end impact model for the larger SC-2, each with 338 g of delta Pu contents is shown in Figure 2-261. Note that each Pu cylinder is located at the bottom of each SC-2 so that its net impact velocity with the top of the T-Ampoule is maximized. The post-impact deformation is shown in Figure 2-262 and its kinetic energy history in Figure 2-263. The top SC-2 is crushed from the subsequent impacts of the lower SC-2, and its Pu contents nearly penetrate its upper wall, which directly impacts the T-Ampoule. The lower SC-2 Pu contents nearly penetrate into the upper SC-2.

Equivalent Plastic Strain (EQPS) in the TB-1 vessel is shown in Figure 2-264 to be less than 3.7%, and only in some localized outer contact regions with the redwood overpack. The von Mises stresses (see Figure 2-265) peak at 147.3 ksi is just above the elevated-temperature minimum yield strength for the TB-1 of 141 ksi but more importantly, through-thickness TB-1 stress values are in the 37 ksi range, below yield. The time at which the peak value of the von Mises stress occurs coincides with the peak value of the contact force (summed over the lid area). A plot of this force as a function of time is shown in Figure 2-266. A maximum contact load of about 49,090 lbs is applied to the inner surface of the TB-1 lid during the impact. No T-Ampoule elements exceeded the tested B-W strain locus and the peak Tearing Parameter value (see Table 2-11, run #16) of 0.0132 was below the critical Tearing Parameter value of 1.012 for Ti-6Al-4V.

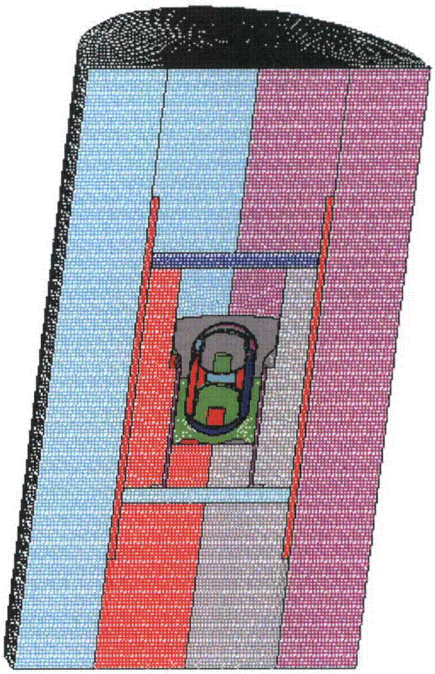

Figure 2-261. Finite Element Mesh for the SC-2, End Impact, 0° Support Structure

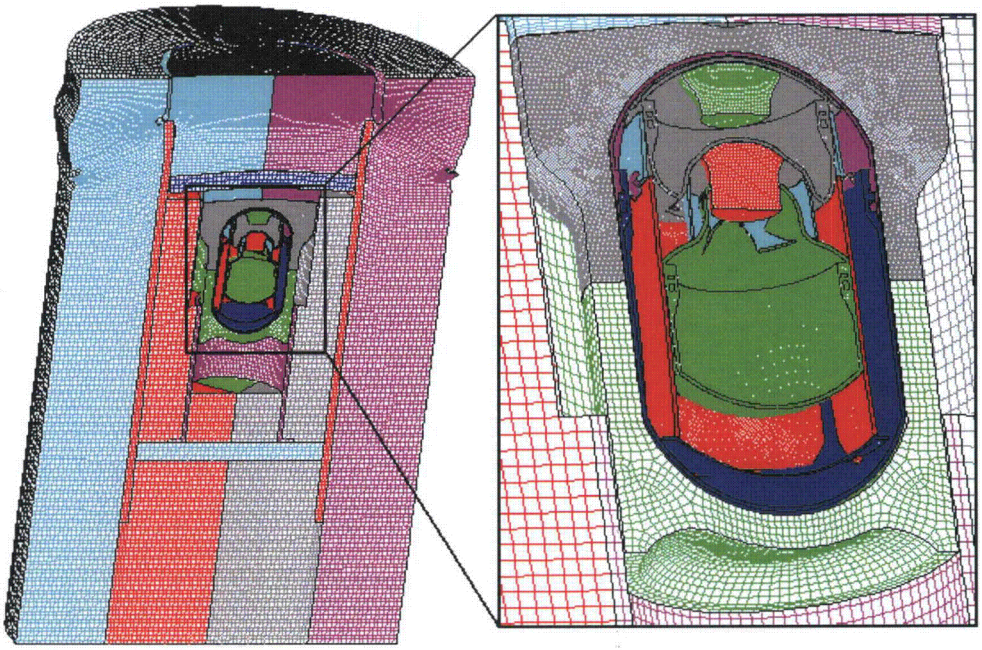

Figure 2-262. Finite Element Mesh for the SC-2, End Impact, 0° Support Structure – Final Displacement

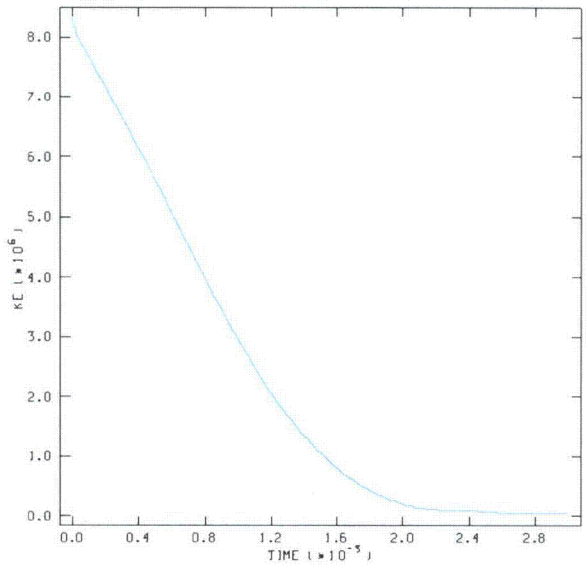

Figure 2-263. Kinetic Energy Time History for the SC-2, End Impact, 0° Support Structure

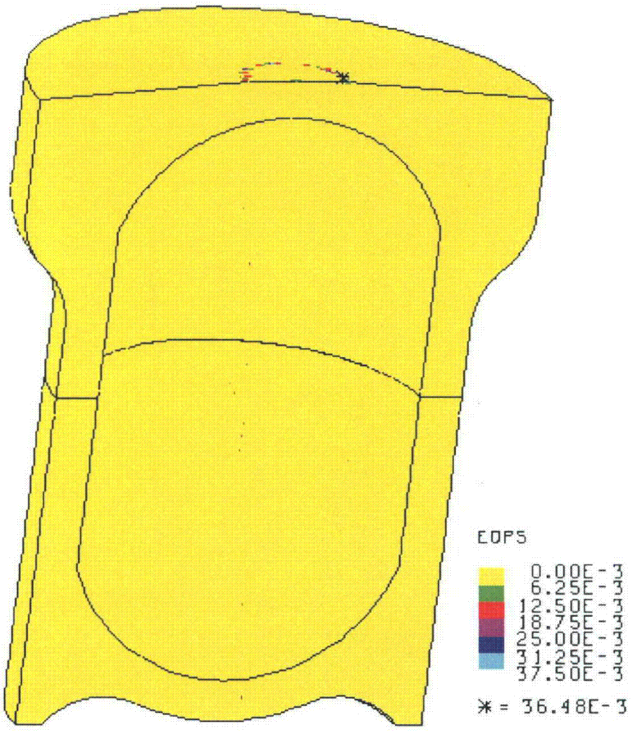

Figure 2-264. Plot of EQPS in the TB-1 for the SC-2, End Impact, 0° Support Structure

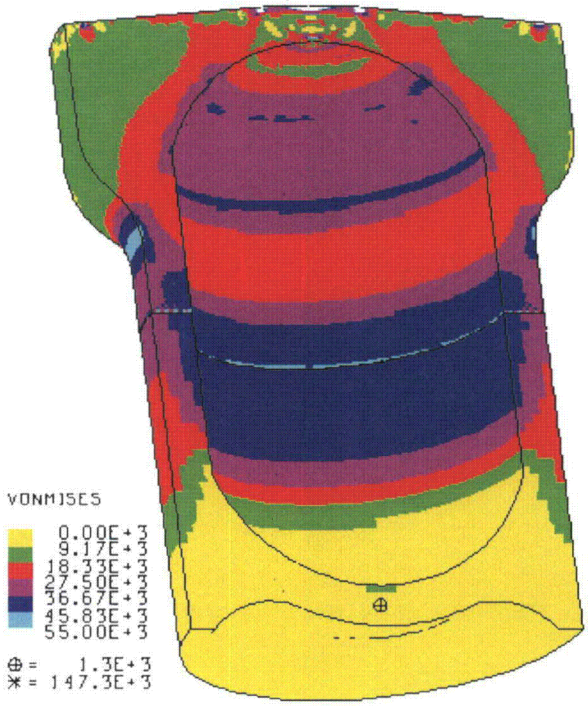

Figure 2-265. Plot of von Mises Stress in the TB-1 for the SC-2, End Impact, 0° Support Structure

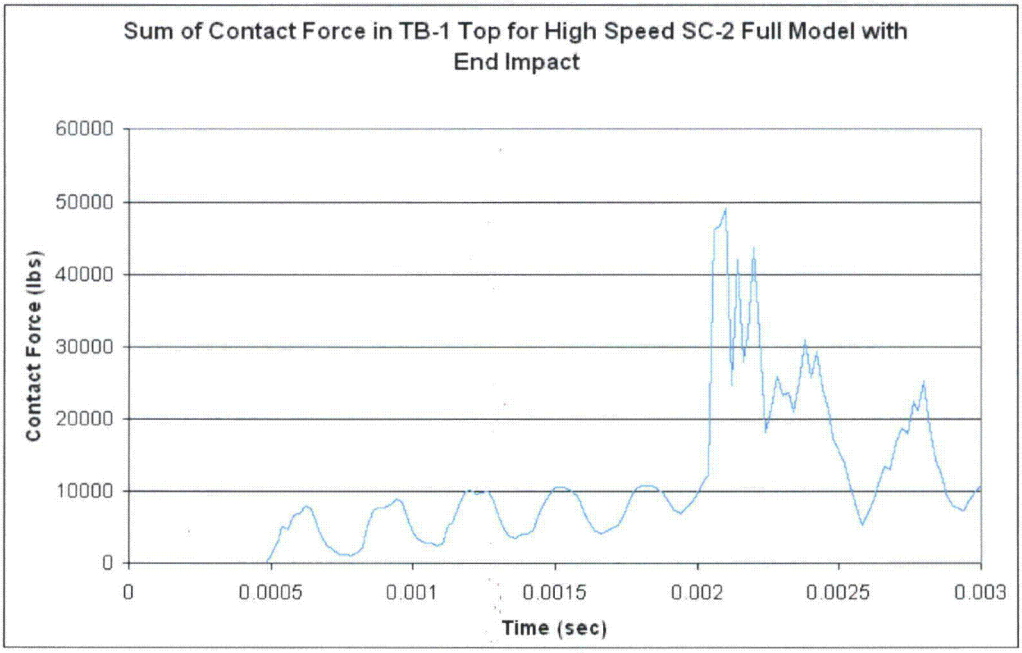

Figure 2-266. Plot of Contact Forces in the TB-1 for the SC-2, End Impact, 0° Support Structure